Centro de Investigación Científica y de Educación Superior de Ensenada, Baja California

Doctorado en Ciencias
en Ciencias de la Tierra
con orientación en Geociencias Ambientales

Soil erosion and sedimentation processes in the transboundary Tijuana River watershed; Case study: Los Laureles Canyon.

Tesis
para cubrir parcialmente los requisitos necesarios para obtener el grado de Doctor en Ciencias

Presenta:

Napoleón Gudiño Elizondo

Ensenada, Baja California, México
2018

Tesis defendida por

Napoleón Gudiño Elizondo

y aprobada por el siguiente Comité

Dr. Thomas Gunter Kretzschmar
Co-Director de tesis

Dr. Trent Biggs
Co-Director de tesis

Dr. Rogelio Vázquez González

Dr. Douglas Stow

Dr. Mathias Hinderer

Dr. Jonas De Dios De Basabe Delgado
Coordinador del Posgrado en Ciencias de Tierra

Dra. Rufina Hernández Martínez
Directora de Estudios de Posgrado

Resumen de la tesis que presenta Napoleón Gudiño Elizondo como requisito parcial para la obtención del grado de Doctor en Ciencias en Ciencias de la Tierra con orientación en Geociencias Ambientales.

Procesos de erosión de suelo y sedimentación en la cuenca transfronteriza del Río Tijuana; Caso estudio: Cañón Los Laureles

Resumen aprobado por:

Dr. Thomas Gunter Kretzschmar Co-Director de tesis	**Dr. Trent Biggs** Co-Director de tesis

La cuenca hidrológica del Río Tijuana se localiza en el extremo noroeste de México y suroeste de Estados Unidos, cuenta con un área de captación de 4,532 kilómetros cuadrados, de los cuales un cuarto de esta área pertenece a Estados Unidos y tres cuartos a México. Durante la temporada de lluvias grandes cantidades de sedimento fluyen hacia la parte americana generando problemas de excesiva sedimentación en el Estuario Tijuana, mientras que en el territorio mexicano la erosión de suelos y otros movimientos de tierra asociados a la escorrentía superficial representan un potencial peligro para la infraestructura civil y el nivel de vida de la población. En este proyecto se desarrolló una metodología para validar un modelo de erosión en la cuenca Los Laureles, una sub-cuenca del rio Tijuana, para cuantificar las contribuciones de los diferentes procesos de erosión (laminar, cárcavas y canales), además de evaluar el potencial efecto de la urbanización en la producción total de sedimentos. Se utilizaron técnicas topográficas de alta resolución para monitorear el comportamiento de las cárcavas y mejorar el entendimiento de los procesos de formación y evolución de éstas en términos hidráulicos, topográficos, geológicos y de uso de suelo. Se instalaron estaciones de monitoreo en las sub-cuencas “Los laureles” para medir la precipitación pluvial, caudal, así como la descarga de sedimentos en la salida de la cuenca para validar las estimaciones del modelo de erosión (AnnAGNPS). Se encontró que los umbrales de formación de cárcavas (área de drenaje y pendiente) son más bajos y que la producción de sedimentos por erosión de cárcavas es mayor en comparada con otros estudios de erosión de cárcavas. El modelo AnnAGNPS simuló bien las cárcavas, la escorrentía total y máxima, así como la producción total de sedimentos (pbias 1.2, RMSE 35% de la media) por un periodo de 17 años. Los parámetros más sensitivos en la erosión de cárcavas fueron la curva número, la profundidad de la capa impermeable y la tensión cortante del suelo. Los resultados del modelo indican que la erosión por cárcavas contribuye con el 57% de la producción total de sedimentos, y que el 50% de la producción total de sedimento es generado en solo el 7% del área total de la cuenca. Se recomienda evaluar medidas de mitigación en la producción de sedimento, así como la incertidumbre y sus posibles implicaciones en el análisis de escenarios para el manejo integral de cuencas urbanas.

Palabras claves: escorrentía, erosión de suelo, cárcavas, producción de sedimento, fotogrametría 3D.

Abstract of the thesis presented by **Napoleon Gudiño Elizondo** as a partial requirement to obtain the Doctor of Science degree in Earth Sciences with orientation in Environmental Geosciences.

Soil erosion and sedimentation processes in the transboundary Tijuana River watershed; Case study: Los Laureles Canyon

Abstract approved by:

Dr. Thomas Gunter Kretzschmar	**Dr. Trent Biggs**
Co-Director de tesis	Co-Director de tesis

The Tijuana River watershed is located in the northwestern Mexico and southwestern USA, the total catchment lies 3,253 km2 in Mexico and 1,212 km2 in the U.S; or 73% and 27 %, respectively. Excessive erosion, transport and deposition of sediment in the watershed have caused many detrimental effects to the people living in the watershed and have resulted in impaired conditions for aquatic life supported in the Tijuana estuary (the outlet of the watershed). This study used Unmanned Aerial Systems (UASs) and Structure-from-Motion (SfM) photogrammetric techniques to quantify gully erosion to calibrated a model (AnnAGNPS) of an ephemeral gully network that formed on unpaved roads following a storm event in an urban watershed (11 km2) in Tijuana, Mexico, a rapidly urbanizing watershed in Tijuana, Mexico. Gullies formed almost exclusively on unpaved roads which had erodible soils and concentrated flow. Management practices (e.g. road maintenance that fill gullies after large storms) contributed to total sediment production at the watershed scale. Sediment production from gully erosion was higher and threshold values of slope and drainage area for gully incision were lower than ephemeral gullies reported for agricultural settings. This indicate high vulnerability to gully erosion which is consistent with high soil erodibility and low critical shear stress measured in the laboratory with a mini jet-erosion- test device. Runoff and soil erosion were simulated for 17 years, and a good correlation between the observed and simulated results was observed (pbias 1.2, RMSE 35% of the mean). Modelled gully erosion was most sensitive to the Soil Conservation Service (SCS) curve number, tillage depth (TD), and critical shear stress. Simulated results show that gully erosion represents about 57% of hillslope sediment production and that 50% of the total sediment yield is produced by only 7% of the watershed area. Future studies evaluating the effect of reduction/prevention of sediment loads from green infrastructure projects, sediment basins, road paving (under different pervious conditions), and the uncertainty of some model estimated parameters, as well as implications in scenario analysis, are crucial for proper sediment management in urbanizing watersheds.

Keywords: Runoff, soil erosion, gullies, sediment production, 3-D photo-reconstruction, AnnAGNPS.

Dedication

A toda mi familia, en especial a mis Padres (Napoleón y Rosario), quienes confiaron en mí desde el primer día. A mi esposa e hijo (Belinda y Napoleón Zion), con quienes afiancé el concepto de que la familia es lo más importante en esta vida. A mis hermanos (Jessica y Norman), por ser mi primer equipo de trabajo y con quien compartí una niñez y adolescencia muy bonita. Y a mis abuelos (Nacho, Ramón, Aurelia y teresa), que adelante están, y que su recuerdo mantendrá por siempre fresca su memoria…

A todos los profesores y amigos que tuvieron fé en mí durante mi formación académica, profesional y deportiva.

Dedico este trabajo también a las próximas generaciones de estudiantes de Geociencias ambientales, en especial a mis exalumnos, con quienes espero haber contribuido positivamente en su formación profesional, y académica.

Acknowledgements

A mi co-director de tesis, el Dr. Trent Biggs, por todo el apoyo, paciencia y confianza depositada en mí durante la realización de este proyecto de tesis.

A mi co-director de tesis, el Dr. Thomas Kretzschmar, por la confianza, consejos y todas las facilidades proporcionadas durante el desarrollo de mis estudios de posgrado. Al resto de mi comité de tesis, el Dr. Rogelio Vazquez, Dr. Douglas Stow y Dr. Matthias Hinderer, por sus muy acertadas observaciones y sugerencias durante el desarrollo de la tesis, las cuales fueron claves para mejorar este trabajo de investigación.

Al Conacyt por las becas de manutención y movilidad estudiantil durante mi formación profesional. Sin estas, hubiese sido imposible solventar mis estudios de postgrado. Al Departamento de ciencias de la tierra de CICESE, en especial a las secretarias Ivonne Pedrin, Ana Rosa Soto y Martha Barrera, al profesor Alejandro Hinojosa, y a los técnicos Jose Mojarro, Sergio Arregui, Mario Vega, entre otros, por toda su ayuda y bonita amistad durante este largo periodo de estudios de posgrado. También agradezco a mis compañeros de cubículo, a los cubanos Yosvanis Batista y Yalina Montececelos, por los buenos momentos que compartimos juntos como tripulación de este barco llamado Doctorado en Ciencias de la Tierra. A muchos otros compañeros, que por motivos de espacio no puedo enlistarlos a todos, pero que considero fueron muy importantes…

A la Agencia de Protección al Ambiente de los Estados Unidos (USEPA) por el equipo de campo, apoyo técnico, capacitación y apoyo económico para llevar a cabo este proyecto. En especial, agradezco a mi equipo de trabajo conformado por: Dr. Ronald Bingner, Dr. Eddy Langendoen, Dra. Yongping Yuan, and Douglas Liden.

Al departamento de Geografía de SDSU, En especial a mis compañeros de laboratorio “Biggs lab”, Kristine Taniguchi, Joel Kramer, Rodney Fedema, Maegan Salinas, Garrett McGurk, et al., por hacerme sentir parte del equipo y por todos los buenos momentos que pasamos en el campus, así como en el *field and labwork….* You guys, rock!!

Un especial agradecimiento para la familia Velazquez-Kidwell por, literalmente, todos los paros que me hicieron durante la maestría y el doctorado en la ciudad de San Diego, la verdad no tengo palabras para agradecerles lo mucho que me apoyaron. ¡Dios bendiga por siempre su hermosa familia!

Table of contents

List of Figures

List of Tables

Capítulo 1. Introduction

1.1 Background

Soil erosion is often associated with land degradation caused by anthropogenic impacts and is commonly related to changes in catchment land uses, such as removal of native vegetation and soil disturbance (Oygarden, 2003). Soil erosion rates have been well documented in agricultural environments, but high erosion rates are also observed in urban areas during construction (Wolman, 1967). Soil erosion rates usually decline as the urban landscape matures (Archibold et al., 2003). Conversely, in developing countries, soil exposure can last for decades following urbanization (Biggs et al., 2010). This can result in increased soil erosion rates compared to undisturbed areas or urban areas with high impervious and/or vegetation cover (Gudino-Elizondo et al., 2018).

Los Laureles Canyon Watershed (LLCW) is a bi-national watershed that flows from Tijuana, Mexico, into the southwestern arm of the Tijuana Estuary, United States. The drainage area is 11.58 km^2, with 10.8 km^2 in Mexico and 0.75 km^2 in the United States (Figure 1). The Tijuana River Estuary National Research Reserve, a protected coastal wetland in California (USA) that supports 400 species of birds. During storms, excessive erosion in Tijuana produces sediment loads that bury native vegetation and block the tidal channels (Weis et al., 2001). It also threatens human life, causing roads and houses in Mexico to collapse (Gudino-Elizondo et al., 2018) and the Tijuana River Valley in the US to flood.

There are few studies assessing soil and gully erosion in urban settings (Castillo and Gomez, 2012). Adejiji et al. (2013) described the relationship between urban land surface characteristics and gully erosion in Nigeria, and found a significant relationship between soil texture and land use. Other studies describe the expansion and headcut retreat of permanent urban gullies. Archibold et al. (2003) surveyed two urban gullies from 1994 to 2000 and measured gully headcut retreat, widening and deepening. They attributed gully erosion to land-use change, as was also found by Guerra and Hoffman (2006) in Brazil and by Imwangana et al. (2014) in Congo. Nevertheless, little has been done to characterize erosion rates for a large network of gullies, due in part to difficulty in surveying them.

Ephemeral gullies can be important contributors to sediment production at the watershed scale (Vandaele et al., 1996), especially in arid and semi-arid environments. Such gullies are small eroded channels formed by concentrated runoff during a storm event (Foster, 1986) and are temporary features removed by tillage operations (Poesen and Govers, 1990) or filled with sediment in urban environments.

Ephemeral gullies form from a complex interaction between physical and management attributes such as topography, rainfall duration and intensity, soil moisture, soil properties, vegetation cover, and management practices (Momm et al., 2012).

Semi-arid watersheds are highly sensitive to soil and stream channel erosion following urbanization (Trimble, 1997; Taniguchi et al., 2015). Gudino-Elizondo et al. (2018) observed that gullies in Tijuana, Mexico, formed almost exclusively on unpaved roads, reflecting the role of roads in routing flow and their vulnerability to gully erosion. Unpaved roads can also be an important component of anthropogenic sediment generation in the study area (Gudino-Elizondo et al., 2018), as has also been reported in other settings (Wemple et al., 2017), including logged forests (Reid and Dunne 1984; Montgomery and Dietrich 1988) and tropical islands (Ramos-Scharron and MacDonald 2007).

An ephemeral gully will form only when a particular interaction between these attributes, or an abrupt change in ground surface elevation, leads to shear stress caused by overland runoff exceeding the soil critical shear stress to produce scour below the soil surface and eventually incision or upstream migration of the gully head (GH). A GH is the location at which gully erosion processes cannot continue upstream under particular combination of rainstorm intensity, storm discharge, land use, vegetation cover and soil type (Torri, 2014). Several studies have documented the relationship between ephemeral gully formation and runoff erosivity using topographic attributes, especially drainage area (Ad) and local slope (S) at the GH, with a threshold defined by $S = aA_d^b$ (Patton and Schumm, 1975; Foster, 1986; Thorne et al., 1986; Montgomery and Dietrich, 1994). In this equation, ‘a’ is a constant which varies with lithology, soils, climate and vegetation cover (Vandaele et al., 1996), and ‘b’ is an exponent related to the dominant processes that form the gully (Gómez-Gutiérrez et al., 2009).

However, measurements and modelling of ephemeral gully erosion rates on unpaved roads have rarely been conducted in urban watersheds. Control of gully erosion could involve road paving, but at the cost of increasing peak discharge. Other best-management practices (BMPs) include revegetation of hillslopes that produce runoff, which could mitigate both runoff and sediment production, but this strategy has not been quantitatively evaluated. The trade-off between sediment control and runoff production is particularly important, but remains unquantified.

Numerical models have been used to simulate soil and gully erosion rates (Merkel et al., 1988; Woodward, 1999; Bingner et al., 2002; Bingner et al., 2015) and to assess the impacts of conservation practices (Taguas et al., 2012). These models differ in terms of their structure, their assumptions and the

input data necessary for model calibration and application (Merrit, 2003). Bull and Kirkby (1997) reviewed the conditions for gully formation and noted that gully modelling must be based on the relationship between flow hydraulics and soil properties (Casali et al., 2009). Nachtergaele et al. (2001) reported a good performance of the Ephemeral Gully Erosion Model (EGEM) predicting gully volumes in agricultural areas of Spain and Portugal.

The Annualized AGricultural Non-Point Source (AnnAGNPS) model was developed to simulate sheet and rill erosion in agricultural environments (Bingner et al., 2002; Bingner et al., 2015), and has been utilized and validated in many studies, including in evaluations of the impact of agricultural BMPs (Yuan et al., 2001, 2003, 2005; Baginska and Milne-Home, 2003; Suttles et al., 2003; Licardello et al., 2007; Shamshad et al., 2008). Gordon et al. (2007) improved on the EGEM using more process-based techniques and this revised EGEM has been incorporated in AnnAGNPS (Bingner et al., 2015). Improvements to the gully widening approach within AnnAGNPS were developed by Bingner et al. (2015). Head-cut migration rates within the model are based on physical approximations of mass, momentum, and energy transfer, described by Alonso et al. (2002). The AnnAGNPS model has not been tested to simulate and monitor ephemeral gully erosion rates in an urban context.

This thesis is organized as follows. Chapter 1 summarizes the background, motivation, and objectives of this research; Chapter 2 aims to map gullies and quantify gully erosion rates using unmanned aerial systems (UASs)-based SfM technology to aid understanding of the processes of gully formation; Chapter 3 aims to generate a set of behavioural gully erosion models in a rapidly urbanizing watershed, and to explore the impact of parameter uncertainty on scenario analysis in a practical management context; and Chapter 4 address the relationship between rainfall and sediment load from different hillslope processes (sheet and rill, gully, and total erosion) at the *Los Laureles canyon* watershed scale. The last chapter, Chapter 5, summarizes the finding of the three papers and concludes with an examination of future research questions

1.2 Objectives

1.2.1 General

Measurement, modeling and better understanding of the erosional processes and sediment production rates in an urban watershed.

1.2.2. Specifics

a) Where do gullies form in an urbanizing landscape in a developing country context?

b) What are the management implications for the control of sediment production?

c) How do the topographic thresholds for gully formation (S and Ad) and sediment production rates from urban gullies compare with gullies in agricultural settings?

d) How well does the AnnAGNPS model predict urban gully erosion, water and sediment loads?

(e) What are the most sensitive AnnAGNPS parameters in urban gully erosion modelling?

(f) What are the implications of parameter uncertainty for evaluation of the impact of road paving and other BMPs on runoff and erosion?

g) What processes generate sediment in the watershed, and what is the role of soil properties and land use?

f) What is the relationship between rainfall and sediment load from different hillslope processes (sheet and rill, and gully erosion)?

g) Where are the hot spot of sediment production, and what watershed characteristics control them?

h) What are the implications of the sediment budget and distribution hotspots for management designed to mitigate sediment loads?

Chapter 2. Measuring ephemeral gully erosion rates and topographical thresholds in an urban watershed using unmanned aerial systems and structure from motion photogrammetric techniques.

2.1 Abstract

Both rural and urban development can lead to accelerated gully erosion. Quantify gully erosion is challenging in environments where gullies are rapidly repaired, and in urban areas where microtopographic complexity complicates the delineation of contributing areas. This study used Unmanned Aerial Systems (UASs) and Structure-from-Motion (SfM) photogrammetric techniques to quantify gully erosion in the Los Laureles Canyon watershed, a rapidly urbanizing watershed in Tijuana, Mexico. Following a storm event, the gully network extent was mapped using an orthomosaic (0.038 m pixel size); the local slope and watershed area contributing to each gully head were mapped with a Digital Surface Model (0.3 m pixel size). Gullies formed almost exclusively on unpaved roads which had erodible soils and concentrated flow. Management practices (e.g. road maintenance that fill gullies after large storms) contributed to total sediment production at the watershed scale. Sediment production from gully erosion was higher and threshold values of slope and drainage area for gully incision were lower than ephemeral gullies reported for agricultural settings. This indicate high vulnerability to gully erosion which is consistent with high soil erodibility and low critical shear stress measured in the laboratory with a mini jet-erosion- test device. Future studies that evaluate effects of different soil types on gully erosion rates on unpaved roads, as well as model effects of management practices such as road paving and their impact on runoff, soil erosion, and sediment loads are crucial for proper sediment management and planning in urban watersheds.

2.2 Introduction

There are few studies assessing gully erosion in urban settings (Castillo and Gomez, 2012). Adejiji et al. (2013) described the relationship between urban land surface characteristics and gully erosion in Nigeria, and found a significant relationship between soil texture and land use. Other studies describe the expansion and headcut retreat of permanent urban gullies. Archibold et al. (2003) surveyed two urban gullies from 1994 to 2000 and measured gully headcut retreat, widening and deepening. They attributed

gully erosion to land-use change, as was also found by Guerra and Hoffman (2006) in Brazil and by Imwangana et al. (2014) in Congo. Nevertheless, little has been done to characterize erosion rates for a large network of gullies, due in part to difficulty in surveying them.

Ephemeral gullies can be important contributors to sediment production at the watershed scale (Vandaele et al., 1996), especially in arid and semi-arid environments. Such gullies are small eroded channels formed by concentrated runoff during a storm event (Foster, 1986) and are temporary features removed by tillage operations (Poesen and Govers, 1990) or filled with sediment in urban environments. Ephemeral gullies form from a complex interaction between physical and management attributes such as topography, rainfall duration and intensity, soil moisture, soil properties, vegetation cover, and management practices (Momm et al., 2012). An ephemeral gully will form only when a particular interaction between these attributes, or an abrupt change in ground surface elevation, leads to shear stress caused by overland runoff exceeding the soil critical shear stress to produce scour below the soil surface and eventually incision or upstream migration of the gully head (GH). A GH is the location at which gully erosion processes cannot continue upstream under particular combination of rainstorm intensity, storm discharge, land use, vegetation cover and soil type (Torri, 2014).

Several studies have documented the relationship between ephemeral gully formation and runoff erosivity using topographic attributes, especially drainage area (Ad) and local slope (S) at the GH, with a threshold defined by $S = aAd^b$ (Patton and Schumm, 1975; Foster, 1986; Thorne et al., 1986; Montgomery and Dietrich, 1994). In this equation, ‘a’ is a constant which varies with lithology, soils, climate and vegetation cover (Vandaele et al., 1996), and ‘b’ is an exponent related to the dominant processes that form the gully (Gómez-Gutiérrez et al., 2009). Montgomery and Dietrich (1994) suggested that b=0.5 for laminar flow and b=0.86 for turbulent flow. S has been measured using different methods such as clinometer, compass, topographic maps, and Digital Elevation Models (DEMs). Recently, 3-D photo-reconstruction techniques have been used to estimate slopes in soil erosion studies (Gomez-Gutierrez et al., 2014; Nadal-Romero et al., 2015, Castillo et al., 2015; Di Stefano et al., 2017), but have not been applied in characterizing ephemeral gullies in an urban context.

Ephemeral gullies can be identified and characterized using aerial imagery because they commonly have distinct color, texture and shadow characteristics (Gómez-Gutiérrez et al., 2009) that differ from the rest of the landscape. Aerial imagery complements ground surveys of gully erosion, especially for rapidly urbanizing watersheds in developing countries, where ground surveys are difficult due to formation of large gullies on unpaved roads, stream channel bank collapse, landslides, and flooding

that impede field access. Urban gullies are often filled in within days of formation, and require rapid assessment after a storm. Remote Sensing (RS) supported by ground control points (GCPs) is often quicker and covers a larger area than manual surveys. GCPs are critical to scale and georeference the RS-derived cartographic products.

Many studies use time series of aerial photographs to map gully erosion, mostly in natural and agricultural areas (Nachtergaele and Poesen, 1999; Ries and Marzolff, 2003; Parkner et al., 2006). DEMs derived from aerial imagery have also been used (Thorne et al., 1986; Martínez-Casasnovas et al., 2002). More recently, structure from motion (SfM) has been used in geomorphic studies, including different spatial scales, environments, and applications (James and Robson, 2012; Turner et al., 2012; Westoby et al., 2012; Gómez-Gutiérrez et al., 2014; Micheletti et al., 2014; Di Stefano et al., 2017). SfM is a photogrammetric technique based on computer visualization tools and image-based, three-dimensional (3D) surface reconstruction algorithms (James and Robson, 2012). SfM creates massive point clouds based on pixel matching from which highly accurate digital surface models (DSM), DEMs and orthophotos can be derived. Accuracy of SfM in assessing gully erosion is very similar to the most accurate topographic methods such as Terrestrial Laser Scanning (TLS) or traditional photogrammetry (Castillo et al., 2012; James and Robson, 2012; Fonstad et al., 2013;), but SfM is cheaper and faster (Westoby et al., 2012; Castillo et al., 2015). High spatial resolution orthophotos derived from SfM can be used to identify the location of gully networks and key characteristics of gully formation such as S and Ad, and their relationship with soil loss within a gully network (Gómez-Gutiérrez et al., 2014).

Gully networks, whether in agricultural or urban areas, have characteristic patterns of sediment production pertaining to Ad. Large watersheds usually have low normalized (per unit area) sediment production compared to small watersheds, because they have more storage capacity to retain sediment and the average slope decreases with increasing watershed size (Walling, 1983; Castillo and Gomez, 2016); this has also been reported for gully erosion rates (Poesen et al., 2003; Vanwalleghem et al., 2005). Poesen et al. (2003) and Castillo and Gomez (2016) compiled gully erosion rates for different agricultural environments, but ephemeral gully erosion rates and topographic thresholds for gully initiation in urbanized watersheds are not available.

This paper aims to map gullies and quantify gully erosion rates using UASs-based SfM technology to aid understanding of the processes of gully formation in Los Laureles Canyon Watershed (LLCW), a rapidly urbanizing watershed that drains into the Tijuana Estuary in the western section of the US – Mexico border. It addresses three questions aligned with the objectives: a) Where do gullies form in an urbanizing

landscape in a developing country context? b) What are the management implications for the control of sediment production? and c) How do the topographic thresholds for gully formation (S and Ad) and sediment production rates from urban gullies compare with gullies in agricultural settings? The study is novel in presenting topographic thresholds for ephemeral gully formation and erosion rates in an urban environment, using a combination of UASs-SfM photogrammetric techniques.

2.3 Methods

2.3.1 Study Area

The San Bernardo (SB) neighborhood (20 ha, Figure 1) is located in the Los Laureles Canyon Watershed (LLCW), a bi-national watershed that flows from Tijuana, Mexico, into the southwestern arm of the Tijuana Estuary, United States. (Figure 1). The climate is Mediterranean, with a wet season from November to April and annual precipitation of ~24 cm/yr. Most storms occur in winter. SB is located on the San Diego formation, which includes deposits of erosive and loosely consolidated sandstone and siltstone, with average slope of 15 degrees. Excessive erosion, transport and deposition of sediment in the LLCW watershed have had many detrimental impacts on the people living in the watershed and have impaired ecosystems in the Tijuana Estuary (Weis et al., 2001).

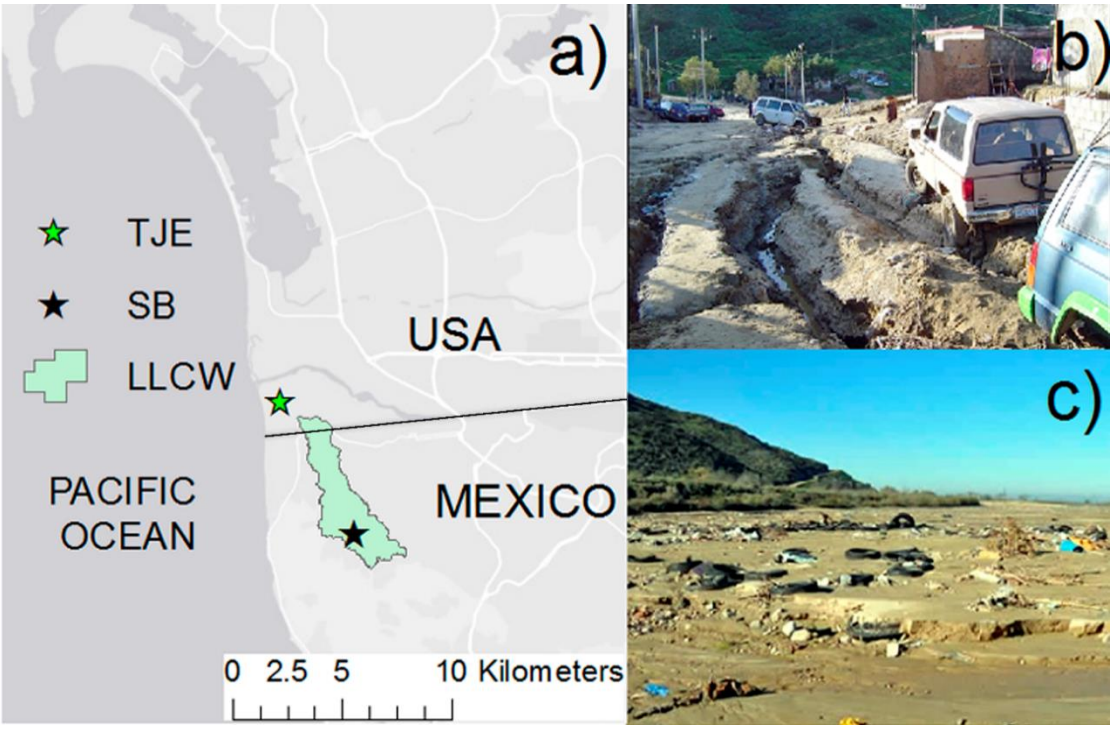

Figure 1. a) Geographic location of Los Laureles Canyon Watershed (LLCW) and San Bernardo (SB), b) one example of land degradation caused by gully erosion in Tijuana, Mexico, c) excessive sedimentation in the Tijuana Estuarine Reserve (TJE), USA.

2.3.2 Image acquisition and processing

Both ground- and UASs-based surveys of a gully network that formed following a large storm event on January 5-7, 2016 were conducted on January 16, 2016 (Figure 2). The storm was the largest of the water year (~50 mm), and had a 15-minute maximum intensity of 4.8 mm, which has a 1-year recurrence interval. Other storms occurred during the year, but were smaller than the threshold precipitation typically required to produce gullies in *SB* (~25-35 mm), as observed on other field visits following storm events during three hydrological years (2013-2016). The volume of sediment generated by the gullies during the January storm is therefore used as the annual total for comparison to other studies. The 2016 water year (October 2015-September 2016) was very dry (155 mm total precipitation vs long-term average of 238 mm), so our results likely underestimate the long-term mean sediment production from gullies in this location.

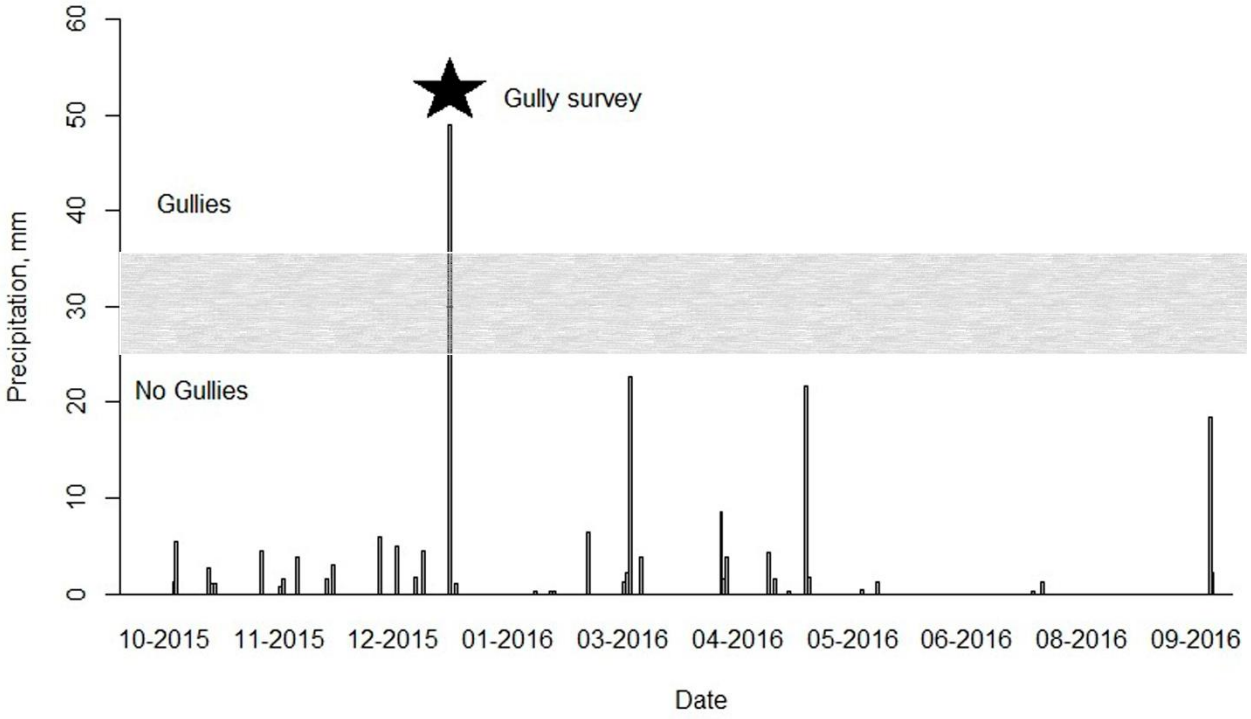

Figure 2. Daily rainfall time series for the 2016 water year. The gray box represents the rainfall threshold (~25-35 mm) for gully formation observed in the study area.

Aerial imagery was acquired during two flights over the *SB* neighborhood. Digital true color images were acquired using a nonmetric, commercially available digital camera (GoPro, 12 megapixels resolution) mounted on a *UASs* (DJI Phantom 2). The camera was set to time-lapse capture mode (1 image per second) and images were acquired at 75 m altitude (above ground level) to ensure 75% side overlap and 75% forward overlap, with the camera mounted facing 15 degrees from vertical to avoid doming deformations (James and Robson, 2014).

SfM was used to create a *DSM* using 7 *GCPs* (calibration points) and 6 Error Control Points (ECPs or validation points) spatially distributed over the study area (Figure 3), and surveyed using differential GPS (Magellan Pro Mart 3) with sub-centimeter to 5 cm vertical accuracy (Magellan Systems Corporation, San Dimas, USA). Other researchers have documented that using 4 to 5 *GCPs* with additional *ECPs* could be considered to determine relatively small but widely distributed surface changes (James et al., 2017) and that root mean square errors (RMSEs) can be reduced by placing *GCPs* on the image perimeter (Vericat et al., 2009). A dense point cloud (11 points/m^2) was generated using the Agisoft Photoscan Professional software (Agisoft LCC, Russia. Version 1.3.0) from which an orthophoto (0.038 m spatial resolution) and a

DSM (0.3 m spatial resolution) were created. The spatial resolution (0.3 m) was calculated as sqrt(1/d), where *d* is the SfM-derived point density, which resulted in one point, on average, in every 0.3 x 0.3 m pixel.

The error of the *DSM* georegistration was measured as the vertical and horizontal difference between validation (ECP) coordinates and corresponding X-Y or Z coordinate values from the *DSM*. The *RMSE* for *ECPs* was calculated as:

$$RMSE = \sqrt{\frac{1}{n}\sum_{i=1}^{n}(dGPScoordinate\_i - DSMcoordinate\_i)^2} \quad (2)$$

where *i* is the index of the points, and 'n' is the number of *ECPs* (6). Additionally, geometry of the orthophoto was tested comparing lengths of 10 different elements (sewer structures) in the image to field data (Table 9). This is the most appropriate measure of accuracy since the goal was to map dimensions of the gullies, not determine their absolute position.

2.3.3 Topographic thresholds

GHs were identified using the orthophoto (Figure 3), and their topographic attributes (*S* and A_d) were measured using *DSM* data. Flow paths and watershed boundaries for each gully head, and for various locations along the gully network, were delineated using Hydrology tools in ArcGIS 10.2. A *GH* was defined as a channel at least 30 cm wide in the upper-most stream cross-section. *GHs* are defined operationally for a given purpose; here we used 30cm based on the resolution of the imagery and the width of *GH* observed in the field. *S* was calculated as the slope gradient of the DSM-derived flowpath over a distance of 2 m upstream from each *GH*. A_d was the area draining into each *GH* calculated from the SfM-derived *DSM* using the Hydrology tools in ArcMap 10.2. The threshold combination of *S* and A_d that generates gullies was determined by fitting the equation $S=aA_d^b$ to the lower envelope of the S-A_d plot.

Our method to calculate *S* follows previous gully erosion studies that use *DSMs* to calculate upslope lengths (i.e. Gomez-Gutierrez et al., 2014). Our use of 2m for the upslope length is similar to Vandekerckhove et al (1998), who used a range from 2 to 4 m. Most studies do not use a constant upslope length, but rather use the nearest two contour lines upslope of each *GH* to define the upslope segment,

and do not report an upslope length (Table 10). In order to determine the sensitivity of *a* and *b* to upslope length, both *a* and *b* were also determined using upslope distances of 2, 3, and 5 m to calculate *S* (see Supporting Information).

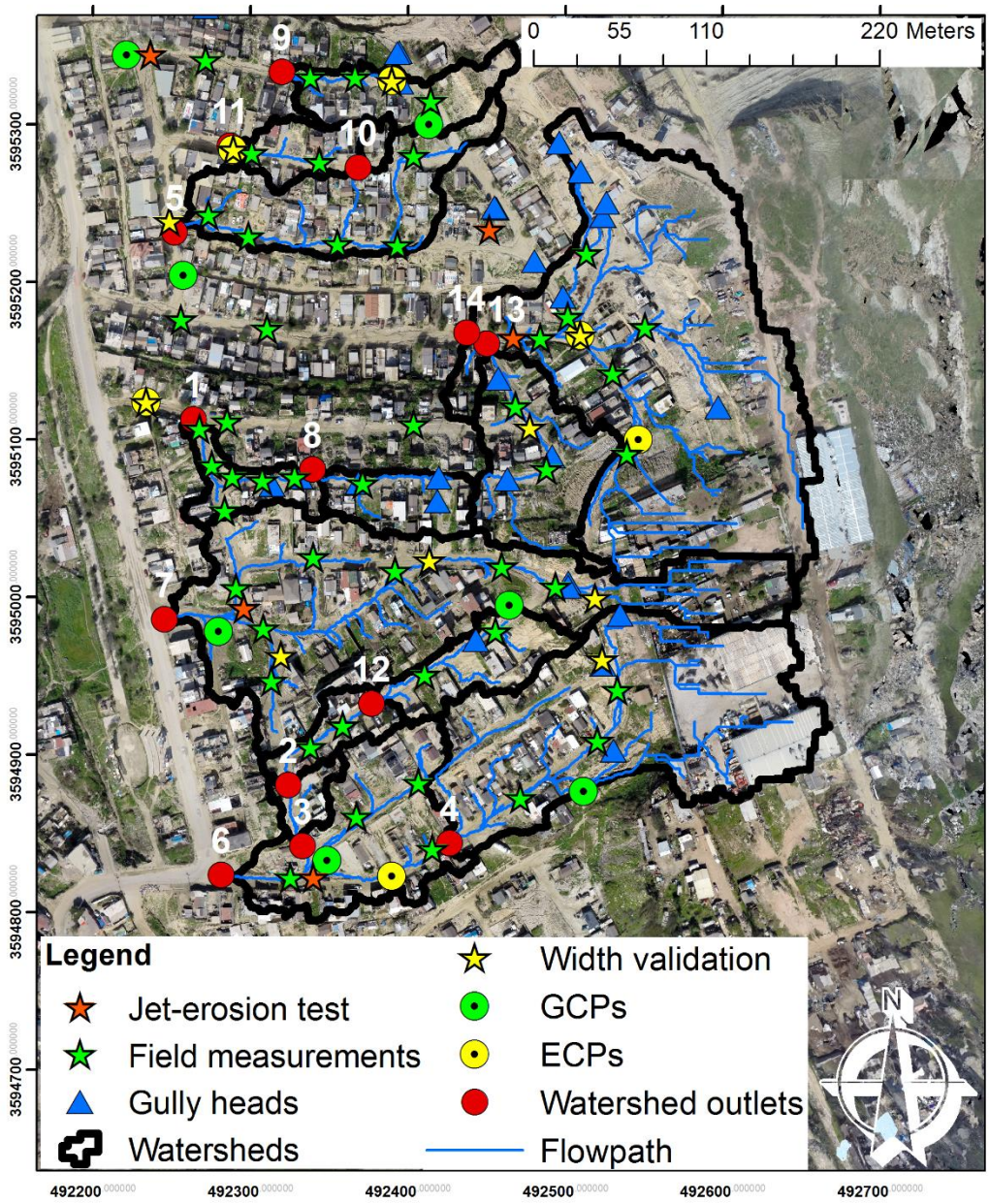

Figure 3. SfM-derived orthophoto and location of the study watersheds, ground control points (GCPs) and gully heads (GHs).

2.3.4 Specific Soil Loss (SSL)

Fourteen watersheds (Figure 3) were delineated using the watershed tool in ArcGIS 10.2, and used to estimate gully erosion rates. Watershed outlets were defined by the downslope terminus of the gully network, and watershed sizes spanned the range observed in *SB*. Gully widths and depths were measured in the field, with a ruler, at 48 locations to calibrate and validate the gully dimensions estimated by remote sensing. Polygons of gully perimeter were delineated manually by visual interpretation of the orthophoto. Gullies were too narrow and deep to estimate depth from the *DSM*, so the imagery was used to interpolate 48 field measurements of depth (Figure 3, Figure 4). First, gully segments with a field measurement of depth were located, and the gully reach having that depth was delineated using visual interpretation of the imagery. The shading and color of the reach were used to delineate a reach with a given depth. Gully segments without a nearby field measurement were delineated and assigned a depth based on the shading and color compared with other segments containing depth measurements. The volume eroded was calculated as the product of the polygon area times estimated depth. The specific soil loss (SSL), the average depth of soil loss in the watershed, was then calculated for each watershed as the total gully erosion (m3) normalized by *Ad* (Figure 4).

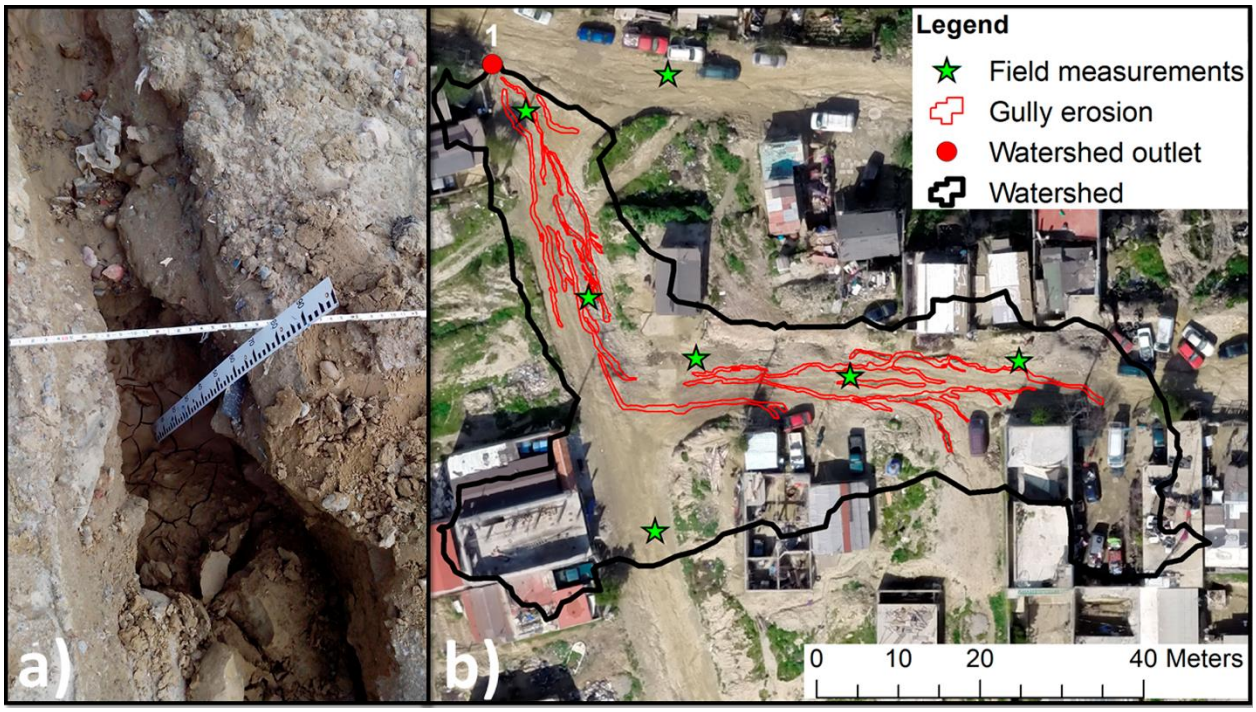

Figure 4. Example of field measurements for watershed 1 (a) and measurement locations, digitized gullies, watershed boundary and outlet used to estimate specific soil loss (b).

2.3.5 Mini-jet test analysis

Five soil samples were collected at representative sites under different land cover conditions (natural, gully walls and filled roads) over the study area to estimate the critical shear stress and soil erodibility using a mini-jet-erosion test following Hanson (1990) and Al-Madhhachi et al. (2013).

2.4 Results

2.4.1 Structure from motion (SfM) derived DSM

The mean absolute error between observed and modeled object lengths was 2 cm (Table 9), which is 7% of smallest features we measured, and is the most appropriate error statistic for mapping gully dimensions. The *RMSE* for *ECPs* was 3 cm in the X-Y and 7cm in the Z, respectively, (Table 8). The SfM-derived *DSM* had relatively similar (i.e. lower) errors compared to other *SfM* applications (Vericat et al., 2009; Javernick et al., 2014; Dietrich, 2016). This magnitude of error is acceptable for the smallest features we mapped, which were ~30 cm wide gullies. The relative precision ratio (measurement precision: observation distance) was 1:833, which is similar to 1:950 reported by James and Robson (2012) to evaluate 3D photo reconstruction quality in *SfM* applications.

2.4.2 Topographic thresholds

A total of 30 *GHs* were identified by the SfM-derived orthophoto. *S* correlated inversely with A_d at the *GHs* (Figure 5), which is consistent with previous studies (Torri et al., 1987; Montgomery and Dietrich, 1992; Vandaele et al., 1996; Vanwalleghem et al., 2005; Kakembo et al., 2009; Castillo and Gomez, 2016). The line fitted through the lower envelope of the S - A_d relationship depicts threshold values required for gully formation (Patton and Schumm, 1975). For instance, an *S* value of 0.015 and/or an A_d of 0.0008 ha ($8m^2$) are needed to initiate gully erosion under the rainfall and erodibility conditions in the study area (Figure 5).

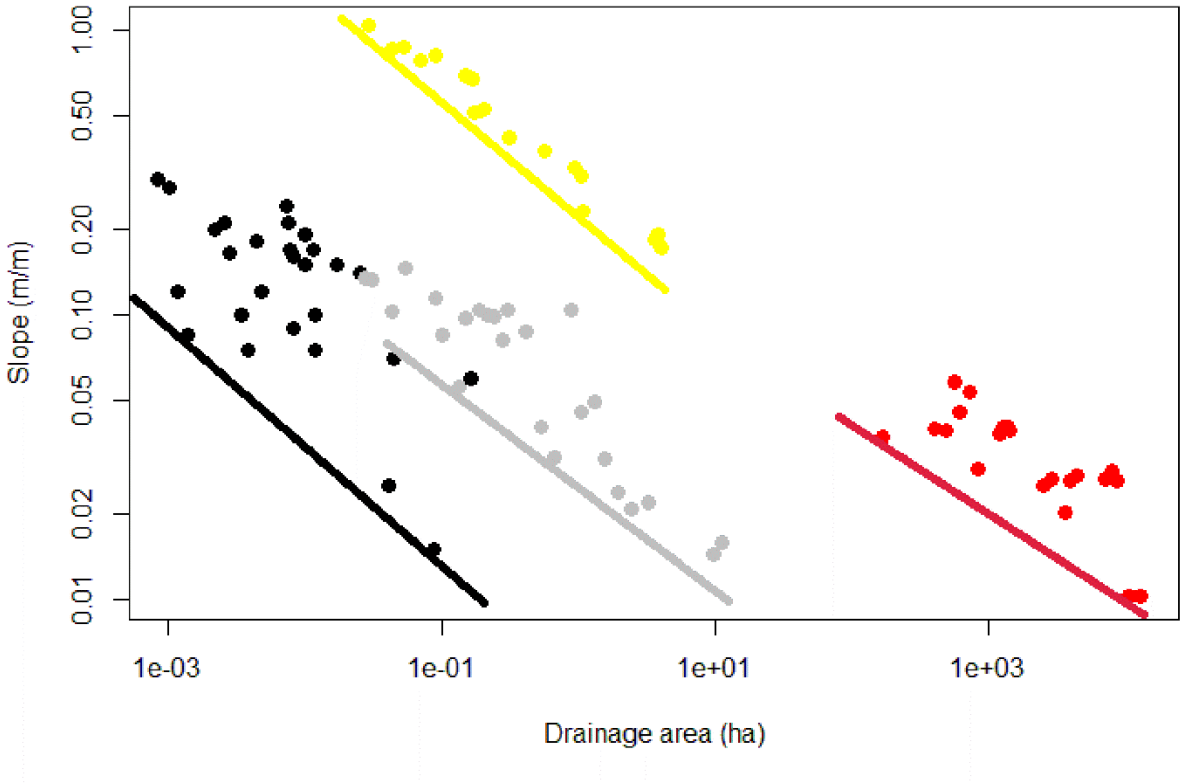

Figure 5. Topographic thresholds (S and A_d) for the mapped headcuts in SB and from selected papers from literature; Colorado (Patton and Schummm, 1975); Oregon and California (Montgomery and Dietrich, 1988); Belgium and Portugal (Vandaele et al., 1995). The line fitted through the lower most points represents the critical conditions for gully initiation.

The mean topographic attributes equation ($S=0.02* A_d^{-0.36}$) was similar to the one reported by Vandaele et al. (1996) for agricultural settings in central Belgium ($S=0.02* A_d^{-0.40}$) under a higher precipitation regime. The spatial distribution of the *SB* point cloud and the values of the *a* and *b* coefficients were not sensitive to different upslope lengths (2, 3, 5 m) defining *S*: coefficient *a* was 0.02, 0.0175 and 0.0158 and *b* was -0.360, -0.355 and -0.387 for upslope lengths of 2, 3, and 5 m (Figure 25, Appendix A), suggesting that both the topographic thresholds for gully formation and the physical characteristics described by these parameters in the system are robust to the upslope length.

Each dataset from the literature that we compared with our data on topographic thresholds (Figure 5) used different cartographic products to measure *Ad* and *S* (especially upslope lengths). Vandekerckhove et al (1998) used an upslope length that range from 2-4 m, which is comparable to our upslope length of 2 m, and sensitivity analysis on our data suggests that the topographical thresholds plot

and regression coefficients *a* and *b* are insensitive to upslope lengths between 2 and 5 m (Figure 25, Appendix A). We conclude that the range of techniques and upslope lengths used by others does not complicate the comparison of results among studies.

2.4.3 Specific soil loss

A total of 311 polygons representing ephemeral gullies within 14 watersheds were identified and mapped from the orthophoto in the *SB* area. The width measured on the orthophoto ranged from 0.3 to 3.1 m, and depth measured in the field ranged from 0.1 to 0.8 m.

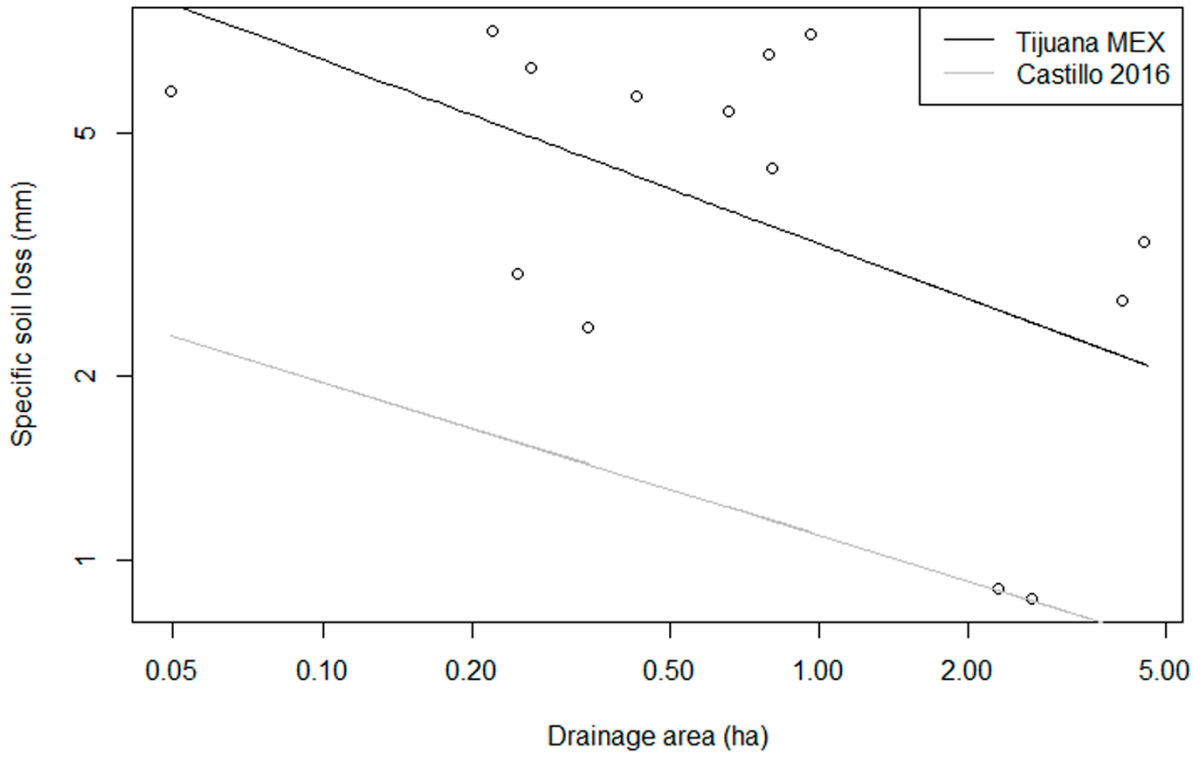

Figure 6. Relationship between watershed size and *SSL* (Specific Soil Loss, the average depth of soil loss in the watershed) from gully erosion in *SB*, Tijuana, Mexico (circle points and black line). The gray line represent the average relationship reported by Castillo and Gomez (2016) for ephemeral gullies.

SSL decreased with increasing A_d in *SB* across two orders of magnitude in A_d (0.04 to 4 ha). *SSL* in *SB* was ~2-5 times higher than the mean of the sites from Castillo and Gomez (2016), which included sites with precipitation ranging from 40-215 mm (Table 10).

2.4.4 Mini-jet test analysis

The critical shear stress values obtained from the jet erosion test ranged from 1.4 - 1.9 Pa (1.6Pa average) and soil detachment coefficient varied from 324 - 879 cm^3/Ns, suggesting high erodibility or low soil resistance values, according to Hanson's soil classification diagram (Hanson, 1990). This is consistent with the difference between regression lines reported in this analysis, compared to area-SSL line from Castillo and Gomez (2016), with both indicating high vulnerability to gully erosion.

2.5 Discussion

2.5.1 Gully mapping

The study of gullies in rapidly urbanizing regions is particularly challenging due to 1) the ephemeral nature of the gullies, which may be filled in by maintenance crews within hours or days of a storm event, precluding use of historical aerial photographs to map them; and 2) the difficulty in delineating the watershed area draining to a given gully due to the complex drainage networks that form in urban areas. While existing *DEMs* can be used to delineate watershed boundaries, they may become outdated as topography changes or have insufficient spatial resolution to accurately identify flowpaths and watershed boundaries in a rapidly urbanizing environment. Microtopographic features like roads, curbs, and ditches can change flowpaths and watershed boundaries, and their relative impact on hydrology can be bigger in small watersheds. Both challenges require rapid, high resolution mapping due to regular management practices implemented on roads that have impacts on gully networks and their contributing areas. *UASs-SfM* imagery and technology were used to address both challenges in *SB*.

Gullies formed almost exclusively on roads, reflecting their role in routing flow and their vulnerability to incision. Most gullies in *SB* are discontinuous because they are usually filled after storms, and the farthest downstream sections have lower slope and are more compacted due to vehicle traffic on the roads, all of which discourage gully formation.

Adediji et al. (2013) reported urban gullies on roads and adjacent to discontinuous concrete channels in Nigeria; gullies in other urban settings were formed in specific sites where runoff is concentrated (Archibold et al., 2003; Imwangana et al., 2014). Roads are the major component of anthropogenic sediment generation in the study area, which has also been reported in other settings, including logged forest (Reid and Dunne, 1984; Montgomery and Dietrich, 1988) and tropical islands (Ramos Scharron, 2007).

The high spatial resolution of the SfM-based *DSM* and orthophoto used in this research provided measurements of sufficient accuracy compared to those derived from other techniques and field-based measurements, representing an effective alternative to ground-based measurements, especially for urban areas where representing complex drainage patterns and microtopographic features is important to accurate mapping of flowpaths and A_d.

2.5.2 Topographical Thresholds

The roads in *SB* showed exceptional vulnerability to gully formation compared to other studies in a range of climates (Figure 5). Topographic thresholds for gully formation observed in *SB* were similar to gullies observed in Belgium and Portugal (annual precipitation of ~700 mm, and silty soils), but low threshold values of S and A_d for gully initiation in *SB* indicate greater vulnerability to gully erosion for a given storm event size, compared to thresholds values reported in Colorado (Patton and Schummm 1975), Portugal and Belgium (Vandaele et al., 1996) as well as California and Oregon (Montgomery and Dietrich, 1988).

Maugnard et al (2014) suggested a potential bias on topographic thresholds using the lower envelope of the S - A_d relationship due to the high sensitivity to outlier values, though the *SB* point cloud is located generally lower than other point clouds from the literature (Figure 5). This vulnerability is explained in part by the fill materials used to repair gullies, which are typically unconsolidated sand and

silt with low critical shear stress and high erodibility that increase gully erosion and sediment yield downstream. Roads also route and focus water flow along straight and steep flow paths, resulting in combinations of *S* and A_d that form gullies.

Comparing gully erosion studies that use different methods to determine gully formation thresholds is complicated, especially when case studies with different soils, geology, and climates are compared. Rainfall events with a high return period generate higher runoff and increase gully erosion for a given A_d (Vandaele, 1993), although ephemeral gully erosion will start only when a specific interaction of hydrologic, soil properties and management produce overland runoff that exceeds the critical soil shear stress to initiate and sustain gully erosion (Vandaele et al., 1996, Patton and Schumm 1975). Rossi et al (2015) noted potential biases in topographic thresholds studies, particularly overestimation of A_d in large watersheds (>30ha), but this is not the case for the small watersheds of *SB*.

Urban development also impacts hydrological connectivity and runoff routing in ways that enhance potential for gully formation. Concrete lots, roofs, and parts of unpaved roads with low infiltration capacity generate runoff and route it to the roads, which increase storm water runoff and gully erosion.

2.5.3 Gully erosion rates

Decreasing sediment yield with increasing A_d was observed in *SB* (Figure 6), which is consistent with a Sediment Delivery Ratio (SDR), the fraction of eroded sediment that is transported past the watershed outlet, of less than 1. Walling (1983) indicated that *SDR* tends to decrease with increased basin size, which has also been reported in other gully erosion studies (Poesen et al., 2003; Vandaele et al., 1996; Castillo and Gomez,2016).

The highest *SSL* estimated in *SB* (7.4 $mm \cdot y^{-1}$) was generally higher than those reported in Castillo and Gomez (2016) for agricultural areas (Table 11, Figure 24, Appendix A), Oygarden (2003) in Norway (3.7 mm· y⁻1); De Santisteban et al (2006) in Spain (5.9 $mm \cdot y^{-1}$); and Capra et al (2012) in Sicily (7.2 mm· y^{-1}). Cases where gully erosion exceeded values observed in this study were reported by Martínez-Casanovas et al (2002) in Spain (16.6 $mm \cdot y^{-1}$), which was associated with large precipitation events (215mm over 135min), and Tebebu et al. (2010) and Zegeye et al. (2016) in sub humid Ethiopia (up to 25 $mm \cdot y^{-1}$), which was associated with land use change and poor land management. Urban watershed characteristics such

as vegetation removal, impervious surfaces, and hydrological connectivity due to roads can lead to increased gully erosion on unpaved roads. To our knowledge, this is the first attempt to quantify ephemeral gully erosion rates in urban environments at developing countries.

Urban gully erosion on unpaved roads from other studies (i.e. Adediji et al., 2013) was not normalized by time, complicating comparison with observed gully erosion rates in *SB*. Management practices in *SB*, especially road maintenance to fill gullies, represent an important contribution to total sediment production in *LLCW*.

2.6 Conclusions

Urbanization has important impacts on soil erosion rates. In the study area, gullies formed almost exclusively on unpaved roads, highlighting them as a major sediment source. Management practices, especially road maintenance that fill gullies with unconsolidated sediment, create an additional and continually replenished source of highly erodible sediment. Lower threshold values of S and A_d for gully incision were found in *SB* compared to agricultural environments, which is consistent with the high soil erodibility and low critical shear stress measured in the laboratory. Gully erosion rates in Tijuana were higher than almost all of those observed in agricultural watersheds described in the literature. Gully erosion may contribute significantly to the total sediment production, but other processes in the sediment budget need to be quantified for comparison. The methodology described in this paper can be used in other watersheds to quantify gully erosion on unpaved roads. Our results suggest urgency in implementing management practices such as pavement or other stabilization of dirt roads to mitigate soil erosion. Future studies evaluating the effect of different soil types on gully erosion rates, as well as modeling the effect of road paving on runoff, soil erosion, and sediment loads, are crucial for proper management of sediment in our study area and potentially in urban areas in developing countries.

Chapter 3. Modelling Ephemeral Gully Erosion from Unpaved Urban Roads: Equifinality and Implications for Scenario Analysis

3.1 Abstract

Modelling gully erosion in urban areas is challenging due to difficulties with equifinality and parameter identification, which complicates quantification of management impacts on runoff and sediment production. We calibrated a model (AnnAGNPS) of an ephemeral gully network that formed on unpaved roads following a storm event in an urban watershed (0.2 km2) in Tijuana, Mexico. Latin hypercube sampling was used to create 500 parameter ensembles. Modelled sediment load was most sensitive to the Soil Conservation Service (SCS) curve number, tillage depth (TD), and critical shear stress (τc). Twenty-one parameter ensembles gave acceptable error (behavioural models), though changes in parameters governing runoff generation (SCS curve number, Manning's n) were compensated by changes in parameters describing soil properties (TD, τc), resulting in uncertainty in the optimal parameter values. The most suitable parameter combinations or "behavioural models" were used to evaluate uncertainty under management scenarios. Paving the roads increased runoff by 146–227%, increased peak discharge by 178–575%, and decreased sediment load by 90–94% depending on the ensemble. The method can be used in other watersheds to simulate runoff and gully erosion, to quantify the uncertainty of model-estimated impacts of management activities on runoff and erosion, and to suggest critical field measurements to reduce uncertainties in complex urban environments.

3.2 Introduction

Both rural and urban development can increase erosion and the delivery of land-based sediment into receiving water bodies, including estuaries, coasts, and inland lakes and reservoirs. Unpaved roads, in particular, represent one of the principal landscape features of rural urbanization in developing countries. Ephemeral gullying, including on unpaved roads, is an important soil erosion process reported in many environments (Poesen et al., 2003). Road drainage impacts erosive processes, increasing flow peaks and total discharge (Montgomery, 1994), which is also observed in monsoonal climates (Ziegler and Giambelluca, 1997).

Ephemeral gullies are important components of sediment budgets in both natural and human-disturbed environments. The term ephemeral indicates that they are temporary features, commonly removed by tillage operations (Poesen and Govers, 1990) or filled by road maintenance in urban environments. Ephemeral gully formation is the product of a complex interaction between terrain topography, climate, soil properties, land cover, and management practices (Momm et al., 2012), and ephemeral gullies can be the primary source of sediment loss in agricultural and urban environments (Bingner et al., 2006; Guerra and Hoffman 2006; Adejiji et al., 2013).

Semi-arid watersheds are highly sensitive to soil and stream channel erosion following urbanization (Trimble, 1997; Taniguchi and Biggs, 2015). Gudino-Elizondo et al. (2018) observed that gullies in Tijuana, Mexico, formed almost exclusively on unpaved roads, reflecting the role of roads in routing flow and their vulnerability to gully erosion. Unpaved roads can also be an important component of anthropogenic sediment generation in the study area (Gudino-Elizondo et al., 2018), as has also been reported in other settings (Wemple et al.., 2017), including logged forests (Reid and Dunne, 1984; Montgomery and Dietrich, 1988) and tropical islands (Ramos Scharron, 2007).

There are few studies assessing gully erosion in urban settings, as documented in a compilation of gully erosion studies by Castillo and Gomez (2016). Adejiji et al. (2013) described the relationship between urban surface characteristics and gully erosion in Nigeria, and found a significant relationship between soil texture, land use, and gully erosion. However, measurements and modelling of ephemeral gully erosion rates on unpaved roads have rarely been conducted in urban watersheds. Control of gully erosion could involve road paving, but at the cost of increasing peak discharge. Other best-management practices (BMPs) include revegetation of hillslopes that produce runoff, which could mitigate both runoff and sediment production, but this strategy has not been quantitatively evaluated. The trade-off between sediment control and runoff production is particularly important, but remains unquantified.

Numerical models have been used to simulate soil and gully erosion rates (Merkel et al., 1988, Woodward, 1999, Bingner and Theurer, 2002; Bingner et al., 2015) and to assess the impacts of conservation practices (Taguas et al., 2012). These models differ in terms of their structure, their assumptions and the input data necessary for model calibration and application (Merritt et al., 2003). Bull and Kirkby (2009) reviewed the conditions for gully formation and noted that gully modelling must be based on the relationship between flow hydraulics and soil properties (Casali et al., 2009). Nachtergaele et al. (2001) reported a good performance of the Ephemeral Gully Erosion Model (EGEM) predicting gully volumes in agricultural areas of Spain and Portugal.

The Annualized AGricultural Non-Point Source (AnnAGNPS) model was developed to simulate sheet and rill erosion in agricultural environments (Bingner and Theurer, 2002; Bingner et al., 2015), and has been utilized and validated in many studies, including in evaluations of the impact of agricultural BMPs (Yuan et al., 2001, 2003, 2005; Baginska et al., 2003; Suttles et al., 2003; Licciardello et al., 2007; Shamshad et al., 2008). Gordon et al. (2007) improved on the EGEM using more process-based techniques and this revised EGEM has been incorporated in AnnAGNPS (Bingner et al., 2015). Improvements to the gully widening approach within AnnAGNPS were developed by Bingner et al. (2015). Head-cut migration rates within the model are based on physical approximations of mass, momentum, and energy transfer, described by Alonso et al. (2002). The AnnAGNPS model has not been tested to simulate and monitor ephemeral gully erosion rates in an urban context.

In hydrologic and soil erosion modelling, several parameter sets may adequately simulate the observed behaviour of the system; such models are called “behavioural” (Beven and Freer, 2001). Hornberger and Spears (1991) rejected the idea of an optimal model structure or parameter set in favour of multiple parameter combinations, which all provide acceptable fits to observed data, called equifinality by Beven (1993). Equifinality suggests that there are multiple interactions among the parameters within a model to produce simulations that may be equally acceptable. Equifinality is especially important when simulating the impacts of changes in climate, land use, or watershed management, since different parameter ensembles can generate different predictions under change (Beven and Freer, 2001). Field measurements may be taken to constrain model parameters, but those measurements may or may not match the parameters obtained through calibration due to either unsampled heterogeneity, problems with model structure, or to other processes operating at spatial scales larger than that of the field measurements. To our knowledge, no study has addressed equifinality in gully erosion modelling and its impact on scenario analysis, particularly in an urban setting.

This paper aims to generate a set of behavioural gully erosion models in a rapidly urbanizing watershed, and to explore the impact of parameter uncertainty on scenario analysis in a practical management context. We address the following research questions: (a) How well does the AnnAGNPS model predict urban gully erosion? (b) What are the most sensitive AnnAGNPS parameters in urban gully erosion modelling? And (c) What are the implications of parameter uncertainty for evaluation of the impact of road paving and other BMPs on runoff and erosion? The study is novel in terms of evaluating AnnAGNPS’s capabilities in assessing gully erosion in urban watersheds, which included using a high-horizontal-resolution (30 cm cell size) Digital Elevation Model (DEM) generated using a combination of Unmanned Aerial Systems (UAS) and Structure from Motion (SfM) photogrammetric techniques (Gudino-

Elizondo et al., 2018) to improve representation of topographic attributes and flow routing to predict ephemeral gully formation. Understanding the process of gully erosion will be critical in describing and quantifying sediment production within urbanized watersheds, and consequent loads of water and sediment to ecosystems downstream.

3.3 Methods

3.3.1 Study Area

The San Bernardo (SB) neighbourhood is located within Los Laureles Canyon Watershed (LLCW), a bi-national watershed that flows from Tijuana, Mexico, into the southwestern arm of the Tijuana River Estuary, Imperial Beach, CA, USA. The LLCW drainage area is 11.58 km2, with 10.8 km2 in Mexico and 0.75 km2 in the United States (Figure 7b). The climate is Mediterranean, with a wet season from November to April and annual precipitation of approximately 240 mm per year. Soils in SB are sandy uplifted marine terraces with steep slopes (mean 15 degrees), resulting in high vulnerability to soil and gully erosion (Gudino-Elizondo et al., 2018). Based on a soils map of San Diego County and samples of soil texture taken in the watershed, the soils are similar to the Las Flores soil group, which are described as having loamy sand A horizons with greyish brown and light brownish grey colour, and a sandy clay B horizon grading to weakly consolidated siliceous marine sandstone in the C horizon (NRCS, 2018). SB has typical mixed urban-rural land cover (Figure 7a) with high population density (~6500 people·km−2). SB was urbanized in 2002, and has unauthorized housing developments (”invasiones”). The construction of unpaved roads on highly erodible soils enhances gully formation, affecting the quality of life for the residents (Grover, 2011), and is likely a significant contributor to total sediment production at the watershed scale. The gully network in SB is filled in with sediment at specified dates to represent road repair. However, road repair was not important, because gully formation was simulated from a single storm event.

Excessive erosion, transport and deposition of sediment have many detrimental effects on the people living in the watershed (Figure 7c) and have impaired conditions for aquatic life in the Tijuana River Estuary (Figure 7b). The Tijuana River National Estuarine Research Reserve, located in the United States, is listed as “impaired” by the State of California due to excessive sediment loads (CalEPA, 2018). Several U.S. government agencies spend approximately $3M per year to remove sediment produced in Mexico (USEPA, personal communication), and it is therefore important to quantify soil erosion rates in the upper watershed in order to identify cost-effective solutions to reduce sediment loads into the Estuary.

3.3.2 Observed gully erosion

Both ground- and UAS-based surveys of a gully network that formed in SB following a large storm event on 5–7 January 2016 were conducted on 16 January 2016 (Figure 8). The storm was the largest of the water year (~50 mm of total rainfall) and had a 15 min maximum rainfall intensity of 4.8 mm, which has a 1 year recurrence interval (Biggs et al., 2017). Other storms occurred during the year, but all were smaller than the threshold precipitation typically required to produce gullies in SB (~25–35 mm), as observed on other field visits following storm events during three hydrological years (2013–2016) (Biggs et al., 2017). The observed sediment production during this storm event was used to test the performance of the AnnAGNPS model in simulating gully erosion on unpaved roads.

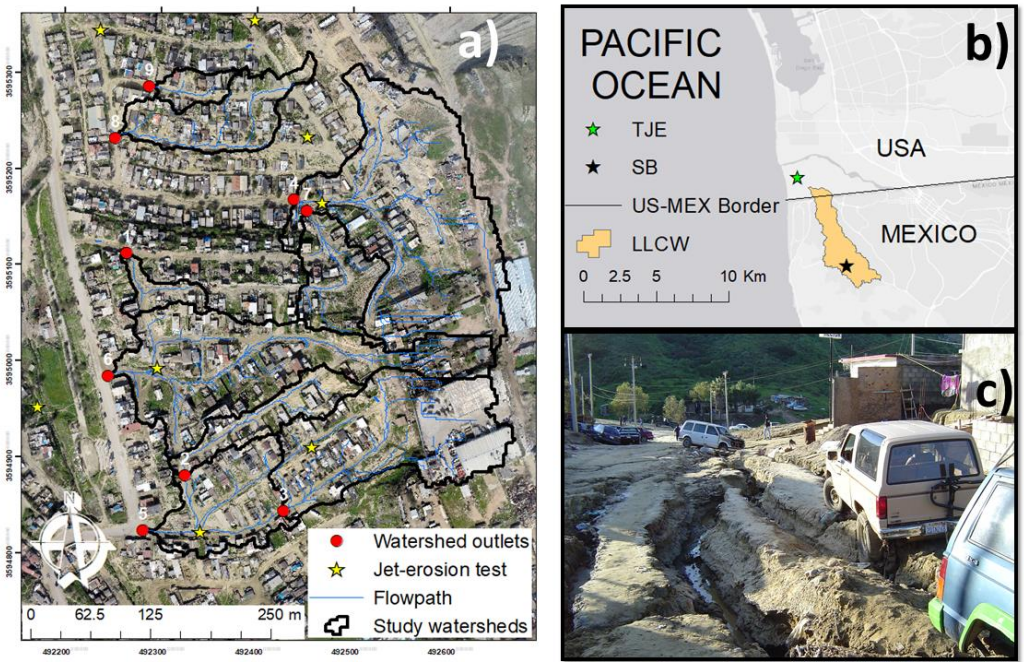

Figure 7. (a) UAS-SfM-derived orthophoto for San Bernardo (SB), and the 9 study watersheds with their outlets; (b) Geographic location of the Los Laureles Canyon Watershed (LLCW), SB, and the Tijuana River Estuarine Reserve (TJE); (c) one example of land degradation caused by gully erosion in Tijuana, Mexico.

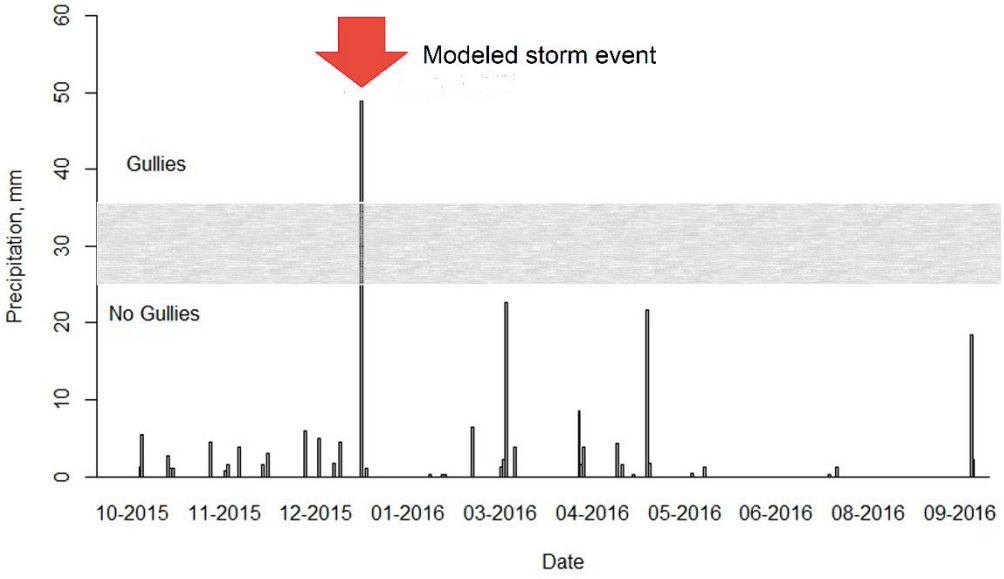

Figure 8. Daily rainfall time series for the 2016 water year. The grey box represents the rainfall threshold (~25–35 mm) for gully formation observed in the study area.

A total of nine sub-watersheds were used to estimate gully erosion rates. Gully perimeters were digitized manually from a UAS-SfM-derived orthophoto, and field measurements were used to assist with visual estimation of the gully depth of each digitized gully in order to calculate Specific Soil Loss (SSL, Gudino-Elizondo et al., 2018). We used the orthophoto to interpolate 48 field measurements (Figure 9b) of gully depth. Polygons delineating gully sections with the same depth were created based on the shadows and colours of the section. Gully sections without a nearby field measurement were identified, delineated, and assigned a depth based on the shadows and colour likeness with other gully sections containing field measurements (Gudino-Elizondo et al., 2018a). The volume of gully erosion was calculated as the product of the gully area times the gully depth. The specific soil loss (SSL, which is the average depth of soil loss in the watershed), was then calculated as the total volume of gully erosion (m3) normalized by each drainage area (Ad) (m2, Figure 9). See Gudino-Elizondo et al., (2018) for a full description of methods.

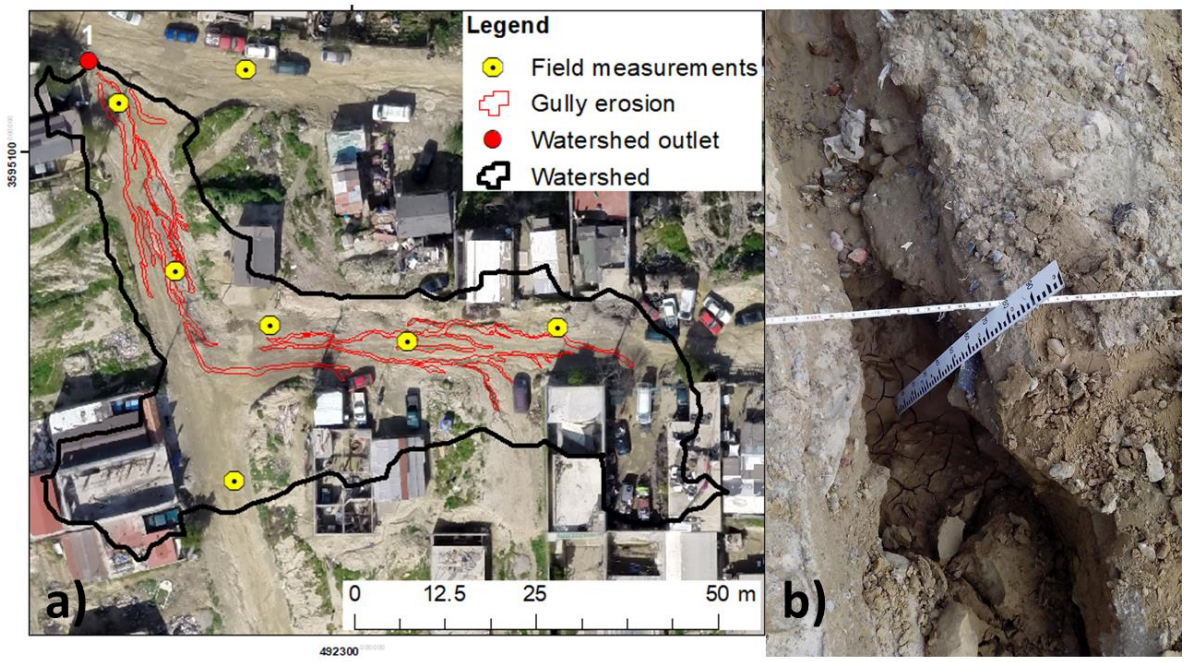

Figure 9. (a) Digitized gullies, watershed boundary, outlet, and locations of field measurements of gully depths; (b) An example of field measurement of gully depth.

3.3.3 AnnAGNPS model

The AnnAGNPS model is a distributed-parameter numerical model developed by the Agricultural Research Service (ARS) and the Natural Resources Conservation Service (NRCS) of the US Department of Agriculture (USDA) to simulate water and sediment loads from any source within a watershed on a daily time step (Bingner et al., 2015). AnnAGNPS has been used to assess watershed response to different conservation practices (Bingner et al., 2015). The spatial distribution of soils, land use, and terrain attributes is used to discretize the watershed into topographically defined sub-watersheds (AnnAGNPS cells) that are assumed to be homogeneous in land cover and soil type. The homogeneous spatial distribution of soils used in this analysis was based on field observations, visual interpretation of high-resolution satellite imagery in GoogleEarthTM and soil samples taken for texture (N = 4) and jet-erosion tests (N = 8). AnnAGNPS simulates the contribution of different erosion processes, including sheet, rill, gullies, and streambed and bank.

Total runoff is calculated following the SCS curve number method (SCS, 1972). Peak discharge, time base and the storm type are calculated using methods described in USDA-NRCS Technical Release 55

(TR-55) (SCS, 1986). A type-II, 24 h rainfall distribution (TR-55) was used, and the type was determined by comparing cumulative rainfall observed at a nearby rain gauge (Biggs et al., 2017) with the cumulative distribution functions from TR-55. Type II is representative of intense rainfall observed during convective events in semi-arid regions of the south-west United States. The model does not distribute the rainfall data over the day (e.g., minute or hourly), but rather uses the storm type distribution (here, type II) to assign regression coefficients that determine the peak discharge as a function of the ratio of initial abstraction to 24 h precipitation that is then used in determining sediment transport. A topography-based method (TopAGNPS) was used to map the location of the most downstream point of the potential ephemeral gullies (Momm et al. 2012). This approach automates identification of the location of potential ephemeral gullies based on the comparison of the runoff erosivity estimated from topographic attributes (i.e., local slope and drainage area) with soil properties. The gully erosion model in AnnAGNPS requires a model estimate of the peak discharge at the incision point (head-cut or nickpoint) where gullies form. If the shear stress exerted by the runoff erosivity exceeds the soil critical shear stress, the gully incises. Once the incision reaches a non-erodible soil layer, defined as TD in AnnAGNPS, the nickpoint migrates upslope at a rate dependent on streamflow conditions and soil resistance to erosion (Gordon et al., 2007; Taguas et al., 2012; Bingner et al., 2015). The gully width was calculated within AnnAGNPS using the Wells' Equation (Wells et al., 2013), which was developed in experimental conditions using packed soil beds under similar soil textures as those observed in SB, expressed as:

$$W=9.0057 * (Q_p * S)^{0.2963} \quad (1)$$

where W is the gully width (m); Qp the peak discharge at the gully head (m3/s); and S is the average bed slope above the gully head (m/m).

Other relationships were investigated for use by AnnAGNPS (Bingner et al., 2016), with the Wells approach providing the best response for gullies that are repaired. Many other empirical relationships have been developed for gullies or channels that were not repaired, but in the watershed for this study, gullies are repaired after precipitation events, and therefore encouraged us to use it for this analysis.

Rainfall intensity and SCS Curve Number (CN) are the most important parameters for the peak discharge and total runoff calculations using the AnnAGNPS model, and both determine the fraction of the rainfall contributing to overland flow. Manning's roughness coefficient is also an important parameter in runoff production and runoff erosivity.

3.3.4 Model setup

The topographic attributes, such as total and individual cell areas, length of channels, and the USLE-LS (Slope Length and Steepness) factors, have been calculated using the TOPAGNPS algorithms (Garbrecht and Martz, 1999) from the DEM generated using a combination of UAS-SfM photogrammetric techniques on the data collected in January 2016 (Gudino-Elizondo et al., 2018a). The DEM has a 0.3 m horizontal spatial resolution, with a Root Mean Square Error (RMSE) of 0.07 m in the vertical and 0.03 m in the horizontal dimensions.

AnnAGNPS can utilize input parameters from the NRCS database developed for any location in the USA, including climate, soil, land use, and management properties (NRCS, 2018). For our field site in Mexico, fieldwork and laboratory analyses were necessary to acquire the needed information to apply AnnAGNPS in an ungauged watershed. Geologic maps may be relatively common, but the utility of such maps and their relationship to soil types must be determined with site-specific data. Soil candidates from the SSURGO database (NRCS, 2018) were tested to choose the most suitable soil data, and were validated with field and laboratory measurements (Biggs et al., in preparation). The Las Flores soil type was the most suitable SSURGO soil type for soils in SB, which are characterized by gentle to strong sloping on marine terraces, being moderately well-drained, having medium to rapid runoff, and very slow permeability. This description matches field observations in SB, and the corresponding soil samples are representatives of highly erodible soils according to Hanson's soil classification diagram (Hanson, 1990). Percentage of impervious cover (IC) was calculated for the study area in SB from a vegetation-impervious-soil (VIS) map by Biggs et al., (2010), as updated in Taniguchi et al., (2018) to support the SCS curve number (CN) values used in this analysis. A land use map was generated by visual interpretation using the GoogleEarthTM imagery (11 November 2012, 2017 DigitalGlobe) into three land use categories: unpaved road (20%), housing (75%), and vacant lots (5%). IC was then calculated for each category and used to determine the default CN values. A composite curve number was calculated as the sum of the product of the fractional area coverage of each land cover category (unpaved road, housing, and vacant lots) multiplied by the CN associated with that category (Dunne and Leopold, 1987). The same value (82 for soil type B) was used for all three cover categories, because in standard tables (Dunne and Leopold, 1987), residential areas have a lower CN than unpaved roads, but in our study area, vegetation was relatively sparse, and there is high connectivity between the roofs and the unpaved roads. Lacking additional data on runoff production from different surfaces, we left the CN for housing equal to the CN of unpaved roads and assume that the increased runoff from roofs is balanced by increased infiltration in vegetated areas on the lots. The USLE soil erodibility factor (K, 0.006 t·h·MJ−1·mm−1), and the saturated hydraulic conductivity (0.77 mm·h−1),

were taken from the NRCS database (NRCS, 2018) for the Las Flores soil type, and were assumed to have a uniform spatial distribution over the study area.

Eight soil samples were collected in the study area to estimate the critical shear stress (τc) and soil erodibility using a mini-jet erosion test following Hanson (1990). The submerged jet-test measures depth-of-scour, manually using a point gauge at known increments over time. τc is determined by the logarithmic-hyperbolic method described in Hanson and Cook (1999). Gordon et al. (2007) noted that measured values of τc would be more accurate than any calculated values due to the large range and temporal and spatial variation of τc in the landscape. In our model, we use the measurements of τc and soil (head-cut) erodibility to set a default value, and use uncertainty analysis to determine if the final parameter range includes the measured values, as described below. Head-cut erodibility can be predicted as a power function of τc with coefficients a and b. The results from the jet-test suggested no consistent exponent value, so we assumed b = 0, and that erodibility was a constant value a, with the default value determined from the jet-test results.

3.3.5 Sensitivity analysis

Sensitivity analysis was performed to explore and quantify the effect of input parameter variability on the output results. Many sensitivity analyses have been conducted on the AnnAGNPS model (Das et al., 2008; Yuan et al., 2003, 2005, 2006; Licciardello et al., 2007; Zema et al., 2012; Chahor et al., 2014). This paper focuses on the input parameters used to evaluate the capability of AnnAGNPS to simulate sediment production from gully erosion on unpaved roads. The sensitivity approach included varying the basic input variables that impact gully erosion modelling, with emphasis on runoff and soil erodibility, using Latin Hypercube Sampling (LHS) (Kim and Yi, 2007; Momm et al., 2014) to analyse the effect on gully erosion modelling, and to explore parameter sets that successfully simulate observed gully erosion. LHS was selected over other techniques such as orthogonal grid sampling because it is more efficient in terms of computational resources requirements. Orthogonal sampling requires more computational resources to perform the same analysis (6 parameters with 5 bins = ~15,000 models). LHS also ensures that each sample is collected in a fully stratified manner (McKay et al., 1979)

The most important parameters for gully erosion modelling (Taguas et al., 2012) selected for LHS were (1) τc, (2) potential maximum soil moisture retention Smax = (1000/CN) − 10, (iii) TD, (iv) saturated

hydraulic conductivity, (v) head-cut erodibility coefficient a, and (vi) Manning's n for overland flow. A feasible parameter range was specified for each parameter (Table 1) based on measured (Jet-erosion test) and literature values (NCRS, 2018; USGS, 2018; Engman, 1986). For runoff generation, ranges were applied to Smax (Smax = (1000/CN) − 10) instead of the CN because the CN assigned to unpaved roads in SB is close to the upper limit value of CN (100) complicating the evaluation of higher values in the LHS.

LHS subdivides the range of each input parameter into N intervals of equal probability (Kim and Yi, 2007; Momm et al., 2014) then one value from each bin is chosen at random for each parameter to fit the desired sampling range. We used 15 bins to generate an initial 15 parameter ensembles. Preliminary tests suggested that these 15 parameter sets were insufficient to generate ensembles with the full range of parameter combinations, so 500 ensembles were generated by randomly selecting one of the 15 LHS-derived parameter values for each of the six parameters (Table 1).

Table 1. Parameter default values, parameter range, and the actual parameter ranges obtained using LHS and for the parameter ensembles that gave acceptable errors (behavioural models).

Parameter	Default Values	Parameter Range		LHS-Derived Parameter Range, All Models (*N* = 500)		Behavioural Models Parameter Range, (*N* = 21)	
		Min	Max	Min	Max	Min	Max
S_{max}	55.75 mm	27.87	83.63	27.93	80.84	35.18	56.85
Saturated conductivity	50 mm·d^{-1}	5	500	5.51	438	5.51	438
Critical shear stress	1 N·m^{-2}	0.04	4	0.05	3.25	0.05	1.79
Manning's *n*	0.15	0.015	0.3	0.017	0.29	0.017	0.22
Tillage depth	0.60 m	0.3	2.4	0.33	2.31	0.63	0.95
Head-cut erodibility	1000 g·N^{-1}·s^{-1}	150	1750	213	1713	213	1562

The sensitivity of the simulated sediment load to variation in each input parameter was quantified using correlation analysis (Momm et al., 2014). The linear correlation coefficient (LCC) measures the strength of the linear association between two parameters (Kim and Yi, 2007). Partial correlation coefficient (PCC) measures the relationship between two parameters, with the effects of all other parameters constant. The PCC values were calculated using the algorithms within the pcor library of the R statistical software package (Kim and Yi, 2007). Percent bias PBIAS was also used to estimate whether the average tendency of the simulated gully erosion rates was higher or lower than the observed data (Chahor et al., 2014).

$$PBIAS = \frac{\sum_{i=1}^{n}(observed - simulated)\times 100}{\sum_{i=1}^{n} observed} \quad (1)$$

According to Gupta et al. (1999), a positive PBIAS value indicates a model underestimation, and a negative PBIAS indicates model overestimation.

3.3.6 Model equifinality and scenario analysis

The 500 parameter ensembles were used to assess parameter identifiability and model equifinality for gully erosion modelling on unpaved roads using the AnnAGNPS model. A threshold of goodness of fit between observed and simulated gully erosion rates (SSL) was used to identify parameter ensembles that could be considered acceptable for a behavioural model. A threshold value of RMSE less than 1.2 mm (41% of the mean) was used as the threshold for behavioural models in this study, based on the comparison between observed and simulated SSL in nine sub-watersheds. An RMSE larger than 1.2 mm (41% of the mean) resulted in models with large errors for individual sub-watersheds, and were not used to test model equifinality. The threshold selected to divide behavioural from non-behavioural models is always subjective (Beven and Binley, 1992), and is based on the objectives of the analysis. Here, we aimed to quantify the impact of parameter uncertainty on scenario analyses, so we selected a threshold that yielded a tractable number of models for analysis (~20).

In order to test for trade-offs and compensation in parameter values, the correlation among parameters for behavioural models was quantified using Pearson's correlation coefficients.

Behavioural models were used to quantitatively evaluate the runoff and sediment production from gully erosion on unpaved roads under two scenarios: (1) current conditions, and (2) paving all roads. Runoff production under the paved condition was simulated by increasing the CN values to reflect the runoff producing potential of impervious surfaces (CNscenario), which was calculated as:

$$CN_{scenario} = CN_{cc}(1 - f_{Aroads}) + (f_{Aroads} \times CN_{paved}) \quad (3)$$

where CNcc is the Curve Number under current conditions; fAroads is the fractional area of roads (0.2), and CNpaved is the Curve Number for paved roads (98).

We assumed that the CN for paved roads would be uniform, with relatively little uncertainty, so we did not perform a sensitivity analysis for the CN of paved roads. Gully sediment production was turned

off under paved conditions since gullies formed exclusively on unpaved roads in the SB area. We assume that the drainage channel network is not modified in the paved scenario, since the change in elevations will be relatively minor. Road paving results in micro-topographic changes, such as routing flow from the centre of the street to side channels, but those alterations should not affect drainage areas or flowpaths at the sub-watershed scale.

3.4 Results

3.4.1 Sensitivity analysis

Smax, TD, and τc were the most sensitive parameters in the gully erosion modelling (Table 2). TD correlated positively with gully erosion (Table 2), because higher scour depths erode more sediment during the upstream migration of the head-cut. Conversely, increasing Smax (decreasing the CN) and increasing τc reduced gully erosion, since increasing Smax reduces runoff, and increasing τc increases the resistance of the soil to detachment and erosion. Head-cut erodibility coefficient, Manning's n, and saturated hydraulic conductivity did not have statistically significant correlations with sediment production from gully erosion.

Table 2. Sensitivity analysis of the effect of variability in potential maximum soil moisture retention, tillage depth, critical shear stress, head-cut erodibility, Manning's n, and saturated hydraulic conductivity on sediment production by gully erosion using the Linear (LCC) and Partial (PCC) correlations.

Variable	LCC	PCC
S_{max}	−0.58 *	−0.77 *
Tillage depth	0.44 *	0.72 *
Critical shear stress	−0.48 *	−0.71 *
Headcut erodibility	−0.10	−0.03
Manning's *n*	0.01	0.05
Saturated conductivity	0.02	0.01

* $p < 0.05$.

3.4.2 Behavioral Models and Parameter Identification

A total of 21 behavioural models were identified using the RMSE < 1.2 mm criterion. Simulated values of gully sediment production correlated with the observed values at the event scale, which illustrates the model's ability to simulate gully erosion on unpaved roads over the study area (Figure 10). The RMSE of the simulated gully erosion rates using the default model was acceptable (2.1 mm, 70% of the mean), but a significant improvement was observed for the behavioural models (Figure 10). The AnnAGNPS behavioural models had relatively low errors (mean percent bias (PBIAS) ranging from −14.2 to 22.7). Model efficiencies were classified by Moriasi et al. (2007) and Parajuli et al. (2009) as being very good for ±16 ≤ PBIAS ≤ ±30 for SSL (Chahor et al, 2014).

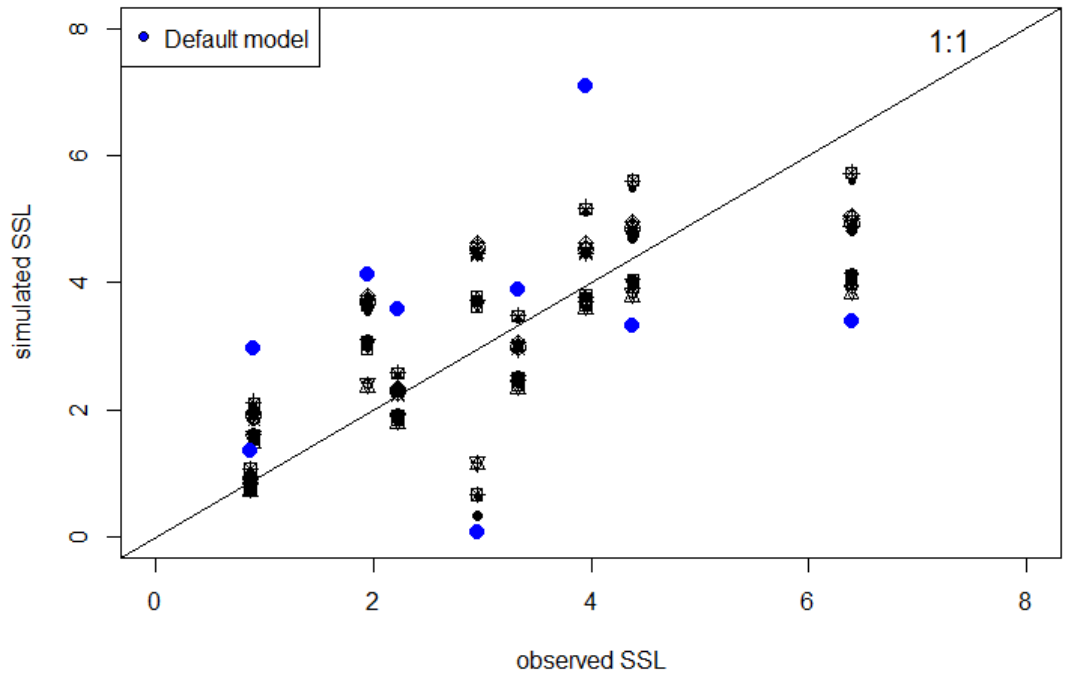

Figure 10. Relationship between observed and simulated Specific Soil Loss (SSL, the average depth of soil loss in the watershed in mm) from gully erosion in San Bernardo, Tijuana, Mexico, obtained from 21 behavioural models. The blue dots show the results from the default model parameters (Table 1).

The behavioural models generally underestimated the largest observed sediment production from gully erosion (SSL > 5 mm) and tended to overestimate sediment production from sub-watersheds with

less gully erosion (SSL < 4 mm) (Figure 10). Gully erosion contributes between 80% and 90% (87% on average) to the total sediment production among the behavioural models under current conditions.

The parameter ranges of the behavioural models were smaller than the initial ranges (Table 1), suggesting that the LHS method improves parameter identifiability in our watersheds. For example, τc in the behavioural models was 0.05–1.79 N·m-2, compared with the original range of 0.04 to 4 N·m−2. This corresponds to a soil texture of fine silt (0.05 N·m−2) to fine gravel (1.79 N·m−2) (USGS, 2018). The parameter range for TD in the behavioural models was 0.63–0.95 m, compared with the original range of 0.3 to 2.4 m. Smax was the most sensitive parameter and was also relatively well constrained in the behavioural models between 35 nm and 57 mm (CN 82–88), compared with the original range of 28–84 mm (CN 75–90). Manning's n, head-cut erodibility coefficient, and saturated hydraulic conductivity were not well constrained, but did not have a large impact on model output.

Some parameters were correlated in the behavioural models, suggesting that their values traded off or compensated for each other, resulting in parameter uncertainty (Table 3). Smax was inversely correlated with τc ($p < 0.05$), where lower values of τc were compensated by higher values of Smax in the behavioural models (Table 3). Higher values of Smax, which resulted in low runoff, required lower values of τc to maintain the same total sediment production.

The τc from the soil samples (N = 8) ranged from 0.15 to 1.9 N·m−2, and the erodibility ranged from 103 to 879 cm3 N−1·s−1 (Figure 11). τc from the samples spanned the range of the τc from the behavioural models, though there were some combinations of τc and erodibility that were slightly outside of the combinations observed, especially where τc was lower than observed for a given erodibility. Note that two behavioural models had the same critical shear stress value from the LHS, so only 20 open circles are visible in Figure 11.

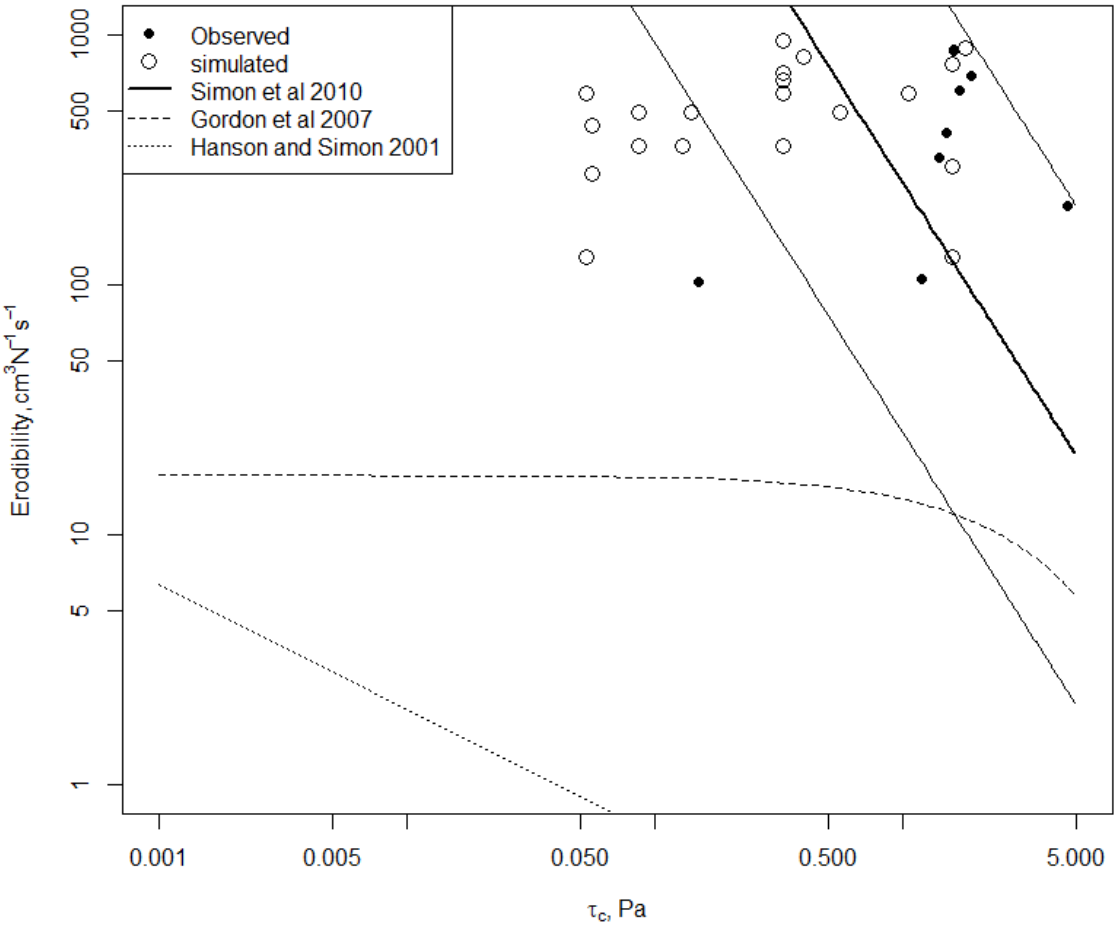

Figure 11. τc and head cut erodibility as measured by the jet-test (black dots) compared with other values from the literature (lines), and with the parameters from the behavioural models (open circles).

Table 3. Correlation coefficients for input parameters of the behavioural models.

Parameter	S_{max}	Head Cut Erodibility	Saturated Conductivity	Critical Shear Stress	Manning's *n*	Tillage Depth
S_{max}	1	0.03	0.05	**−0.51** *	−0.18	−0.31
Head cut erodibility		1	−0.42 †	0.14	−0.27	0.24
Saturated conductivity			1	0.11	0.11	0.10
Critical shear stress				1	−0.21	0.43 †
Manning's *n*					1	−0.44 †
Tillage depth						1

* Bold numbers indicate p < 0.05; Numbers with the symbol (†) indicate p < 0.10.

3.4.3 Scenario Analysis: Equifinility

Total sediment loads and total and peak runoff for all of the behavioural models under the current conditions and roads paved scenarios are presented in Table 4.

Among the twenty-one behavioural models, sediment reduction from paving all roads varied from 90 to 94%, while total runoff was 1.46 to 2.27 times the unpaved condition, and peak runoff was 1.78 to 5.75 times the unpaved condition. The decrease in discharge under unpaved conditions results from higher potential maximum soil moisture retention for the modelled event. Other events that occur under higher antecedent moisture conditions may show a lower impact of paving.

A total of 3 out of the 21 behavioural models were identified as outliers in the equifinality analysis for scenario implications (Figure 12a,b). These 3 parameter ensembles, which showed the highest impacts on total and peak discharge, were characterized by high values of Smax, which results in lower runoff production under unpaved conditions and a larger percentage increase in overland flow under the road paved scenario. The sediment production ratio showed more robust results on the total sediment reduction (90 to 94%) for all the behavioural models (Figure 12c).

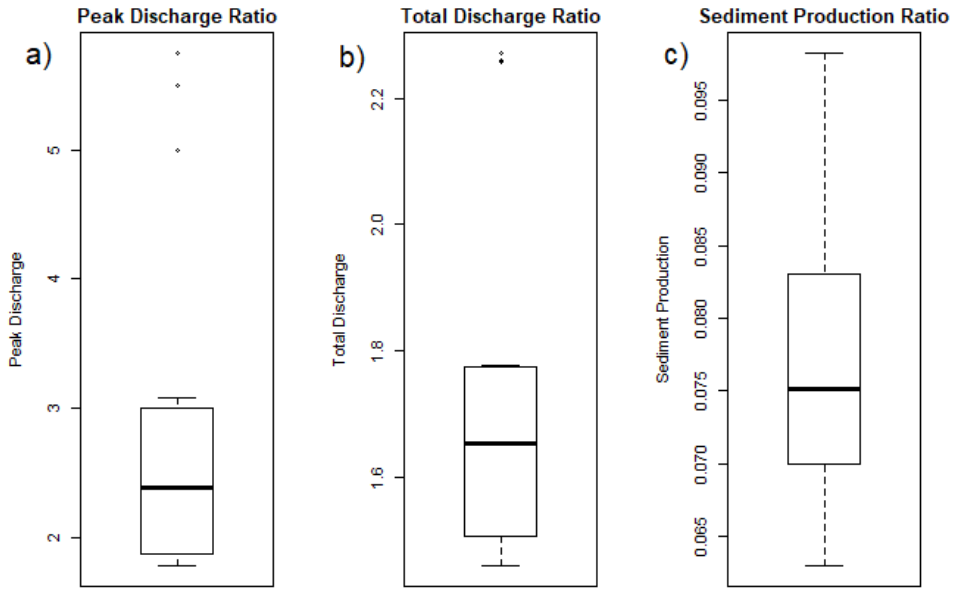

Figure 12. Impacts on water and sediment load ratios between current conditions and paving-all-roads scenario using the 21 behavioural models.

Table 4. Modelled peak discharge (L/s), total discharge volume (Q, m3), and sediment load (tons) at the outlet under unpaved and paved conditions for 21 behavioural models.

	Peak (L/s)	Q (m^3)	Sediment (tons)
Unpaved			
min	4	148	513
mean	50	500	787
max	101	739	1048
Paved			
min	20	337	49
mean	105	799	59
max	181	1078	67
Ratio of Paved: Unpaved			
min	1.78	1.46	0.06
mean	2.73	1.70	0.08
max	5.75	2.27	0.10

3.5 Discussion

Simulated sediment production from gullies was similar to the observed gully erosion in SB, suggesting that the AnnAGNPS model is able to estimate sediment production from unpaved roads in the study watersheds. The AnnAGNPS behavioural models had relatively similar errors (mean percent bias (PBIAS) ranged from −14.2 to 22.7, and 9 of 21 models have PBIAS less than 10) compared to previous AnnAGNPS applications simulating annual sediment loads (PBIAS = −7.1, Chahor et al. 2014), which used nine years of observed data for model calibration in a Mediterranean agricultural watershed.

Smax, TD and τc were the most sensitive parameters for the gully erosion model (Table 2). These results were consistent with previous studies that showed the importance of the runoff production in generating ephemeral gullies (Yuan et al., 2001; Licciardello et al., 2007; Taguas et al., 2012), and suggests that field measurements that can determine these parameters are useful for decreasing model uncertainty.

Runoff and soil resistance-to-erosion properties play an important role in gully erosion. The influence of these parameters on modelling the erosive process were reflected in the sensitivity analysis, where a trade-off was observed between the parameters related to runoff and soil erodibility (especially Smax and τc) in order to balance their respective influence in the gully erosion modelling, which is consistent with the significant correlation ($p < 0.05$) between Smax and τc (Table 3). Other parameters (saturated hydraulic conductivity, head-cut erodibility, Manning's n) were correlated with other parameters in the behavioural models ($p < 0.10$), but these three parameters did not have significant impacts on sediment production from gullies, and further analysis on those correlations are beyond the scope of this paper.

Smax, TD, and τc were well-constrained in the behavioural models (Table 1). Manning's n, head-cut erodibility and saturated hydraulic conductivity showed a wider range of values in the behavioural models, suggesting that these parameters are more influenced or compensated by other parameter combinations, complicating parameter identification.

High soil infiltration rates due to low antecedent soil moisture played a critical role in surface runoff generation in SB during the simulated storm event. CN Type II under "normal" soil moisture conditions was 82, while the CN for the modelled storm event, which was adjusted for antecedent soil moisture, was much lower (30), showing the impact of soil moisture on CN and runoff production. Low runoff production on dry soils had very important implications on the scenario analysis, resulting in a large increase in peak discharge (~1.8 to 5.7 times) under paved conditions. Other events that occur under conditions of higher antecedent moisture condition may show less impact of paving.

Field-measured values of τc helped to constrain the initial value for modelling. For example, the parameter range for τc in the behavioural models was 0.05–1.79, compared with the original range of 0.05 to 4. Approximately 80% of the behavioural models spanned the range of τc from of 0.05 to 1.1 $N \cdot m-2$, which corresponds to a soil texture of fine silt (0.05) to very coarse sand (1.1) (USGS, 2018). This suggests that field-measured τc is representative of the τc that controls the simulated sediment production in the study area.

Using different parameter ensembles generated by LHS allowed us to identify the range of the parameters and resulted in a better fit between the observed and the simulated gully erosion rates. Observed gully erosion rates were successfully reproduced using the 21 behavioural models (RMSE < 1.2

mm, < 41% of the mean), indicating robust simulated sediment production by gully erosion from unpaved roads.

The 21 behavioural models were consistent in terms of total sediment reduction (90–94%). Conversely, total runoff of the behavioural models increased from approximately 1.5 to 2.3 times and peak runoff increased by 1.8 to 5.7 times under the paved condition compared to the current condition. This could have significant impacts on the receiving earthen stream channels. The large increase in runoff generation under the paved roads scenario could be related to the large range in Smax in the behavioural models, and suggests that field data on infiltration rates, which could be used to generate values of Smax, is most critical for reducing model uncertainty. Soil compaction by car traffic on unpaved roads, which reduces infiltration rates, also has an impact on parameter uncertainty.

Increased runoff and changes in soil erosion rates due to road construction are well-known processes (Reid and Dunne, 1984; Ramos-Scharrón and MacDonald, 2007). However, to our knowledge, this is the first attempt to simulate and evaluate model equifinality and implications for scenario analysis of ephemeral gully erosion rates in an urban environment. The AnnAGNPS model provides the capability of evaluating the impact of sediment management activities designed to mitigate gully erosion on unpaved roads. Road paving can be an effective sediment conservation practice, but the overall impact at the watershed scale—for example, the effect on receiving stream channels—needs to be assessed.

3.6 Conclusion

Gully formation and sediment yield were successfully simulated in an urban setting. Simulated Specific Soil Loss (SSL) using a model of gully erosion (AnnAGNPS) was similar to the observed SSL from gully erosion, with RMSE in SSL ranging from 0.96 to 1.2 mm for the twenty-one behavioural models, compared to 2.1 mm for the default parameter (Smax, TD, Manning's n, saturated hydraulic conductivity, and head-cut erodibility) set. In the study area, gullies formed almost exclusively on unpaved roads, highlighting them as a major sediment source. Gully erosion may contribute significantly to the total sediment production, but other processes in the sediment budget need to be quantified for comparison. Smax (curve number), TD and τc were the most sensitive parameters in gully erosion modelling. The 21 behavioural models were consistent in their estimates of total sediment reduction when paving all roads

(decrease of 90–94%). Conversely, total runoff of the behavioural models increased by approximately 1.5 to 2.3 times under the paved condition compared to under the current conditions. Our results suggest urgency in implementing management practices such as pavement or other stabilization measures of unpaved roads to mitigate soil erosion, but that paving may increase peak discharge significantly (by 1.8–5.7 times) at the neighbourhood scale. Our sensitivity analysis also identified the most uncertain parameters requiring further investigation to quantify the impacts of management on runoff and sediment production, especially parameters relating to infiltration capacity and runoff production. Future studies evaluating the effect of different soil types on gully erosion modelling using AnnAGNPS, as well as modelling the effect of other management actions (i.e., revegetation of hillslopes) on soil erosion and sediment loads, are crucial for proper management of sediment in our study area, and potentially in other urban areas in developing countries.

Chapter 4. Contribution of hillslope and gully erosion to total sediment loads in a rapidly urbanizing watershed of the US-Mexico Border using the AnnAGNPS model.

4.1 Abstract

Both rural and urban development can lead to accelerated soil erosion, including sheet, rill, gully and channel erosion processes. Measuring and modelling erosional processes is challenging in ungauged watersheds, especially in developing countries, where rapid urbanization complicates parameter identification and model structure. We calibrated a model (AnnAGNPS) to quantify the sediment budget in the Los Laureles Canyon watershed, a rapidly urbanizing watershed in Tijuana, Mexico. The simulated results were calibrated and validated with data on runoff and sediment load from 14 storm events and with annual sediment load data collected for one sediment trap at the watershed outlet. Runoff and soil erosion were simulated for 17 years, and a good correlation between the observed and simulated results was observed (pbias 1.2, RMSE 35% of the mean). Our simulated results show that gully erosion represents about 57% of hillslope sediment production and that 50% of the total sediment yield is produced by only 7% of the watershed area. Future studies evaluating the effect of reduction/prevention of sediment loads from green infrastructure projects, sediment basins, road paving (under different pervious conditions), and the uncertainty of some model estimated parameters, as well as implications in scenario analysis, are crucial for proper sediment management in urbanizing watersheds.

4.2 Introduction

Soil erosion, defined as the detachment, transport, and redistribution of soil particles (Govers et al., 1990; Flanagan, 1995), is considered to be a primary cause of land degradation around the world (Fu and Gulinck, 1994). Urbanization can lead to increase soil and gully erosion and the delivery of land-derived materials into receiving water bodies, including estuaries, coasts, and inland lakes and reservoirs.

Hillslope and gully erosion is often associated with land degradation caused by anthropogenic impacts and is commonly related to changes in catchment land uses, such as removal of native vegetation and soil disturbance (Oygarden, 2003). Soil erosion rates have been well documented in agricultural settings, but high erosion rates are also observed in urban areas (Wolman, 1967). Soil erosion rates

typically decline as the urban landscape matures (Archibold et al., 2003). Conversely, in developing countries, soil exposure can last for decades following urbanization (Biggs et al., 2010). This can result in increased soil erosion rates compared to undisturbed areas or urban areas with high impervious and/or vegetation cover (Gudino-Elizondo et al., 2018).

Soil erosion and sediment transport at the watershed scale can be estimated using water and sediment balance models that consider topography, soil properties, land cover and land use (Bisantino et al., 2013). These models differ in structure, assumptions and input data necessary for model calibration and application (Merrit el at., 2003; Gudino-Elizondo et al., 2018). Soil erosion modeling is often used to simulate soil erosion by different sources, such as sheet, rill, gully and channel erosional processes to address sediment budgets and to assess the impacts of conservation practices on total sediment reduction. The sediment budget is defined as the quantitative tracking of contributing sources, sinks and redistribution of sediments in a unit area over unit time (Slaymaker, 2003).

Most soil erosion studies have only dealt with measuring sheet and rill erosion process (Gomez et al., 2008), but ephemeral gullies can also be an important source of sediment at the watershed scale (Vandaele et al., 1996; Poesen et al., 2003; Martinez-Casasnovas et al., 2005), especially in arid and semi-arid environments (Taguas et al. 2012; Gudino-Elizondo et al., 2018). Ephemeral gullies are small eroded channels formed by concentrated runoff during a storm event (Foster, 1986) and are temporary features removed by tillage operations (Poesen and Govers, 1990) or filled with sediment in urban environments. Ephemeral gullies form from a complex interaction between physical and management attributes such as topography, rainfall duration and intensity, soil moisture, soil properties, vegetation cover, and management practices (Momm et al., 2012).

The Annualized AGricultural Non-Point Source (AnnAGNPS) model has been used to simulate sheet and rill erosion in many agricultural applications (Bingner et al., 2002; Bingner et al., 2015), and has been calibrated once to model ephemeral gully erosion from unpaved urban roads to study model equifinality and implications for scenario analysis (Gudino-Elizondo 2018). Gordon et al., (2007) incorporate the gully erosion modelling technology from the Ephemeral Gully Erosion Model (EGEM) into the AnnAGNPS model (Bingner et al., 2015). Later, progress in the gully widening algorithm within AnnAGNPS were developed by Bingner et al., (2015). Head-cut migration rates were also improved by Alonso et al. (2002) based on physical approximations of mass, momentum, and energy transfer.

In semi-arid Mediterranean environments AnnAGNPS has been tested in small catchments (Licciardello and Zimbone, 2002; Licciardello et al., 2007; Taguas et al., 2009; Taguas et al., 2012). Licciardello and Zimbone (2002) and Licciardello et al. (2007) applied AnnAGNPS in a mountainous grazing watershed (130 ha) in Eastern Italy. Taguas et al. (2012), evaluated the influence on total soil losses of the different management strategies in marginal olive orchards in a mountainous area in Córdoba, Spain, where ephemeral gullies are a significant source of sediment. However, the AnnAGNPS model has not been tested to simulate soil and ephemeral gully erosion rates in an urban context at watershed scale under different soil types and land uses.

In this study, the main objectives are to 1) evaluate the capabilities of the AnnAGNPS model in a small urban watershed and to extend the knowledge about the model's application in semi-arid environments, where the initial soil moisture conditions of the watershed strongly influence runoff generation (Milella et al., 2012) and 2) to use the model to constrain the sediment budget in order to inform management and policy designed to mitigate sediment loads downstream. The Los Laureles Canyon Watershed (LLCW) drains 11.6 km^2 and is located in Northwestern Mexico. It has been monitored since 2013 to provide continuous water discharge from a stream gauge, and annual sediment loads from a sediment trap constructed in 2004 at the watershed outlet. This paper addresses the following research questions: a) How well does AnnAGNPS simulate water and sediment loads in an urban watershed? B) What processes generate sediment in the watershed, and what is the role of soil properties and land use? C) What is the relationship between rainfall and sediment load from different hillslope processes (sheet and rill, and gully erosion)? d) Where are the hot spots of sediment production, and what watershed characteristics control them? E) What are the implications of the sediment budget and distribution hotspots for management designed to mitigate sediment loads?

4.3 Methods

4.3.1 Study area

Los Laureles Canyon Watershed (LLCW) is a bi-national watershed that flows from Tijuana, Mexico, into the southwestern arm of the Tijuana Estuary, United States. The drainage area is 11.6 km2, with 10.8 km2 in Mexico and 0.8 km2 in the United States (Figure 13). The climate is Mediterranean, with a wet season from November to April and annual precipitation of ~240 mm/yr. Most of the erosional storm

events occur during the winter. The regional geology (San Diego formation) includes marine and fluvial sediment deposits of conglomerate, sandy conglomerate, and siltstone. Soils are sandy with a wide range of cobble fraction, and are dominated with steep slopes (15 degrees, mean value), resulting in high vulnerability to soil and gully erosion.

LLCW is a typical mixed urban and rural dominated watershed in the north western highlands of Tijuana with high population density (~6500 people/km2) that leads to increased soil erosion. It was urbanized in 2002 and has unauthorized housing developments ("invasiones"). The construction of unpaved roads on highly erodible soils enhances gully formation, affecting the quality of life for the residents (Grover, 2011), and can be a significant contributor to total sediment production at the watershed scale (CalEPA, 2018). The gully network is filled in with sediment following storms, and this management has to be taken into account during the simulation period.

During storms, excessive erosion in upper watershed produces sediment loads that bury native vegetation and block the tidal channels. It also threatens human life, causing roads and houses in Tijuana, Mexico to collapse and the Tijuana River Valley in the US to flood. The primary sources of sediment from LLCW are gully formation on unpaved roads, channel erosion, and sheet and rill erosion from unoccupied lots in Tijuana (Biggs et al., 2010). The construction of unpaved roads on highly erodible sediment enhances gully formation, affecting the quality of life for the residents (Grover, 2011; Gudino-Elizondo et al., 2018), and is likely a significant contributor to the total sediment production at LLCW scale.

4.3.2 Field collection

The AnnAGNPS model requires precipitation data that describes daily climate data. A rain gauge station was installed in LLCW on February 2013, and these precipitation data were correlated with data from nearby stations (Figure 13) to decide the best data source candidate to fill the gap on precipitation data used for the simulation period. The entire simulation period was sixteen years, from January 2001 to the end of 2017.

We also installed a stream gauge monitoring station at the watershed outlet to record stream flow data using a pressure transducer (Solinst, water level logger) to determine the stage-discharge relationship. This data was also correlated with one stream gauge in the USA side to complete our

observations when our equipment (pressure transducer) malfunctioned using time-lapse photographs of the water stage at our stream gauge station.

Sediment was collected in traps at the watershed outlet in the United States (Figure 13). The sediment traps were constructed in late 2004. Data on sediment removed from the traps were available from the Tijuana River National Estuarine Research Reserve (TRNERR) and were used to validate simulated sediment production at watershed scale.

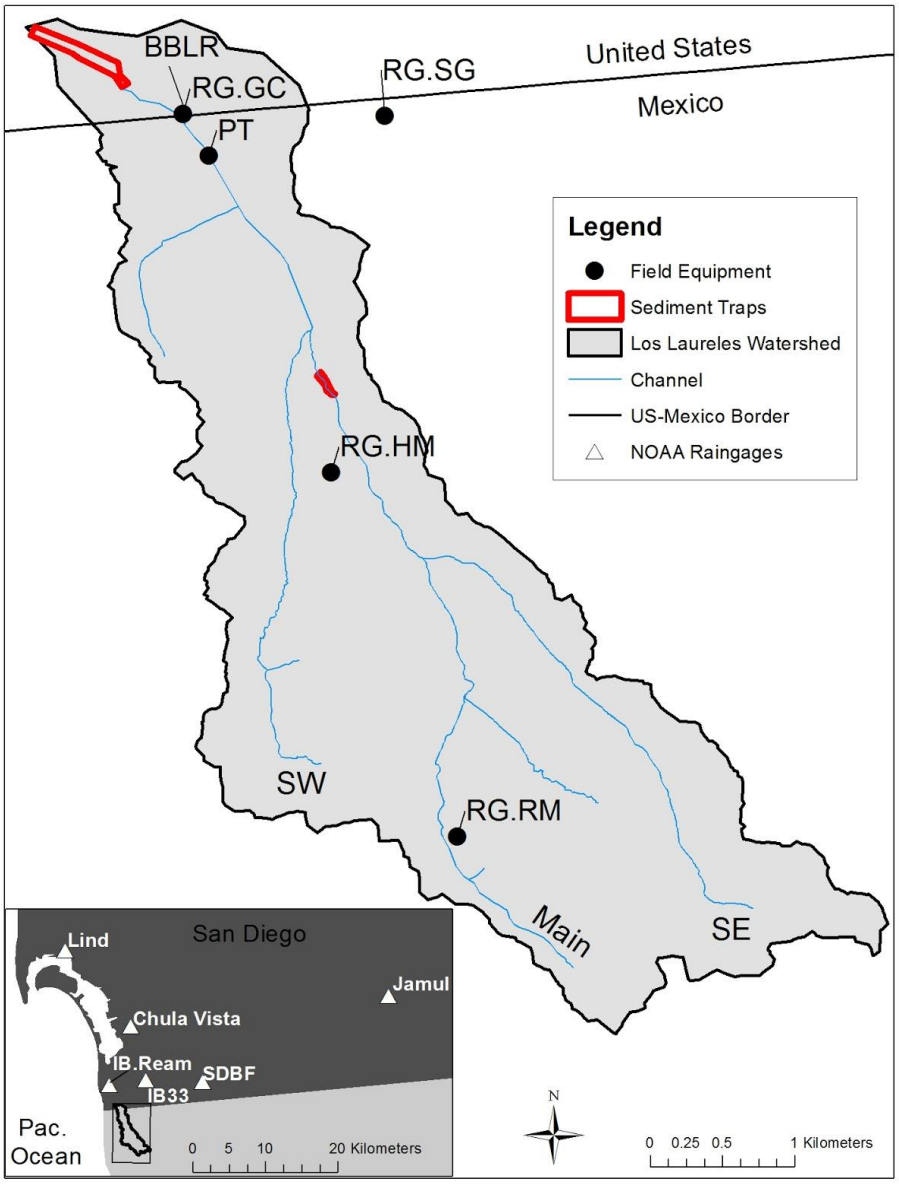

Figure 13. Location of the Los Laureles Canyon Watershed, flow paths (SW, Main and SE), and monitoring station of sediment traps and rain gauges (R.G.). Modified from Biggs et al, 2018.

Field campaigns were conducted on 09/02/2015 and 09/03/2015 to collect surface and subsurface soil samples in representative sites on the two distinct geology types (sandy-conglomerate and conglomerate) within the watershed to compare the soil texture with the observed soil texture in the sediment traps at the watershed outlet (Figure 14). A bulk sample of sediment smaller than coarse gravel (<32mm) was collected for texture analysis using dry sieving to separate 2 mm fraction and pipette method for fines (<2mm).

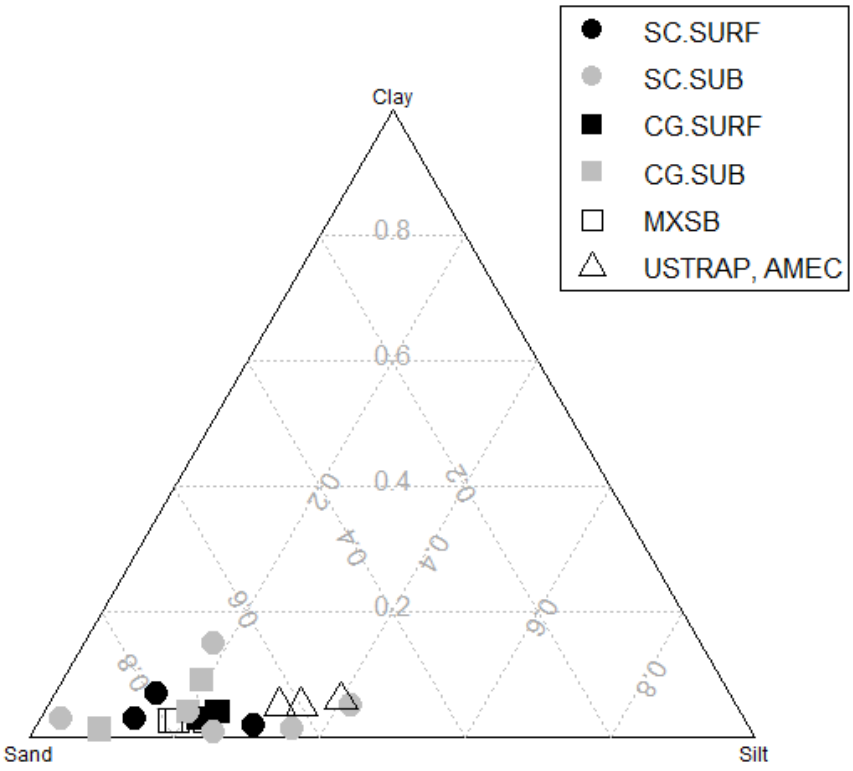

Figure 14. Ternary diagram of grain sizes observed in samples collected within the watershed for sandy-conglomerate surface (SC.SURF) and sub-surface (SC.SUB), conglomerate surface (CG.SURF) and sub-surface (CG.SUB),sediment trap in Mexico (MXSB) and at the watershed outlet (USTRAP, AMEC).

The geology in LLCW was taken from IMPLAN survey 2001 and modified based on field data collection during September 2015 and visual interpretation using Google Earth imagery. First, a seamless cross-border geological map was created (Figure 15). US soils that occurred on geologic types found in LLCW were identified as candidate soils for the study watershed. Overlays of the soils map in Google EarthTM imagery were also used to correlate geomorphological features with soil units across the border. Road cuts were identified and the cobble percentage was determined through point counts along a 1 m

transect through each distinct horizon. See Biggs et al. (2018) for a full description of field and laboratory data collection.

Once candidate soils were determined from the US geology and soils maps, the SSURGO soil characteristics were extracted from SSURGO for all horizons for comparison with data collected in the field. Soil texture for all soil samples collected in LLCW and near the US-Mexico border was plotted in ternary diagrams and compared to SSURGO surface and subsurface soil texture. For each soil group, the SSURGO soil type that most closely matched the mean texture from the soil samples were selected and used to update the soils map for LLCW.

Finally, polygons delineating soil types were created in Google Earth by first determining the relationship between soil color, landform, and soil type for soils in the US, and then extrapolating those relationships to map similar soils in the LLCW (Figure 15).

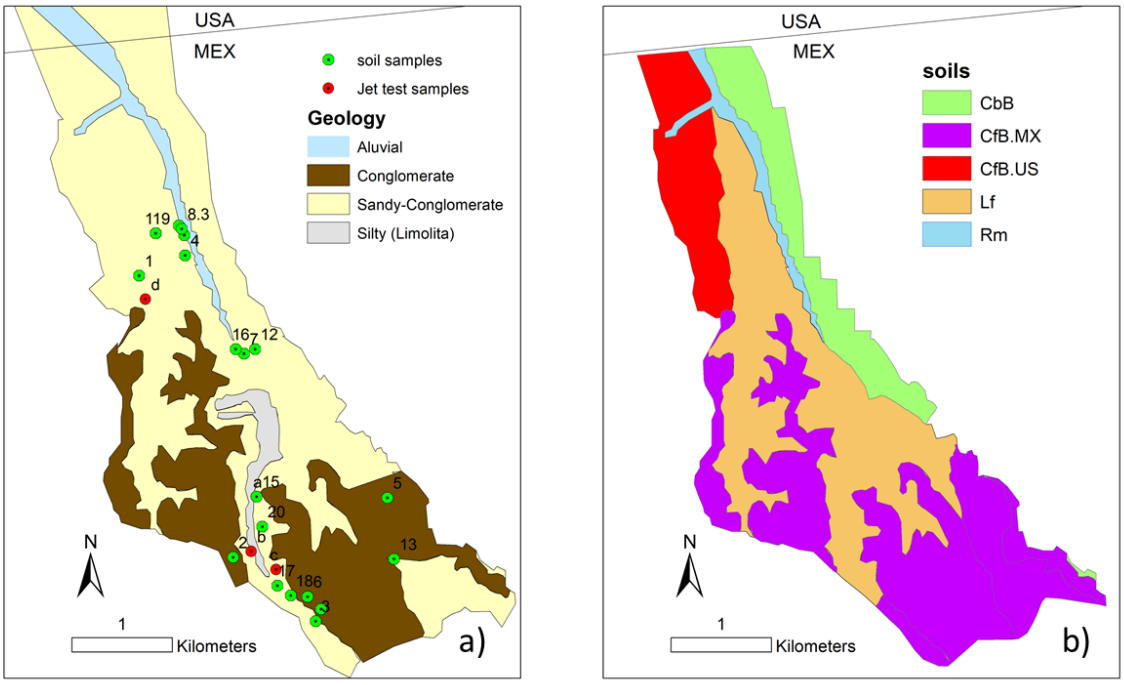

Figure 15. Geology map (left) and updated soils map for LLCW (right). Las Flores (Lf), fine sandy loam, dominates the central portion of the watershed (orange). CfB.MX represents the Chesterton sandy loam (CfB), but with a cobbly surface soil. Carlsbad (CbB) and Chesterton (CfB.US) soils extend from the US/Mexico border.

Additionally, nine soil samples were collected in the study area to estimate the critical shear stress (τc) and soil erodibility using a mini-jet erosion test following Hanson (1990). The submerged jet-test measures depth-of-scour over time-lapse records. τc is determined by the method described in Hanson and Cook (1999). Gordon et al. (2007) suggested that τc measurements would be more appropriate for gully erosion modeling than any calculated values due to the large range variation of τc in the landscape. In our model, we use the measurements of τc on sandy soils to set a default value and use uncertainty analysis to determine if the final parameter range includes the measured values, as described in Gudino-Elizondo et al (2018). Initial values of Tc for conglomerate soil were taken from USGS (2018) dataset, and were modified during calibration.

4.3.3 AnnAGNPS model

The AnnAGNPS model is an advanced simulation model developed by the USDA-Agricultural Research Service and NRCS to evaluate watershed response to management practices (Bingner et al., 2015). The spatial variability of soils, land use, and topography within a watershed can be determined by discretizing the watershed into many user-defined, homogeneous, drainage-area-determined cells. AnnAGNPS simulates runoff and sediment leaving the land surface and while tracking their transport through the channel system to the watershed outlet on a daily time step. Additionally, AnnAGNPS is capable different erosional processes (i.e., sheet, rill, and gullies) as well as streambed and bank sources. This model provides an integrated approach for simulating ephemeral gully erosion as the headcut is induced and evolves upstream with varying widths, depths and migration rates as a result of climatic regimes, watershed characteristics, and management practices. A topographic analysis technique has been developed based on digital elevation models (DEM) that is combined with Geographic Information Systems (GIS) technology to map potential ephemeral gullies throughout a watershed system (Momm et al. 2012). This approach can provide an automated estimate of the location of the most downstream locations potential ephemeral gullies (knickpoints), when combined with AnnAGNPS, can be used to determine the extent of actual ephemeral gully erosion within a watershed resulting from a combination of precipitation, watershed characteristics and management practices.

The hydrology component of AnnAGNPS applies the SCS Curve Number technique (SCS — Soil Conservation Service, 1985) to generate daily runoff in the cells from precipitation. The total daily runoff is determined for each channel and for the outlet, using the TR-55 (SCS — Soil Conservation Service, 1986)

by adding the travel times. The time of concentration (calculated from AGFLOW and TOPAGNPS), the calculated runoff volume and the storm type of TR-55 are required for the calculation of the value of the peak discharge and the corresponding time (Bingner et al., 2015). Simulated total and peak discharge were compared with data measured at the gage (outlet) for 14 storm events.

A LIDAR-derived Digital Elevation Model (DEM) (3 m, horizontal resolution) of the watershed was acquired from NOAA, 2018. The DEM was used to obtain the necessary input data for running the TOPAG-NPS program. The DEM was used (i) to identify and measure topographic features, (ii) to define surface drainage channels, (iii) to subdivide watersheds into cells along drainage divides and (iv) to calculate representative cell parameters, including cell area, slope and length. The size of the cells depends on the values of the Critical Source Area (CSA) and Minimum Source Channel Length (MSCL). The CSA is defined as the minimum upstream drainage area above which a source channel is initiated and maintained; while the MSCL is the minimum acceptable length of the cell swale for the source channel to exist.

CSA and MSCL are required by TOPAGNPS algorithms to represent the landscape in cells and streams. These two parameters control the topology and properties of the network and sub-catchments generated by TOPAZ. In this study, a critical source area of 1 ha and a minimum source channel length of 50m were selected, based on field observations, to effectively characterize the hillslope and reach units of the study area. As a result of processing the DEM, the study watershed was discretized into 1147 sub-catchments (AnnAGNPS cells) and 462 reaches. The cell size ranges from 9E-6 to 0.1 km^2 (Figure 16).

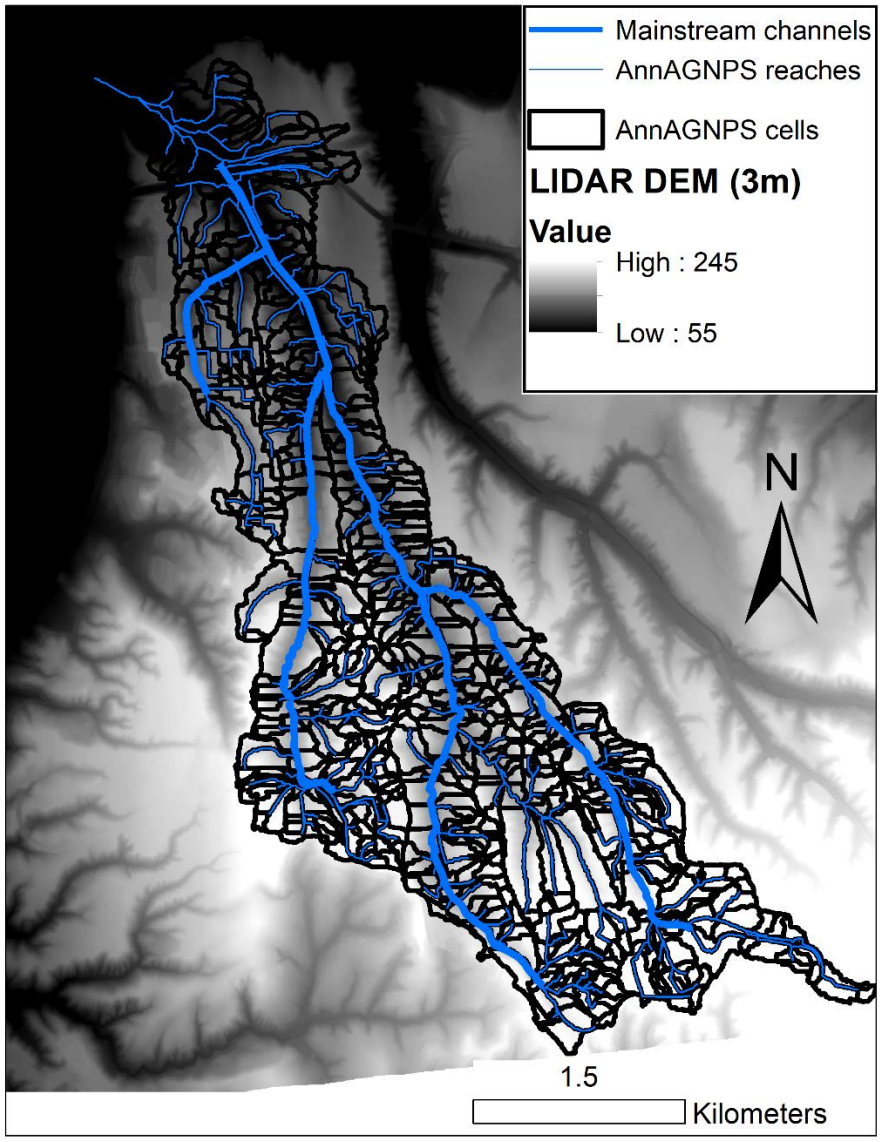

Figure 16. AnnAGNPS cells, reaches, and mainstream channels in the Los Laureles Canyon watershed (LLCW).

The effect of resolution of the digital elevation model (DEM) on terrain attributes within an AnnAGNPS model simulation has little impact on runoff, as runoff does not vary much with a decrease in DEM resolution. Soil erosion and sediment loads can change prominently with DEM resolution, as resolution impacts on slope (Wang and Lin, 2011). Hancock et al. (2006) found that area–slope and area–elevation (hypsometry) properties are well depicted by the DEMs at 90-m resolution. So a LIDAR-derived 3-m DEM should improve the model performance in the study watershed compared with applications that use more-commonly available 10 or 30m resolution DEMs.

The 24 h rainfall distribution used was type II (TR-55), which is representative of most of the USA territory and represents intense rainfall observed during convective events in semi-arid regions of the south-west (USA), and is consistent with the storm type calculated for the modeled storm event using raingage data collected in the study area (Biggs et al., 2018). Fourteen storm events observed during 2013–2017 (Table X) were used for the application of the AnnAGNPS model, excluding those few that had missing data because of a temporary malfunction of the sensor, caused by the extreme flow (Table X, Storm 7 late December 2016). The complete time series of the daily rainfall has been used for the simulations from 2001 to 2017.

4.3.4 Model setup

AnnAGNPS can include input parameters from NRCS database for any location in the U.S., such as climate, soil and management properties. For our field site in Mexico, fieldwork and laboratory analyses were necessary to acquire the needed information to apply AnnAGNPS in an ungauged watershed. Geologic maps may be relatively common, but the utility of such maps and their relationship to soil types must be determined with site-specific data. Soils candidates from SSURGO database were tested to choose the most suitable soil data validated with actual field and laboratory measurements (Biggs et al., 2018).

A land use map was created by visual interpretation using the Google Earth (11/11/2012, 2017 DigitalGlobe) imagery into seven land use categories (agriculture, rangeland, paved urban, dispersed unpaved urban (5-15% urbanized), urban unpaved (15-30% urbanized), unpaved graded land, and sediment trap). The accuracy of the land use data has been validated by comparing images with ground-based photography and field surveys. All of these data were used to populate the required hydrologic settings for AnnAGNPS simulations.

4.3.5 Sediment budget

Data on sediment removed from the sediment traps at the watershed outlet (Figure 13) were available from the Tijuana River National Estuarine Research Reserve (TRNERR). Both upper and lower traps were cleaned out in spring and fall 2005, winter 2006, and each fall from 2007-2012. Starting in

2013, the lower trap was not excavated (Biggs et al., 2017). Topographic surveys were conducted in Fall 2011 (both upper and lower traps) and Fall 2015 (upper trap only). The total sediment yield includes sediment retained in the trap, and sediment that was lost through the trap and entered the estuary. The trap efficiency, or the proportion of the total sediment yield that is retained in the sediment basin, for medium sand, fine sand, silt, and clay was estimated by following the guidelines for sedimentation under turbulent, non-ideal conditions (Morris and Fan, 1998). The trap efficiency, as a function of the settling velocity ratio, was calculated based on Urbonas and Stahre (1993), See Biggs et al., (2018) for a full description of methods.

These data were used to compare our simulated results on sheet, rill and gully erosion for the same time periods. Channel evolution is an important source of sediment that the AnnAGNPS technology may not be addressing adequately in this watershed, so we should consider that limitation in order to address the sediment budget at the LLCW scale. We compared the simulated sediment production as the total amount of sediment by source (sheet and rill, and gully erosion) that makes into the mainstream channel network (Figure 16), plus the estimated channel erosion contribution, with the total amount of sediment excavated from the sediment traps at specific dates in the watershed outlet. One estimate of channel erosion was taken from the estimates of Taniguchi et al (2018), who calculated channel erosion from the difference between the cross sections observed in 2014 with the cross section under reference conditions. Taniguchi et al. (2018) estimated that channel erosion accounted for 25-40% of total sediment yield to the estuary over 2002-2017. Here, we add 15% and 30% to the total sediment load to the channel in order to calculate total sediment yield including channel erosion.

4.3.6 Model calibration

The model was calibrated as follows: First, the CN were assigned based on literature values. No adjustments were needed for the CN as the fit was adequate between the observed Rainfall-runoff relationship with several SCS CN rainfall-runoff relationships (Figure 18) which correspond to urban environments (Dunne and Leopold, 1987). Second, the values of Tc and sediment delivery ratio were varied to match the observed sediment in the traps at the outlet. Tc was set to 1.6 N·m−2 for sandy soils based on the average value obtained from laboratory measurements on nine samples collected on the "Las Flores" soil type within the watershed. Initial values of Tc for conglomerate soils were taken from USGS (2018) dataset for fine cobbles (64 N·m−2) and were modified during calibration for Tc=32 N·m−2

which correspond to very coarse gravel, that we considered that fits better with the observed diameters of rocky materials present on conglomerate soil types.

4.4 Results

4.4.1 Rainfall data

For the events that have rainfall data in the LLCW watershed at Hormiguitas (RG.HM), the gauge at San Diego Brownfields (SDBF) has the highest correlation coefficient and smallest RMSE of the stations with good data availability. Rainfall at RG.HM was higher than that at all other stations for larger events (>60mm), but matched the SDBF data well for rainfall 10-50 mm (Figure 17). The SDBF gage has a higher correlation coefficient and lower error compared with stations closer to the LLCW in the Tijuana Estuary (IB3.3), so SDBF can be considered to be the best available option for estimating rainfall for 2001-2014 (Figure 17).

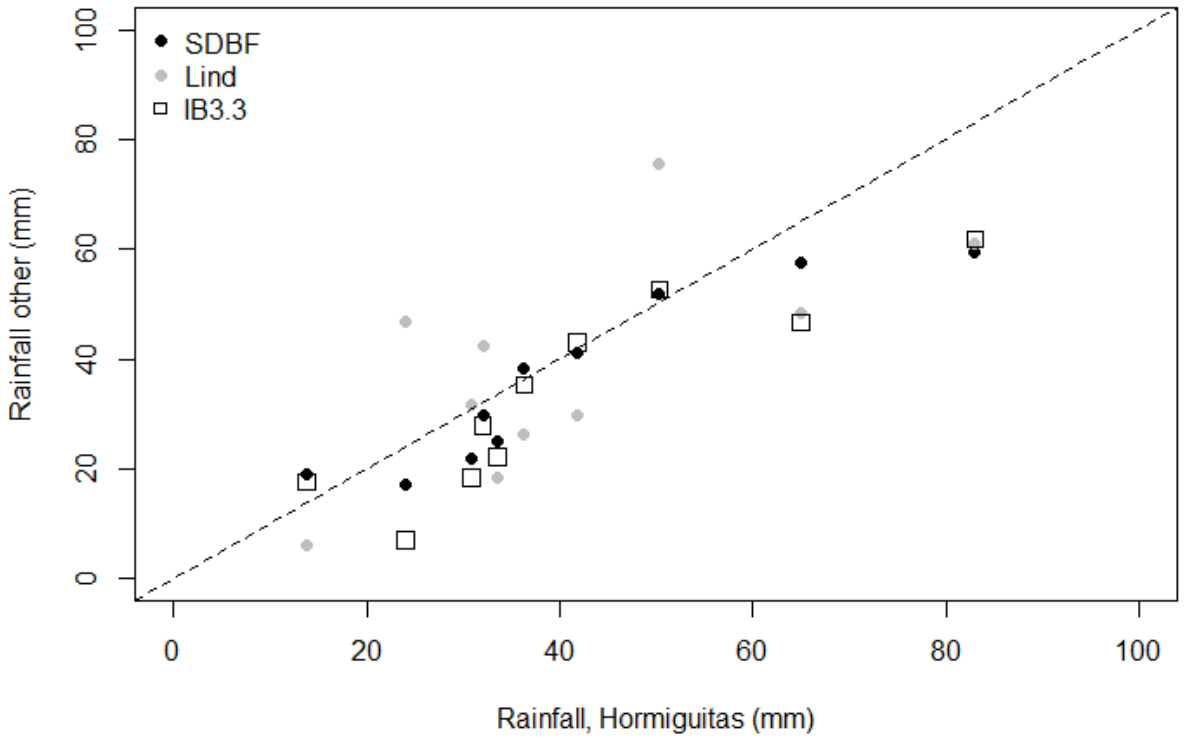

Figure 17. Event-total precipitation for the 10 storm events for the Hormiguitas gage (RG.HM) and three other nearby stations. The dashed line is the 1:1 line. Taken from Biggs et al, 2017.

4.4.2 Rainfall-runoff relationships

Event rainfall for the 14 events ranged from 7 to 83 mm (Table 5). Event total runoff increased with event-total rainfall. The runoff coefficients (Q:P) ranged from 0.02 to 0.67. The 24 h rainfall distribution that showed the best simulated results was type II (TR-55). The comparison of observed-simulated values at the storm event scale is presented in Table 5 and Figure 18. The RMSE for total runoff was 59 m3 (85% of mean), and 13 m3/s (177% of the mean) for peak discharge. RMSE was dominated by a single large storm; RMSE without that storm was 25.6 m3 (61% of the mean) for total runoff and 6.9 m3/s (105% of the mean) for peak discharge.

Table 5. Summary of storm events used for model calibration/validation

Event	Rainfall	Peak discharge (cms)		Total Runoff (m^3)	
		observed	simulated	observed	simulated
Storm 1					
2014-02-28	12.25	1.13	0.43	0.27	0.74
2014-03-01	7.50	1.54	0.08	0.33	0.20
2014-03-02	7.50	6.14	0.58	1.08	0.90
Storm 2					
2015-03-01	23.25	3.36	2.69	1.36	3.91
2015-03-02	9.25	1.43	0.31	0.48	0.56
Storm 3					
2015-05-15	22.50	19.46	2.46	5.93	3.62
Storm 4					
2015-09-15	30.75	5.27	5.69	6.40	7.27
Storm 5					
2016-01-05	22.25	17.72	3.58	3.76	4.79
Storm 6					
2016-03-06	6.50	1.03	0.00	0.93	0.01
2016-03-07	23.00	5.07	2.55	4.23	3.74
Storm 7					
Storm 8					
2017-01-19	13.00	5.37	2.85	2.57	3.51
2017-01-20	28.00	6.86	15.91	18.66	17.24
Storm 9					
2017-02-17	33.25	11.16	13.88	7.03	15.31
Storm 10					
2017-02-27	81.00	16.69	58.23	42.07	63.12
RMSE			**13**		**59**

For storm 7, no PT data was available and IBWC rating curve discharge was zero.

The correlation coefficient for total discharge was 0.96, which showed a high linear association between the observed and simulated discharge, as the test of significance indicated to be highly significant at $p < 0.01$. Comparing the mean values of measured and predicted total discharge, the model over predicted total discharge only by 28%. The AnnAGNPS model works better for medium sizes events (2-20mm, Figure 18) which represent the more important events in the long term basin. The model under estimated higher observed peak discharge values where rainfall intensity is higher compared with other observed events in the study area (Biggs et al., 2018).

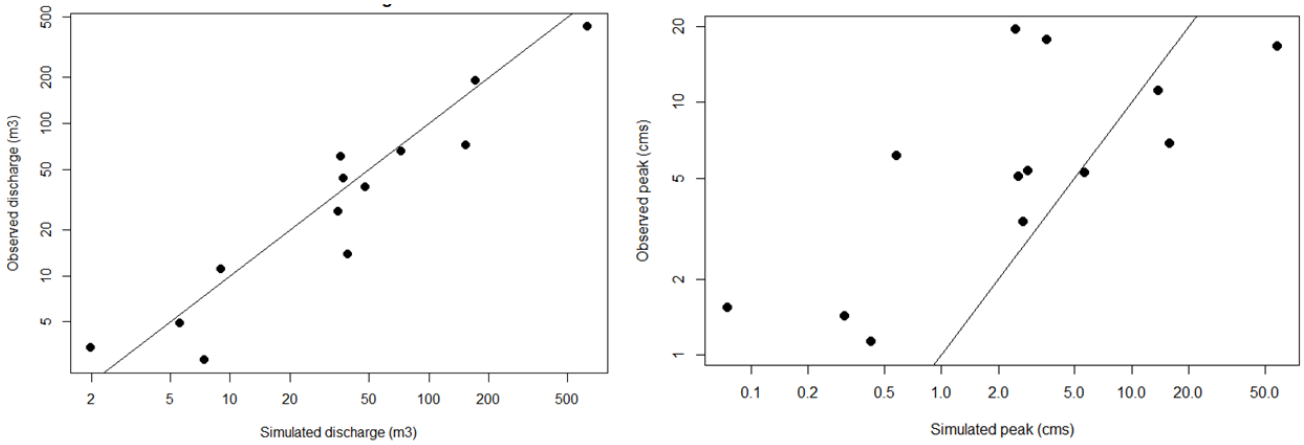

Figure 18. Relationship between observed and simulated total discharge for 13 events. Lines in each plot are the 1:1 lines.

The CN was highest for the smallest events and generally decreased with event size. This is consistent with runoff production from surfaces with low infiltration capacity during small events, and from all surfaces, including those with high infiltration capacities, during large events. The largest event (rainfall 81 mm) had a runoff coefficient of 0.51, and most points fell between SCS Curve Numbers (CN) 80 and 90, which is consistent with the urban land cover in the watershed (Figure 19).

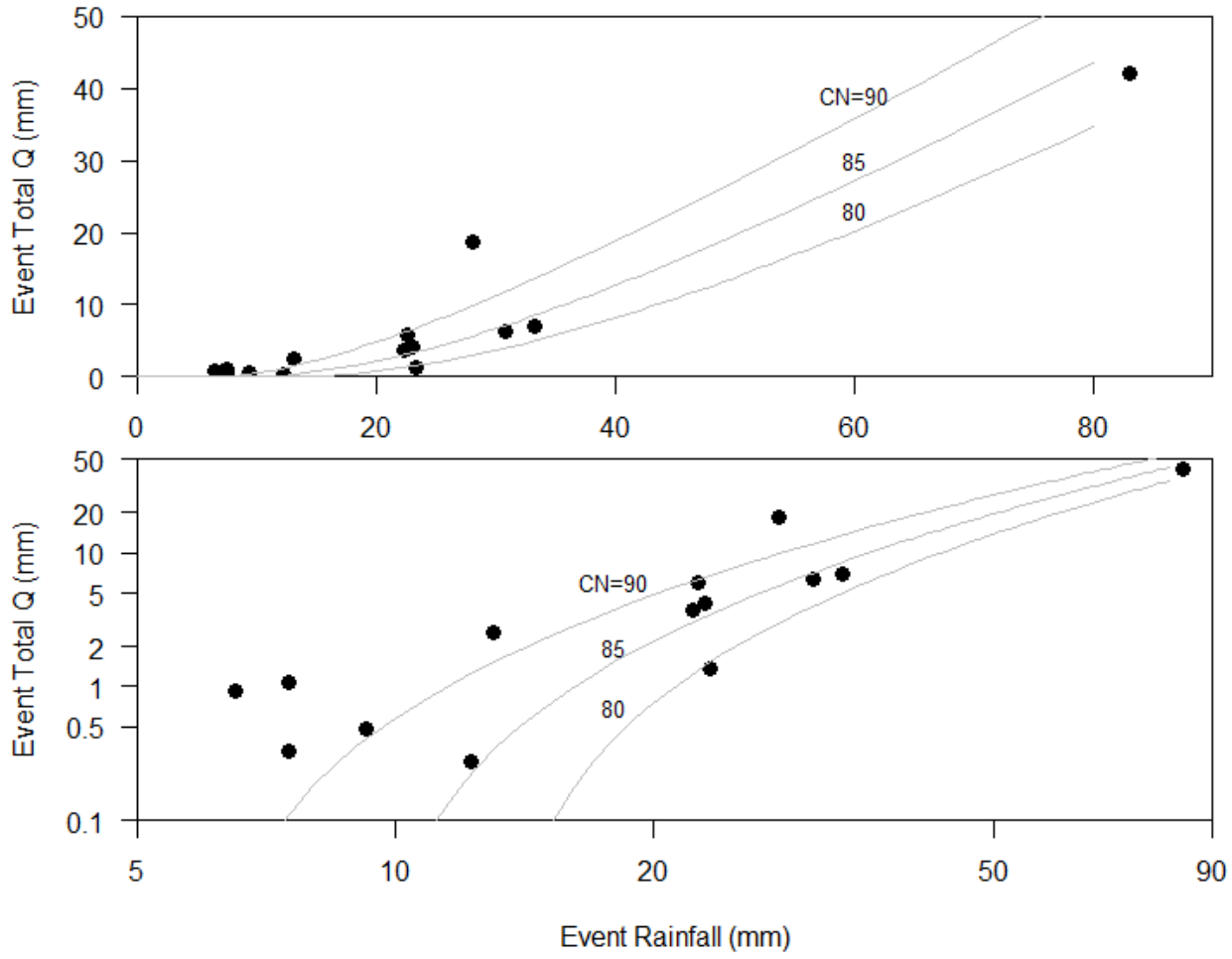

Figure 19. Rainfall-runoff relationship for all observed storm events, with several SCS CN rainfall-runoff relationships, in non-log (top) and log-log (bottom). Taken from Biggs et al, 2017.

4.4.3 Sediment budget

Total sediment accumulation in the traps correlates with precipitation at both Lindbergh Field (Lind) and San Diego Brownfields stations (Figure 20). The relationship is linear, which is unexpected given the usually non-linear relationship between rainfall and sediment load (Inman and Jenkins, 1999). The annual trap efficiency varied from 0.79 to 0.98, and was 0.89 for the cumulative mass removed over 2006-2012.

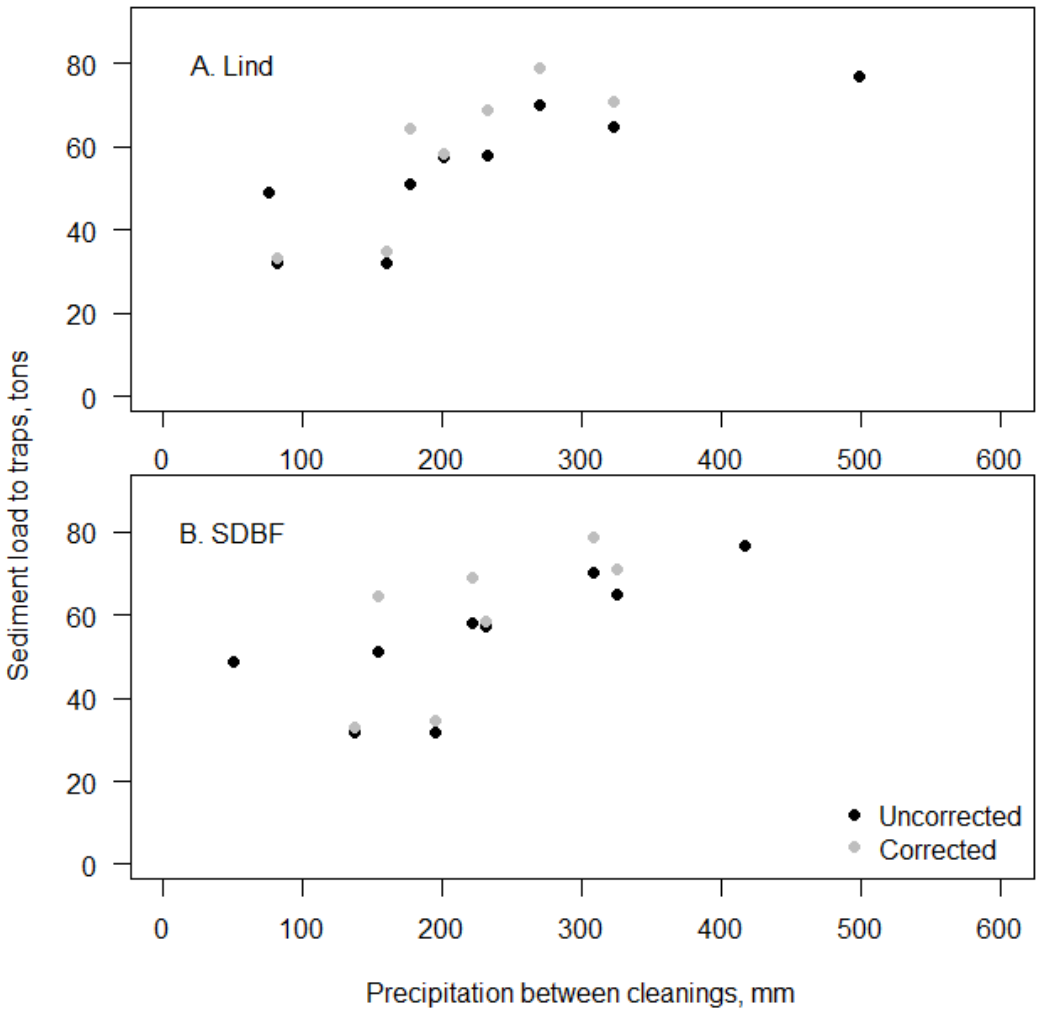

Figure 20. Total sediment removed from the Goat Canyon traps versus total annual precipitation between removal events, 2005-2012. The uncorrected or raw amount of sediment removed is in black and corrected sediment removed based on trap efficiency is in grey. Annual precipitation is from A. Lindbergh and B. San Diego Brownfield stations. Taken from Biggs et al, 2017.

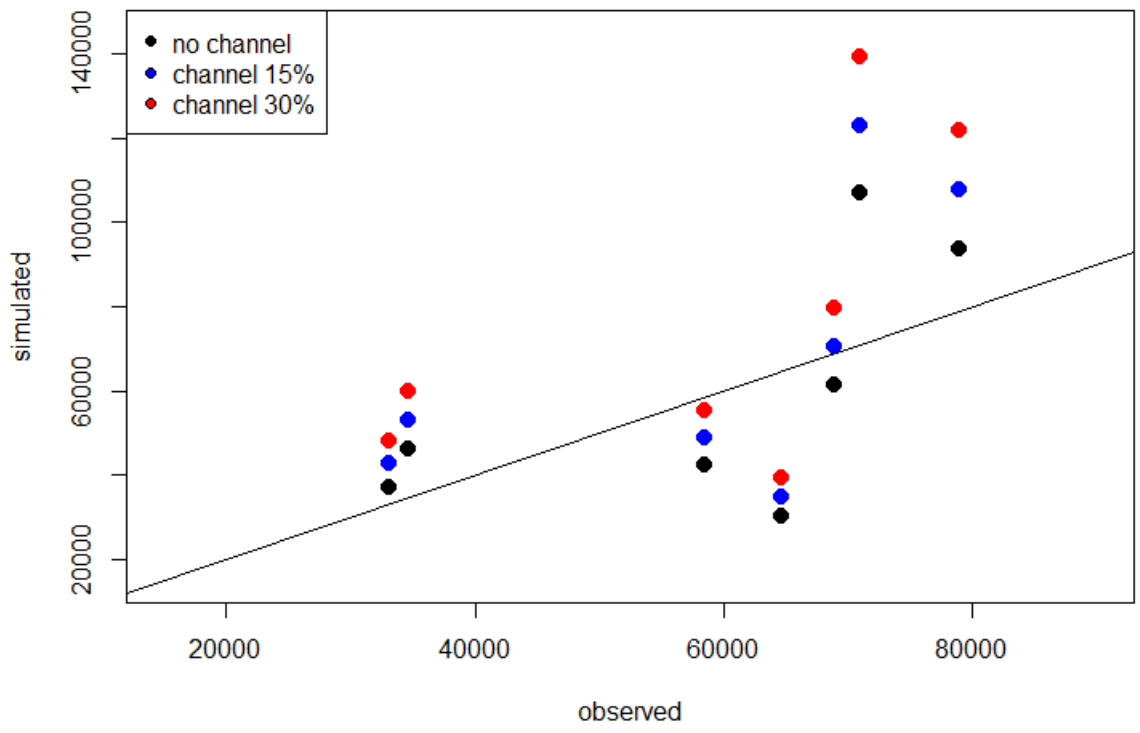

Figure 21. Observed and simulated sediment yield at the watershed outlet.

Total sediment yield from AGNPS correlated with sediment observed at the outlet, with a percent bias of 1.2, RMSE of 20,406 tons (35% of the mean, Figure 21). Actual trap efficiency may have impacts on the underestimation of sediment load at the traps; fine sediment is probably flowing as wash load to the ocean limiting the accuracy of the AnnAGNPS model to simulate sediment yield.

The default values of τ_c for conglomerate soil types (τ_c =64 $N \cdot m^{-2}$) resulted, on average, in approximately 200% overestimation of total sediment load at the outlet, so it was changed during calibration for τ_c =32 $N \cdot m^{-2}$ to match better with the observed sediment yield in the sediment traps. The τ_c value set in the calibrated model corresponds to very coarse gravel (USGS, 2018) which is consistent with the observed diameters on rocky materials in the study area (Biggs et al., 2018).

Precipitation correlates with sediment production from sheet and rill, gully and total sediment production, Though sediment production by sheet and rill erosion correlates better with rainfall than gully

sediment production. A rainfall threshold (~25-35mm) for gully formation was observed by Gudino-Elizondo et al. (2018) in the upper watershed, which seems to be consistent with the significant contribution by gullies to the total sediment production for those storm events with higher precipitation than such a threshold. Figure 22 shows the contribution of each process (sheet and rill, gullying) to the total sediment production as a function of rainfall.

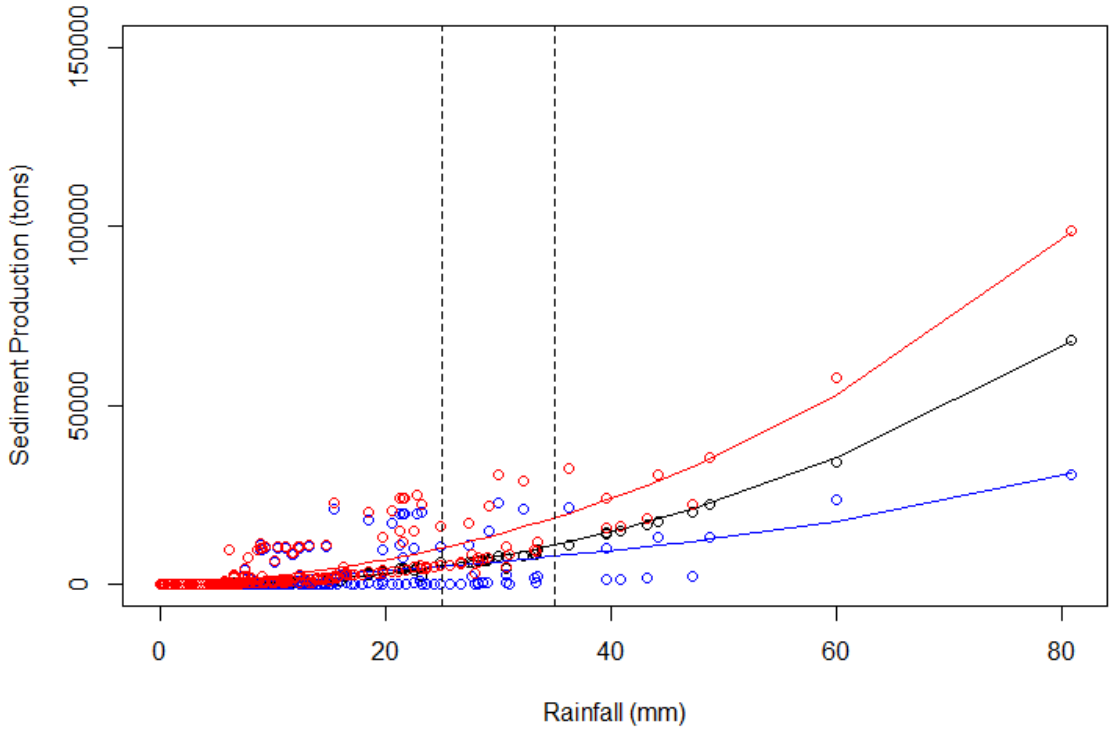

Figure 22. Simulated sediment production by erosion processes in LLCW. The vertical dashed lines shown the range of rainfall threshold for gully erosion observed in the field during (2013-2018).

Simulated sheet and rill erosion rates were generally the dominant erosional processes within the watershed, which has important contribution to the total sediment production at the watershed scale (Figure 23), which was also reflected in the event wise regressions (Figure 22), especially for larger events. Total sediment production at the sub-watershed scale (AnnAGNPS cells) was dominated by cells characterized by sandy soil types on steep slopes, encouraging gully erosion formation (Figure 23). The simulated results showed that 50% of the total sediment production at watershed scale is generated by only 7% of the total watershed area (Appendix B). These cells are hot spots of sediment production and have to be prioritized for management activities to reduce sediment production.

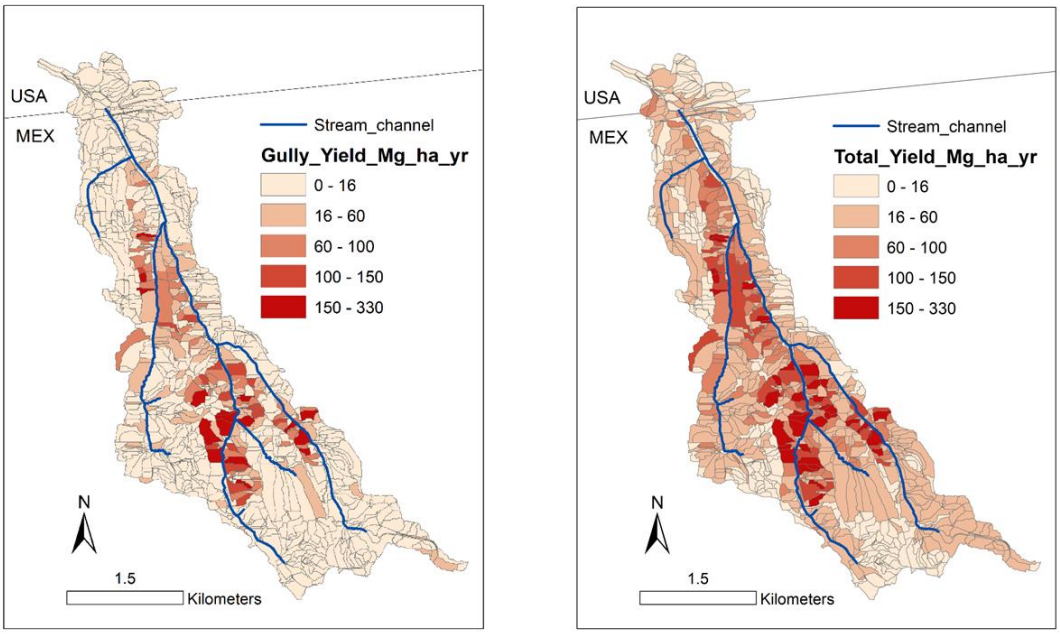

Figure 23. a) Sediment yield by gully erosion, and b) Total sediment yield by subwatershed within the Los Laureles Canyon watershed.

The simulated sediment load does not account for the timing and interactions between land clearance and impervious soil fraction changes due to non-uniform urbanization rates within the watershed during the simulation period, and instead represents the long-term rate of that we use to compare with rates of total sediment yield observed at the watershed outlet.

Table 6. Simulated sediment yield (by source) and total observed at the watershed outlet by periods between sediment trap cleanings.

Year	Sheet and Rill	Gullies	Total	Observed	Ratio of modelled to observed			Rainfall (mm)
					No channel	+Ch 15%	+ Ch 30%	
2006	8,483	34,742	43,226	34,642	**1.25**	**1.43**	**1.62**	193
2007	15,257	21,632	36,889	33,079	**1.12**	**1.28**	**1.45**	136
2008	10,204	20,080	30,284	64,580	**0.47**	**0.54**	**0.61**	154
2009	38,058	23,147	61,205	68,949	**0.89**	**1.02**	**1.15**	218
2011	48,347	45,340	93,687	78,935	**1.19**	**1.36**	**1.54**	298
2012	51,752	53,399	105,151	70,965	**1.48**	**1.70**	**1.93**	323
2011	16,992	27229	44,221	58,513	**0.76**	**0.87**	**0.98**	234
Mean	42 %	58 %						

* Ratio simulated to observed (NC=No channel erosion contribution; 15, 30=15 and 30% of channel erosion contribution.

On average, gully erosion contributes more to the total sediment production than sheet and rill erosion processes in the annual budget. Although, storm-wise simulated sediment yield shows that sheet and rill processes contribute generate more sediment for larger storm events, indicating that gully erosion is more important than sheet and rill for small storm events in terms of sediment production (Figure 22).

4.5 Discussion

Simulated total discharge and sediment yield estimations compared favorably with the observed data at the watershed outlet. AnnAGNPS model has the capability to identify areas with high sediment production within the watershed for prioritizing areas to mitigate soil erosion. Model outputs shows that 50% of the sediment production is generated only from 7% of the watershed area (Appendix B). This application can be critical in developing countries where economical resources are usually limited to implement BMPs, especially in marginal areas like LLCW. Total sediment production at subwatershed scale (AnnAGNPS cells) was dominated by cells characterized by sandy soils on steep slopes, which encourage gully erosion vulnerability.

Calculated runoff coefficients using stream gauge measurements help to constrain curve number values, one of the most sensitive parameters in runoff and soil erosion (Yuan et al., 2001; Licardello et al., 2007; Taguas et al., 2012; Gudino-Elizondo et al., 2018). Uncertainties in soil-resistance-to-erosion parameters, especially critical shear stress for cobbly soils, may impact sediment production by gully erosion, suggesting that more field and laboratory data are necessary to have more accurate sediment yield estimations at LLCW scale.

A systematic overprediction of sediment yield was observed. This could be due either to model errors, or to problems with the validation dataset. Fine sediment is flowing as wash load over the sediment traps into the ocean, reducing the trap efficiency, and limiting the comparison of the observed data with the simulated sediment yield from AnnAGNPS, particularly for wet years when the trap is full at the end of the season. Moreover, channel evolution is not well characterized by the AnnAGNPS model, reducing the capability of the model to simulate the observed behavior of the system. Taniguchi et al. (2018) noted that urbanization and channel structures had caused extreme channel enlargement in the LLCW, suggesting the necessity to implement, or even better, couple a more sophisticated channel evolution

model to AnnAGNPS such as the channel evolution computer model (CONCEPTS) to better simulate the sediment production at the LLCW scale.

Gully erosion represented 57% of total sediment production. This is relatively similar compared with other estimates for human-disturbed watersheds. Bingner et al. (2006) reported that ephemeral gullies are the primary source of sediment (73% of the total) in agricultural settings within the Maumee River basin in Ohio, USA. De Santiesteban et al. (2006) found that ephemeral gullies contributed for 66% to total soil loss in a small agricultural watershed. Taguas et al. (2012) found that contribution of gully erosion to the total soil loss varies substantially depending on the management, on average, from 46% to 19% under spontaneous grass cover and under conventional tillage management. Our results suggest urgency in implementing management practices such as pavement or other stabilization of dirt roads to mitigate soil erosion as well as modeling the effect of management activities (i.e. revegetation of hillslopes) in soil erosion and sediment loads. Future studies evaluating the uncertainty of the model estimated parameters as well as implications in scenario analysis are crucial for proper management of sediment in the study watershed and potentially in other urban areas in developing countries.

4.6 Conclusion

Rural and urban development has important impacts on soil erosion rates. Severe soil and gully erosion in the Los Laureles Canyon watershed is adversely impacting the Tijuana River Estuary. Management practices, especially road maintenance that fills gullies with unconsolidated sediment, create an additional source of sediment. Simulated total discharge correlated with the observed (r^2=0.96) and simulated peak discharge was better predicted for medium sizes events which are more frequent in the study area and hence contribute more to the total sediment production on a medium to long-term basis. Simulated sediment yield using the AnnAGNPS model was similar to the observed sediment excavated rates in the sediment traps at the watershed outlet, with ratios ranging from 0.47 to 1.51 between observed and simulated results. Simulated gully erosion contributes significantly to the total sediment production at watershed scale (57%, annual average). We identified hot spots of sediment production within the watershed that contributes on 50% of the total sediment production that only represent 7% of the total catchment area. Our results suggest urgency in implementing management practices such as pavement or other stabilization of dirt roads to mitigate soil erosion as well as modeling the effect of best

management practices (i.e. revegetation of hillslopes) in soil erosion and sediment loads. Future studies evaluating the uncertainty of the model estimated parameters as well as implications in scenario analysis are crucial for proper management of sediment in the study watershed and potentially in other urban areas in developing countries. Our maps of the spatial distribution of sediment yield are uncertain due to the coarse resolution of land use and soil properties for such small sub-watersheds (AnnAGNPS cells), so future research should include more detailed spatial information to improved model estimated parameters and have more accurate sediment production estimates and BMP's evaluations within the watershed.

Chapter 5. Conclusions

5.1 Conclusions

The present analysis was motivated by a growing conceptual gap in the use of soil erosion modeling to address sediment production in urban watersheds, and this research showed that urbanization has important impacts on soil erosion rates. In the study area, gullies formed almost exclusively on unpaved roads, highlighting them as a major sediment source. Management practices, especially road maintenance that fill gullies with unconsolidated sediment, create an additional and continually replenished source of highly erodible sediment. Lower threshold values of S and Ad for gully incision were found in the study area compared with agricultural environments, which is consistent with the high soil erodibility and low critical shear stress measured in the laboratory. Gully erosion rates in Tijuana were higher than almost all of those observed in agricultural watersheds described in the literature. Gully formation and sediment yield were successfully simulated using de AnnAGNPS model. Simulated Specific Soil Loss (SSL) was similar to the observed SSL from gully erosion, with RMSE in SSL ranging from 0.96 to 1.2 mm for the twenty-one behavioural models, compared to 2.1 mm for the default parameter (Smax, TD, Manning's n, saturated hydraulic conductivity, and head-cut erodibility) set. Smax (curve number), TD and τc were the most sensitive parameters in gully erosion modelling. The 21 behavioural models were consistent in their estimates of total sediment reduction when paving all roads (decrease of 90–94%). Conversely, total runoff of the behavioural models increased by approximately 1.5 to 2.3 times under the paved condition compared to under the current conditions. Simulated gully erosion contributes significantly to the total sediment production at watershed scale (57%, annual average). We identified hot spots of sediment production within the watershed that contributes on 50% of the total sediment production that only represent 7% of the total catchment area. Our results suggest urgency in implementing management practices such as pavement or other stabilization measures of unpaved roads to mitigate soil erosion, but that paving may increase peak discharge significantly (by 1.8–5.7 times) at the neighbourhood scale. Our sensitivity analysis also identified the most uncertain parameters requiring further investigation to quantify the impacts of management on runoff and sediment production, especially parameters relating to infiltration capacity and runoff production.

5.2 Future work

Future studies that evaluate effects of different soil types on actual and modeled gully erosion rates on unpaved roads, as well as model effects of management practices such as road paving with different infiltration rates to explore their impact on runoff, soil erosion, and sediment loads are crucial for proper sediment management and planning in urban watersheds. Chapter 2 also highlight the necessity to evaluate the performance of the AnnAGNPS to simulate gully erosion on different soil types, as well as modelling the effect of other management actions (i.e., revegetation of hillslopes) on soil erosion and sediment loads.

Future studies evaluating the uncertainty of the model estimated parameters at watershed scale as well as implications in scenario analysis are crucial for proper management of sediment in the study area, and potentially in other urban areas in developing countries. Our maps of the spatial distribution of sediment yield are uncertain due to the coarse resolution of land use and soil properties for such small sub-watersheds (AnnAGNPS cells), so future research should include more detailed spatial information to improved model estimated parameters and have more accurate sediment production estimates and BMP's evaluations within the watershed.

References

Adediji, A., Jeje, L.K., Ibitoye, M.O. 2013. Urban development and informal drainage patterns: Gully dynamics in Southwestern Nigeria. Applied Geography, 40, 90-102. doi:10.1016/j.apgeog.2013.01.012

Al-Madhhachi, A.S.T., Hanson, G.J., Fox, G.A., Tyagi, A.K., Bulut, R. 2013. Measuring soil erodibility using a laboratory “mini” jet. Transactions of the ASABE 56(3), 901–910. doi:10.13031/trans.56.9742

Alonso, C.V., Bennett, S.J., Stein, O.R. 2002. Predicting headcut erosion and migration in concentrated flows typical of upland areas. Water Resour. Res., 38, 39–15, doi:10.1029/2001WR001173.

Archibold, O.W., Levesque L.M.J., de Boer D.H., Aitken A.E., Delanoy L., Gully retreat in a semi-urban catchment in Saskatoon, Saskatchewan. Applied Geography, 23: 261-279. doi:10.1016/j.apgeog.2003.08.005

Baginska, B., Milne-Home, W.A. 2003. Parameter sensitivity in calibration and validation of an annualized agricultural non-point source model. Water Sci. Appl., 6, 331–345, doi:10.1029/WS006p0331.

Beven, K.J., Freer, J. 2001. Equifinality, data assimilation, and uncertainty estimation in mechanistic modelling of complex environmental systems using the GLUE methodology. J. Hydrol., 249, 11–29, doi:10.1016/S0022-169400421-8.

Beven, K.J. 1993. Prophecy, reality and uncertainty in distributed hydrological modelling. Adv. Water Resour., 16, 41–51, doi:10.1016/0309-170890028-E.

Beven, K.J., Binley, A. 1992. The future of distributed models: Model calibration and uncertainty prediction. Hydrol. Process., 6, 279–298, doi:10.1016/j.jhydrol.2005.07.007.

Biggs, T.W., Atkinson, E., Powell, R. Ojeda, L., 2010. Land cover following rapid urbanization on the US-Mexico border: Implications for conceptual models of urban watershed processes. Landscape and Urban Planning, 96, 78-87. doi:10.1016/j.landurbplan.2010.02.005.

Biggs, T.W., Taniguchi, K.T., Gudino-Elizondo, N., Yongping Y., Bingner R.L., Langendoen, E.J., Liden, D. 2018. Field Measurements to Support Sediment and Hydrological Modelling in Los Laureles Canyon; U.S. Environmental Protection Agency: Washington, DC, USA, EPA/600 /X-18/0XX.

Biggs, T.W., Taniguchi, K.T., Gudino-Elizondo, N., Yongping Y., Bingner, R.L., Langendoen, E.J., Liden, D. Geology, soil properties and erosion on marine terraces along the US-Mexico Border. (Manuscript in preparation).

Bingner, R.L., Czajkowski, K., Palmer, M., Coss, J., Davis, S., Stafford, J., Widman, N., Theurer, F., Koltum, G., Richards, P. 2006. Upper Auglaize Watershed AGNPS Modelling Project: Final Report; Research Report No. 51; USDA-ARS National Sedimentation Laboratory: Oxford, MS, USA.

Bingner, R.L., Theurer, F.D. 2002. Physics of suspended sediment transport in AnnAGNPS. In: Proceedings of the 2nd Federal Interagency Hydrologic Modeling Conference, Las Vegas, NV, USA, 28 July–1 August.

Bingner, R.L., Theurer, F.D., Yuan, Y.P. AnnAGNPS technical processes. Washington, D.C. US Department of Agriculture (USDA)—Agricultural Research Service (ARS). 2015. Accessed on 5 July 2017, fromhttps://www.wcc.nrcs.usda.gov/ftpref/wntsc/HandH/AGNPS/downloads/AnnAGNPS_Technical_Documentation.pdf

Bingner, R.L., Wells, R.R., Momm, H.G., Rigby, J.R., Theurer, F.D. 2016. Ephemeral gully channel width and erosion simulation technology. Nat. Hazards, 80, 1949–1966, doi10.1007/s11069-015-2053-7.

Bisantino T., Bingner R., Chouaib W., Gentile F., Trisorio Liuzzi G. 2013. Estimation Of Runoff, Peak Discharge And Sediment Load At The Event Scale In A Medium-Size Mediterranean Watershed Using The Annagnps Model. Land Degrad. Dev. doi:10.1002/ldr.2213.

Bull, L.J., Kirkby, M.J. 1997. Gully processes and modelling. Progress Physical Geography, 21, 354–374.

CalEPA, California Environmental Protection Agency. 2018. Accessed on 4 February 2018, fromhttps://www.waterboards.ca.gov/sandiego/water_issues/programs/tmdls/TijuanaRiverValley.shtml

Capra, A., Ferro, V., Porto, P., Scicolone, B., 2012. Quantifying interrill and ephemeral gully erosion in a small Sicilian basin. Z. Geomorphology, 56, 9–25. doi:10.1127/0372-8854/2012/S-00070.

Casali, J., Gimenez, R., Bennett, S. 2009. Gully erosion processes: Monitoring and modelling. Earth Surface Processes and Landforms, 34, 1839–1840, doi:10.1002/esp.1867

Castillo, C., Pérez, R., James, M.R., Quinton, N.J., Taguas, E.V., Gómez, A., 2012. Comparing the accuracy of several field methods for measuring gully erosion. Soil Science Society of America Journal 76, 1319–1332.

Castillo, C., James, M.R., Redel-Macías,M.D., Pérez, R., Gómez, J.A., 2015. SF3M software: 3-D photo-reconstruction for non-expert users and its application to a gully network. Soil 1, 583–594. doi:10.5194/soil-1-583-2015.

Castillo, C., Gómez, A., 2016. A century of gully erosion research: Urgency, complexity and study approaches. Earth-Science Reviews, 160, 300–319.

Chahor, Y., Casalí, J., Giménez, R., Bingner, R.L., Campo, M.A., Goñi, M. 2014. Evaluation of the AnnAGNPS model for predicting runoff and sediment yield in a small Mediterranean agricultural watershed in Navarre (Spain). Agricultural Water Management, 134, 24–37, doi:10.1016/j.agwat.2013.11.014.

Das, S., Rudra, R.P., Gharabaghi, B., Gebremeskel, V., Goel, P.K., Dickinson, W.T. 2008. Applicability of AnnAGNPS for Ontario conditions. Canadian Biosystems Engineering, 50, 1.1–1.11.

De Santisteban, L.M., Casali, J., Lopez, J.J., 2006. Assessing soil erosion rates in cultivated areas of Navarre (Spain). Earth Surface Processes and Landform 31, 487–506. doi:10.1002/esp.1281.

Di Stefano, C., Ferro, V., Palmeri, V., Pampalone, V. 2017. Measuring rill erosion using structure from motion: A plot experiment. Catena, 153, 383-392. doi:10.1016/j.catena.2017.04.023

Dietrich, JT. 2015. Riverscape mapping with helicopter-based Structure-from-Motion photogrammetry. Geomorphology, 252, 144–157. doi:10.1016/j.geomorph.2015.05.008

Dunne, T., Leopold, L.B. 1987. Water in Environmental Planning, W.H. Freeman and Company: New York, NY, USA, p. 818, ISBN 0-71670079-4.

Engman, E.T. 1986. Roughness coefficients for routing surface runoff. Journal of irrigation and drainage engineering, 112, 39–53, doi:10.1061/(ASCE)0733-9437112:1.

Flanagan, D.C., and Nearing M. A. 1995. Water Erosion Prediction Project Hillslope Profile and Watershed Model Documentation. SERL Report No.10. West Lafayette, IN: National Soil Erosion Research Laboratory.

Fonstad, M., Dietrich, J.T., Courville, B.C., Jensen, J.L., Carbonneau, P.E. 2013. Topographic structure from motion: a new development in photogrammetric measurement. Earth Surface Processes and Landform 38, 421–430.

Foster, G.R., 1986. "Understanding Ephemeral Gully Erosion," Soil Conservation, Assessing the National Resource Inventory, National Academy of Science Press, 2, 90-125.

Fu, B., Gulinck, H. 1994. Land evaluation in an area of severe erosion: the Loess Plateau of China. Land Degradation & Rehabilitation, 5, 33–40.

Garbrecht, J., Martz, L.W. 1999. TOPAGNPS, An Automated Digital Landscape Analysis Tool for Topographic Evaluation, Drainage Identification Watershed Segmentation and Subcatchment Parameterization for AGNPS. Watershed Modelling Technology; Agricultural Research Service: Beltsville, MD, USA. Accessed on 1 June 2017, from https://www.ars.usda.gov/ARSUserFiles/60600505/AGNPS/Dataprep/TOPAGNPS_userman.pdf

Gómez, J.A., Giráldez, J.V., Vanwalleghem, T., 2008a. Comments on "Is soil erosion in olive groves as bad as often claimed?" By L. Fleskend and L. Stroosnijder. Geoderma 147, 93–95.

Gómez-Gutiérrez, A., Schnabel, S., Lavado-Contador, F. 2009. Gully erosion, land use and topographical thresholds during the last 60 years in a small rangeland catchment in SW spain. Land Degradation and. Development 20 (5), 535–550. doi:10.1002/ldr.931

Gómez-Gutiérrez, A., Schnabel, S., Berenguer-Sempere, F., Lavado-Contador, F., Rubio-Delgado, J. 2014. Using 3D photo-reconstruction methods to estimate gully headcut erosion. Catena 120, 91–101.

Gordon, L.M., Bennett, S.J., Bingner, R.L., Theurer, F.D., Alonso, C.V. 2007. Simulating ephemeral gully erosion in AnnAGNPS. Trans. ASAE, 50, 857–866, doi:10.13031/2013.23150.

Govers, G., Everaert, W., Poesen, J., Rauws, G., De Ploey, J. and Lautridou, J.P., 1990. A long flume study of the dynamic factors affecting the resistance of a loamy soil to concentrated flow erosion. Earth Surf. Process. Landforms, 15, 313-328. doi:10.1002/esp.3290150403

Grover, R. 2011. Local Perspectives on Environmental Degradation and Community Infrastructure in Los Laureles Canyon, Tijuana. Master's Thesis, San Diego State University, San Diego, CA, USA.

Gudino-Elizondo, N., Biggs, T., Castillo, C., Bingner, R., Langendoen, E., Taniguchi, K., Kretzschmar, T., Yuan, Y., Liden, D. 2018. Measuring ephemeral gully erosion rates and topographical thresholds in an urban watershed using Unmanned Aerial Systems and Structure from Motion photogrammetric techniques. Land Degrad. Dev., 1-10. doi:10.1002/ldr.2976

Guerra, A.J.T., Hoffman, H. 2006. Urban gully erosion in Brazil. Geography 19(3), 26-29.

Gupta, H.V., Sorooshian, S., Yapo, P.O. 1999. Status of automatic calibration for hydrologic models: Comparison with multi-level expert calibration. Journal of Hydrologic Engineering, 4, 135–143.

Hancock, G.R., Martinez, C., Evans, K.G., Moliere, D.R. 2006. A comparison of SRTM and high-resolution digital elevation models and their use in catchment geomorphology and hydrology: Australian examples. Earth Surface Processes and Landforms, 31, 1394–1412

Hanson, G.J. 1990. Surface erodibility of earthen channels at high stresses part II – developing an in situ testing device. Transactions of the ASAE, 33(1), 132−137.

Hanson, G.J., Cook, K.R. 1999. Procedure to estimate soil erodibility for water management purposes. In Proceeding of the Mini-Conference Advance in Water Quality Modeling, Toronto, ON, Canada, 18–21 July 1999, ASAE 1999, Paper No. 992133, ASAE: St. Joseph, MI, USA,.

Hornberger, G.M., Spear, R.C. 1981. An approach to the preliminary analysis of environmental systems. Journal of Environmental Management, 12, 7–18.

Inman, D. L., Jenkins, S. A. 1999. Climate Change and the Episodicity of Sediment Flux of Small California Rivers. The Journal of Geology, 107, 251-270.

Imwangana, F.M., Dewitte, O., Ntombi, M., Moeyersons, J. 2014. Topographic and road control of mega-gullies in Kinshasa (DR Congo). Geomorphology, 217, 131–139. doi: 10.1016/j.geomorph.2014.04.021

James, M.R., Robson, S. 2012. Straightforward reconstruction of 3D surfaces and topography with a camera: Accuracy and geosciences applications. Journal of Geophysical Research, 117, 1–17.

James, M.R., Robson, S. 2014. Mitigating systematic error in topographic models derived from UAV and ground-based image networks. Earth Surface Processes and Landform 39: 1413–1420. doi:10.1002/esp.3609.

James, M.R., Robson, S., d'Oleire-Oltmanns, S., Niethammer, U. 2017. Optimising UAV topographic surveys processed with structure-from-motion: Ground control quality, quantity and bundle adjustment. Geomorphology, 280: 51–66. doi:10.1016/j.geomorph.2016.11.021

Javernick, L., Brasington, J., Caruso, B. 2014. Modeling the topography of shallow braided rivers using Structure-from-Motion photogrammetry. Geomorphology, 213, 166–182. doi:10.1016/j.geomorph.2014.01.006

Kakembo, V., Xanga, V.W., Rowntree, K. 2009. Topographic threshold in gully development on the hillslopes of communal areas in Ngqushwa local municipality, Eastern Cape, South Africa. Geomorphology, 110: 188–194.

Kim, S.H., Yi, S. 2007. Understanding relationship between sequence and functional evolution in yeast proteins. Genetica, 131, 151–156, doi:10.1007/s10709-006-9125-2.

Liden, T.D. 2016. US Environmental Protection Agency, San Diego, CA, USA. Personal communication.

Licciardello, F., Zimbone, S.M. 2002. Runoff and erosion modeling by AGNPS in an experimental Mediterranean watershed. In: Proc. ASAE Annual Intl. Meeting/CIGR XVth World Congress. St. Joseph, Mich.: ASAE.

Licciardello, F., Zema, D.A., Zimbone, S.M., Bingner, R.L. 2007. Runoff and soil erosion evaluation by the AnnAGNPS Model in a small Mediterranean watershed. Trans. ASAE, 50, 1585–1593, doi:10.13031/2013.23972.

McKay, M.D., Beckman, R.J., Conover, W.J. 1979. A Comparison of Three Methods for Selecting Values of Input Variables in the Analysis of Output from a Computer Code. American Statistical Association and American Society for Quality Stable, 21, 239–245, doi:10.2307/1268522.

Martínez-Casasnovas, J.A., Ramos, M.C., Ribes-Dasi, M., 2002. Soil erosion caused by extreme rainfall events: mapping and quantification in agricultural plots from very detailed digital elevation models. Geoderma, 105, 125–140. doi:10.1016/S0016-7061(01)00096-9.

Maugnard, A., Van Dyck, S., Bielders, C.L. 2014. Assessing the regional and temporal variability of the topographic threshold for ephemeral gully initiation using quantile regression in Wallonia (Belgium). Geomorphology, 206: 165–177. doi:10.1016/j.geomorph.2013.10.007

Merkel, W.H., Woodward, D.E., Clarke, C.D. Ephemeral gully erosion model (EGEM). 1988. In Modeling Agricultural, Forest, and Rangeland Hydrology, In: Proceedings of the International Symposium, Chicago, IL, USA, 12–13 December, American Society of Agricultural Engineers St. Joseph, MI, USA, 1988, pp. 315–323.

Merritt, W.S., Letcher, R.A., Jakeman, A.J. 2003. A review of erosion and sediment transport models. Environmental Modelling & Software, 18, 761–799. doi:10.1016/S1364-815200078-1.

Micheletti, N., Chandler, J. H., and Lane, S. N., 2014: Investigating the geomorphological potential of freely available and accessible structure-from-motion photogrammetry using a smartphone, Earth Surface Processes and Landform, 40, 473–486. doi:10.1002/esp.3648.

Milella, P., Bisantino, T., Gentile, F., Iacobellis, V., Trisorio, L.G. 2012. Diagnostic analysis of distributed input and parameter datasets in Mediterranean basin streamflow modeling. Journal of Hydrology, 472–473: 262–276.

Momm, H. G., Bingner, R. L., Wells, R. R., Wilcox, D., 2012. AGNPS GIS-based tool for watershed-scale identification and mapping of cropland potential ephemeral gullies. Applied engineering in agriculture, 28 (1), 1-13. doi:10.13031/2013.41282.

Momm, H.G., Bingner, R.L., Yuan, Y., Locke, M.A., Wells, R.R. 2014. Spatial Characterization of Riparian Buffer Effects on Sediment Loads from Watershed Systems. J. Environ. Qual., 43, 1736–1753.

Montgomery, D.R., Dietrich, W.E., 1988. Where do channels begin? Nature 336, 232-234.

Montgomery, D.R., Dietrich, W.E. 1992. Channel initiation and the problem of landscape scale. Science, 255, 826–830.

Montgomery, D.R., Dietrich, W.E., 1994. Landscape dissection and drainage area-slope thresholds — Chapter 11. In: Kirkby, M.J. (Ed.), Process Models and Theoretical Geomorphology. John Wiley and Sons Ltd, pp. 221–246.

Moriasi, D., Arnold, J., Van Liew, M., Bingner, R.L., Harmel, R., Veith, T. 2007. Model evaluation guidelines for systematic quantification of accuracy in watershed simulations. Trans. ASABE, 50, 885–900, doi:10.13031/2013.23153.

Morris, G.L. and Fan, J. 1998. Reservoir Sedimentation Handbook: Design and Management of Dams, Reservoirs and Watersheds for Sustainable Use. New York: McGraw-Hill Companies, Inc.

Nachtergaele, J., Poesen, J., 1999. Assessment of soil losses by ephemeral gully erosion using high-altitude (stereo) aerial photographs. Earth Surface Processes and Landform 24, 693–706. doi:10.1002/(SICI)1096-9837(199908)24:8<693::AID-ESP992>3.0.CO;2-7

Nachtergaele, J., Poesen, J., Vandekerckhove, L., Oostwould-Wijdenes, D.J., Roxo, M. 2001. Testing the ephemeral gully erosion model (EGEM) for two Mediterranean environments. Earth Surface Processes and Landform, 26, 17–30, doi:10.1002/1096-983726:1<17::AID-ESP149>3.0.CO;2-7.

Nadal-Romero, E., Revuelto, J., Errea, P., López-Moreno, J.I., 2015. The application of terrestrial laser scanner and SfM photogrammetry in measuring erosion and deposition processes in two opposite slopes in a humid badlands area (central Spanish Pyrenees). SOIL 1: 561–573. doi:10.5194/soil-1-561-2015

Natural Resources Conservation Service Soils. 2018. Accessed on 4 February 2018, from https://www.nrcs.usda.gov/wps/portal/nrcs/main/soils/survey/

Oygarden, L., 2003. Rill and gully development during an extreme winter runoff event in Norway. Catena 50, 217–242. doi:10.1016/S0341-8162(02)00138-8.

Parajuli, P.B., Nelson, N.O., Frees, L.D., Mankin, K.R. 2009. Comparison of AnnAGNPS and SWAT model simulation results in USDA-CEAP agricultural watersheds in south-central Kansas. Hydrological Processes, 23, 748–763.

Parkner, T., Page, M.J., Marutami, T., Trustrum, N.A. 2006. Development and controlling factors of gullies and gully complexes. East coast, New Zealand. Earth Surface Processes and Landforms, 31, 187–199.

Patton, PC, Schumm, SA, 1975. Gully Erosion, Northwestern Colorado: a threshold phenomenon. Geology, 3, 88–90.

Poesen, J., Govers, G. 1989. Gully erosion in the loam belt of Belgium. In Soil Erosion on Agricultural Land, Proceedings of a Workshop Sponsored by the British Geomorphological Research Group, Coventry, Chicester, UK, January 1989, Boardman, J., Foster, I.D.L., Dearing, J., Eds., Wiley: Chicester, UK, pp. 513–530.

Poesen, J., Govers, G., 1990. Gully erosion in the loam belt of Belgium. In: Boardman, J., Foster, I.D.L., Dearing, J. Eds.., Soil Erosion on Agricultural Land. Wiley, Chicester, pp. 513–530.

Poesen, J., Nachtergaele, J., Verstraeten, G., Valentin, C., 2003. Gully erosion and environmental change: importance and research needs. Catena 50, 91–133. doi:10.1016/S0341-8162(02)00143-1

Poesen, J.W.A., Torri, D., Vanwalleghem, T., 2011. Gully erosion: procedures to adopt when modelling soil erosion in landscapes affected by gullying. Chapter 19. In: Morgan, R.P.C., Nearing, M.A. (Eds.), Handboook of Erosion Modelling. Wiley-Blackwell. ISBN: 978-1-4051-9010-7, pp. 360–386.

Ramos-Scharrón CE, MacDonald LH. 2007. Runoff and suspended sediment yields from an unpaved road segment, St. John, US Virgin Islands. Hydrological Processes 21: 35–50. doi:10.1002/hyp.6175.

Reid LM, Dunne T. 1984. Sediment production from forest road surfaces. Water Resources Research 20(11): 1753–1761. doi:10.1029/WR020i011p01753.

Ries, J.B., Marzolff, I., 2003. Monitoring of gully erosion in the Central Ebro Basin by largescale aerial photography taken from a remotely controlled blimp. Catena 50, 309–328. doi:10.1016/S0341-8162(02)00133-9.

Rossi M, Torri D, Santi E. 2015. Bias in topographic thresholds for gully heads. Natural Hazards 79:S51–S69. doi:10.1007/s11069-015-1701-2.

SCS. Hydrology, National Engineering Handbook; Natural Resources Conservation Service, US Department of Agriculture: Washington, DC, USA, 1972. Chapter 4. Accessed on 15 November 2017, from: https://www.nrcs.usda.gov/wps/portal/nrcs/detailfull/national/water/?andcid=stelprdb1043063.

SCS. Technical Release 55: Urban Hydrology for Small Watersheds; Natural Resources Conservation Service, US Department of Agriculture: Washington, DC, USA,. Accessed on 15 November 2017, from: https://www.nrcs.usda.gov/Internet/FSE_DOCUMENTS/stelprdb1044171.pdf

Shamshad, A., Leow, C.S., Ramlah, A., Wan Hussin, W.M.A., Mohd Sanusi, S.A. 2008. Applications of AnnAGNPS model for soil loss estimation and nutrient loading for Malaysian conditions. Applications of AnnAGNPS model for soil loss estimation and nutrient loading for Malaysian conditions, 10, 239–252, doi:10.1016/j.jag.2007.10.006.

Slaymaker, O. 2003. The sediment budget as conceptual framework and management tool. Hydrobiologia, 494, 71–82

Suttles, J.B., Vellidis, G., Bosch, D., Lowrance, R. Sheridan, J.M., Usery E.L. 2003. Watershed-scale simulation of sediment and nutrient loads in Georgia Coastal Plain streams using the Annualized AGNPS model. Trans. ASAE, 46, 1325–1335, doi:10.13031/2013.15443.

Taguas, E.V., Peña, A., Ayuso, J.L., Yuan, Y., Pérez, R., 2009. Evaluating and modelling the hydrological and erosive behaviour of an olive orchard microcatchment under nontillage with bare soil in Spain. Earth Surface Processes and Landforms, 34 (5), 738–751.

Taguas, E.V., Yuan, Y., Bingner, R.L., Gomez, J.A. 2012. Modeling the contribution of ephemeral gully erosion under different soil managements: A case study in an olive orchard microcatchment using the AnnAGNPS model. Catena, 98, 1–16, doi:10.1016/j.catena.2012.06.002.

Taniguchi, K., Biggs, T.W. 2015. Regional impacts of urbanization on stream channel geometry: A case study in semi-arid southern California. Geomorphology, 248, 228–236, doi: 10.1016/j.geomorph.2015.07.038.

Taniguchi, K.T., Biggs, T.W., Langendoen, E.J., Castillo, C., Gudino-Elizondo, N., Yongping, Y., Liden, D. 2018. Stream channel erosion in a rapidly urbanizing region of the US–Mexico border: Documenting the importance of channel hardpoints with Structurefrom-Motion photogrammetry. Earth Surface Processes and Landforms, doi:10.1002/esp.4331.

Tebebu TY, Abiy AZ, Zegeye AD, Dahlke HE, Easton ZM, Tilahun SA, Collick AS, Kidnau S, Dadgari F, Steenhuis TS. 2010. Surface and subsurface flow effect on permanent gully formation and upland erosion near Lake Tana in the northern highlands of Ethiopia. Hydrology and Earth System Sciences 14(11): 2207–2217. doi:10.5194/hess-14-2207-2010.

Thorne, C.R., Zevenbergen, L.W., Grissinger, E.H. and Murphey, J.B., 1986. Ephemeral gullies as sources of sediment. Proc. Fourth Federal Interagency sedimentation Conf., Las Vegas, Nevada, 1, 3.152-3.161.

Torri, D., Sfalanga, M. and Chisci, G., 1987. Threshold conditions for incipient filling. In: R.B. Bryan (Editor), Rill Erosion: Processes and Significance. Catena 8, 97-105.

Torri, D., Poesen, J., 2014. A review of topographic threshold conditions for gully head development in different environments. . Earth-Science Reviews 130, 73–85. doi:10.1016/j.earscirev.2013.12.006.

Trimble, S.W. 1997. Contribution of stream channel erosion to sediment yield from an urbanizing watershed. Science, 278, 1442–1444, doi:10.1126/science.278.5342.1442

Turner, D., Lucieer, A., Watson, C., 2012. An automated technique for generating georectified mosaics from ultra-high resolution unmanned aerial vehicle (UAV) imagery, based on structure from motion (SfM) point clouds. Remote Sensing 4, 1392–1410.

Urbonas, B., and Stahre, P., 1993. Stormwater Best Management Practices and Detention. PTR Prentice Hall, Englewood Cliffs, New Jersey.

U.S. GEOLOGICAL SURVEY, Scientific Investigations Report 2008–5093, Table 7. 2018. Available online: https://pubs.usgs.gov/sir/2008/5093/table7.html (accessed on 5 January 2018).

Vandaele, K., 1993. Assessment of factors affecting ephemeral gully erosion in cultivated catchments of the Belgian Loam Belt. In: S. Wicherek (Editor), Farm Land Erosion in Temperate Plains Environment and Hills. Elsevier, Amsterdam, pp. 125-136.

Vandaele, K., Poesen, J., Govers, G., van Wesemael, B., 1996. Geomorphic threshold conditions for ephemeral gully incision. Geomorphology 16, 161–173.

Vandekerckhove L, Poesen J, Oostwoud Wijdenes D, De Figueiredo T. 1998. Topographical thresholds for ephemeral gully initiation in intensively cultivated areas of the Mediterranean. Catena 33 (3–4), 271–292.

Wang, X., Lin, Q.. 2011. Effect of DEM mesh size on AnnAGNPS simulation and slope correction. Environmental Monitoring and Assessment, 179, 267–277.

Vanwalleghem, T., Poesen, J., Nachtergaele, J., Verstraeten, G., 2005. Characteristics, controlling factors and importance of deep gullies under cropland on loess-derived soils. Geomorphology 69, 76–91. doi:10.1016/j.geomorph.2004.12.003.

Walling, D. 1983. The Sediment Delivery Problem. Journal of Hydrology 65, 209–237. doi:10.1016/0022-1694(83)90217-2

Wemple, B.C., Browning, T., Ziegler, A.D., Celi, J., Chun, K.P., Jaramillo, F., Leite, N., Ramchunder, S.J., Negishi, J.N., Palomeque, X. 2017. Ecohydrological disturbances associated with roads: Current knowledge, research needs, and management concerns with reference to the Tropics. Ecohydrology, doi:10.1002/eco.1881.

Weis, D. A., Callaway, J. C., Gersberg, R. M. 2001. Vertical accretion rates and heavy metal chronologies in wetland sediments of the Tijuana Estuary. Estuaries, 24, 840-850.

Wells, R.R., Momm, H.G., Rigby, J.R., Bennett, S.J., Bingner, R.L., Dabney, S.M. 2013. An empirical investigation of gully widening rates in upland concentrated flows. Catena, 101, 114–121, doi:10.1016/j.catena.2012.10.004.

Westoby MJ, Brasington J, Glasser NF, Hambrey MJ, Reynolds JM. 2012. 'Structure-from-Motion' photogrammetry: A low-cost, effective tool for geoscience applications. Geomorphology 179: 300–314. doi:10.1016/j.geomorph.2012.08.021

Wolman, M.G., 1967. A cycle of sedimentation and erosion in urban river channels. Geografiska Annaler A 49, 385–395.

Woodward, D.E. 1999. Method to predict cropland ephemeral gully erosion. Catena, 37, 393–399, doi:10.1016/S0341-816200028-4.

Yuan, Y., Bingner, R.L., Rebich, R.A. 2001. Evaluation of AnnAGNPS on Mississippi Delta MSEA watersheds. Trans. ASAE, 44, 1673–1682, doi:10.13031/2013.6448.

Yuan, Y., Bingner, R.L., Rebich, R.A. 2003. Evaluation of AnnAGNPS nitrogen loading in an agricultural watershed. J. Am. Water Resour. Assoc., 39, 457–466.

Yuan, Y., Bingner, R.L., Theurer, F.D., Rebich, R.A., Moore P.A. 2005. Phosphorus component in AnnAGNPS. Trans. ASAE, 48, 2145–2154, doi:10.13031/2013.20100.

Zegeye AD, Langendoen EJ, Stoof CR, Tilahun SA, Dagnew DC, Zimale FA, Guzman CD, Yitaferu B, Steenhuis TS. 2016. Morphological dynamics of gully systems in the subhumid Ethiopian Highlands: the Debre Mawi watershed. SOIL 2(3): 443–458. doi: 10.5194/soil-2-443-2016.

Zema, D.A., Bingner, R.L., Denisi, P., Govers, G., Licciardello, F., Zimbone, S.M. 2012. Evaluation of runoff, peak flow and sediment yield for events simulated by the AnnAGNPS model in a Belgian agricultural watershed. Land Degrad. Dev., 23, 205–215, doi:10.1002/ldr.1068.

Ziegler, A.D., Giambelluca, T.W. 1997. Importance of rural roads as source areas for runoff in mountainous areas of northern Thailand. J. Hydrol., 196, 204–229, doi:10.1016/S0022-169403288-X

Appendix

Appendix A (Chapter 2)

This appendix contains tables of the errors in Ground Control Points (GCPs, or calibration points); Error Control Points (ECPs, or validation points); mean absolute error of actual/modeled lengths of objects in the orthophoto; and sensitivity analysis for local slope (S) calculation using different distances upstream from gully heads (GHs).

It also contains details of other studies used to compare our findings, relative to topographic thresholds (Table 10) and gully erosion rates (Table 11 and Figure 24).

1.1 DSM georegistration error.

Table 7. Error of the Ground Control Points (GCP) reported by AGISOFT.

ID	XY error (cm)	Z error (cm)
1	0.009	-0.001
2	0.007	0.002
3	0.005	0.002
4	0.017	-0.004
5	0.009	0.005
6	0.007	-0.003
7	0.010	0.001
RMSE	**0.009**	**0.002**

Table 8. Absolute error and RMSE of the Error Control Points (ECP).

ID	XY error (cm)	Z error (cm)
1	3.67	-3.40
2	3.57	-12.42
3	0.99	-4.94
4	2.29	0.01
5	5.75	-11.80
6	3.07	4.45
RMSE	**3.53**	**7.63**

Table 9. Mean absolute error of actual/modeled lengths of objects.

Object measurement	Modeled (m)	Actual (m)	Absolute error (m)
1	1.62	1.60	0.02
2	1.59	1.60	0.01
3	2.34	2.33	0.01
4	0.67	0.66	0.01
5	1.66	1.62	0.04
6	0.68	0.66	0.02
7	1.67	1.60	0.07
8	1.65	1.65	0.00
9	1.56	1.56	0.00
10	1.68	1.66	0.02
Average			**0.02**

1.2 Literature review of existing studies related to topographic thresholds and gully erosion rates.

Table 10. Topographic thresholds taken from Vandaele et al. (1996)

Region	**Author**	**Annual rainfall (mm)**	**Soil texture**	**Land use**	**S method**	**Incison by**
Colorado	Patton and Schummm (1975)	700-800	Soil on sandstone	Sagebrush and scattered trees	Topographic map (1:50,000)	Discontinuous gullies
Portugal	Vandaele et al., 1995	500-600	Red schist soil	cultivated	Topographic map (1:25,000)	Ephemeral gullying
California	Montgomery and Dietrich (1988)	760	Soil on greywacke	Coastal Prairie	Field measurements (Brunton compass)	Small scale landsliding and overland flow
Oregon	Montgomery and Dietrich (1988)	1500	Soil on Sandstones	Logged forest		
Belgium	Vandaele et al., 1995	700-800	Loam	Cultivated	Topographic map (1:25,000)	Ephemeral gullying
Mexico	This study	240mm	Sandy	Urban	SfM-derived DEM (30cm resolution)	Ephemeral gullies

Table 11. Ephemeral gully erosion rates taken from Castillo and Gomez (2016)

Region	**Author**	**Rainfall**	**Soil texture**	**Geology**	**Land use**	**Erosion rates (mm)**
Norway	Oygarden	112mm	clay and silt	Marine sediments	Cultivated	3.7
Spain	Martinez-Casanovas et al., 2002	215mm	Highly Calcareous	Sedimentary rocks and conglomerates	Cultivated	16.6
Sicily	Capra et al., 2012	66mm	Silty clay loam	Not reported	Experimental plot	7.2
Spain	De Santisteban et al., 2006	40mm	Silty sand loam	Not reported	Cultivated	5.9
Mexico	This Study	50 mm	Sandy	Sedimentary rocks	Urban	7.4

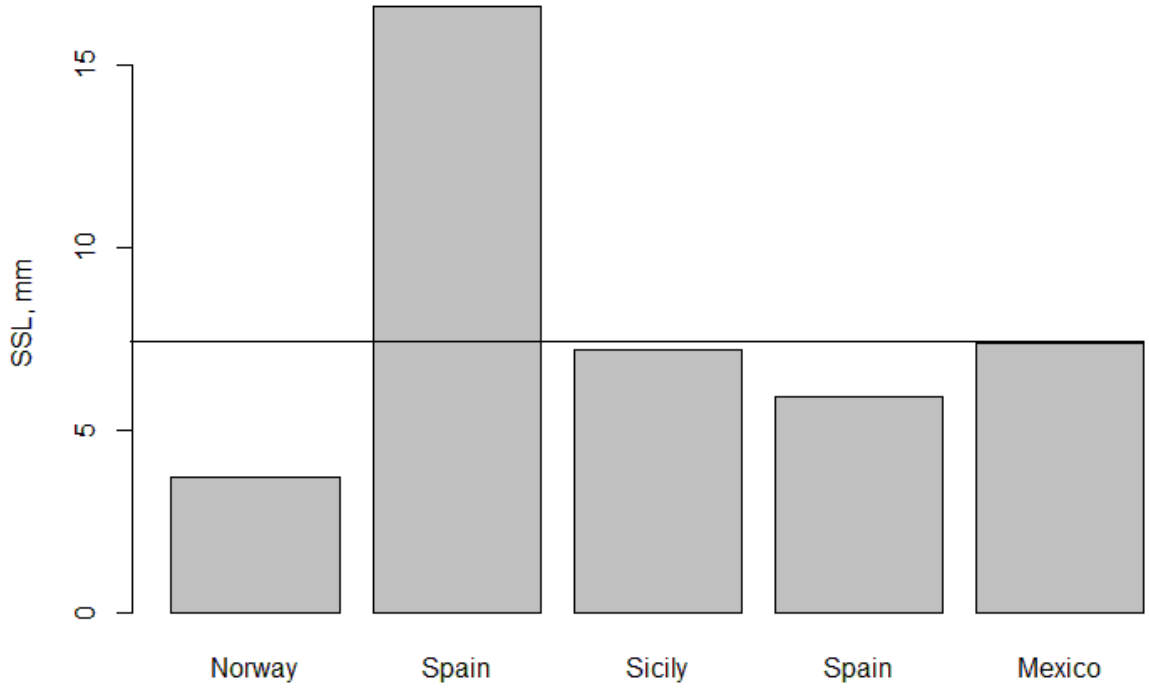

Figure 24. Ephemeral gully erosion rates reported in the literature.

1.3 Sensitivity analysis for Local slope calculation.

Local slope (S) calculation was tested using different distances upstream from the GHs (2, 3 and 5m), and added to Figure 25 for comparison. The results were stable using different upstream lengths to calculate S. Topographical thresholds were consistently lower than those reported in the literature (Figure 25).

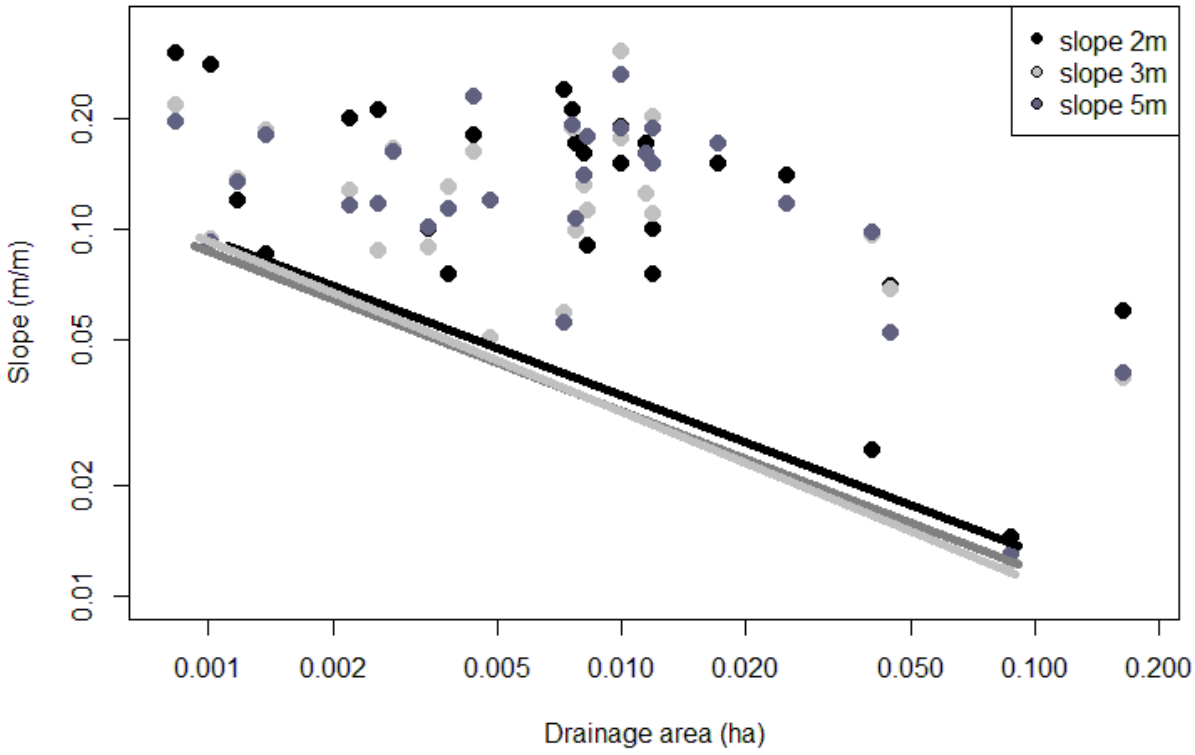

Figure 25. Topographical thresholds using different upstream lengths to calculate S.

The mean topographic threshold equation presented in the manuscript using 2 m was $S=0.02* Ad^{-0.36}$, which is similar to the equation using 3m ($S=0.0175* Ad^{-0.355}$) and 5m ($S=0.0158* Ad^{-0.387}$).

Appendix B (Chapter 4)

Table 12. Summary of storms and partitioning of rainfall into daily totals for analysis and AnnAGNPS modeling. The "*" indicates events that were not included in further analysis but were included for reallocation of rainfall. E1, E2 or E3 indicate the events retained for analysis. Observed and revised rainfall are from the Hormiguitas gage (RG.HM). Taken from Biggs et al., 2017.

	Daily rainfall (mm)	Event total rainfall (mm)	Event start	Event end	Maximum Intensity (mm)			SCS Storm Type
Storm 1					15 min	1 hr	6 hr	
2/27/2014*	1.25	1.25	2014-02-27 07:40	2014-02-28 00:00	0.75	0.75	1	-
E1: 2/28/2014	19.75	12.25	2014-02-28 00:00	2014-02-28 15:50	2.75	5.75	9.75	24T2
E2: 3/1/2014	10.50	7.50	2014-02-28 15:50	2014-03-01 00:00	6.0	7.25	7.75	6T2
E3: 3/2/2014	0.50	7.50	2014-03-01 00:00	2014-03-01 15:57	3.25	6.0	7.25	-
3/3/2014*	0	3.5	2014-03-01 15:57	2014-03-02 12:13	1.5	1.5	3	-
Total	32	32						
Storm 2								
2015-02-28*	1.25	1.25	2015-02-28 11:26	2015-03-01 00:00	1.25	1.25	1.25	-
E1: 2015-03-01	29.50	23.25	2015-03-01 00:00	2015-03-01 22:19	1.75	5.75	16.0	24T1
E2: 2015-03-02	5.25	9.25	2015-03-01 22:19	2015-03-02 11:29	2.75	6.25	7.75	24T1
2015-03-03*	0.25	2.50	2015-03-02 11:30	2015-03-03 02:00	2.5	2.5	4.0	-
Total	36.25	36.25						
Storm 3								
2015-05-14*	1.50	1.50	2015-05-14 14:31	2015-05-15 00:00	0.5	0.5	1.75	-
E1: 2015-05-15	22.50	22.50	2015-05-15 00:00	2015-05-15 13:14	4.25	10.25	19	12T2
Total	24.00	24.00						
Storm 4								
E1: 2015-09-15	29.50	30.75	2015-09-15 10:47	2015-09-16 05:52	3.5	11.25	21	24T1
2015-09-16*	1.25	0	2015-09-16 05:52	--				-
Total	30.75	30.75						
Storm 5								
2016-01-04*	14.25	15	2016-01-04 02:27	2016-01-05 09:18	3	3.5	7	-
E1: 2016-01-05	23.00	22.25	2016-01-05 09:18	2016-01-05 18:33	4.75	8.5	20	12T2

2016-01-06*	5.5	5.5	2016-01-05 18:33	2016-01-06 20:08	2.5	2.5	4.25	-
2016-01-07*	6.5	6.5	2016-01-06 20:08	2016-01-07 23:56	0.5	2	3.5	-
2016-01-08*	1	1	2016-01-07 23:56	2016-01-08 04:28	1	1	1	-
Total	50.25	50.25						
Storm 6								
2016-03-05*	1	0	-	-				
E1: 2016-03-06	5.5	6.5	2016-03-05 20:44	2016-03-06 08:55	0.25	0.5	1.25	16T2
E2: 2016-03-07	23	23	2016-03-06 9:00	2016-03-08 10:07	4.75	8.5	16.25	12T2
2016-03-09*	0.25	0.25	2016-03-09 5:12	2016-03-11 15:55	0.25	0.25	0.25	
2016-03-11*	3.75	3.75	2016-03-11 15:55	2016-03-11 17:36	1	2.25	3.75	
Total	33.5	33.5						
Storm 7								
2016-04-07*	8.75	8.75	2016-04-07 6:37	2016-04-07 14:46	1.5	2.5	8	
2016-04-08*	1.25	1.25	2016-04-07 14:50	2016-04-08 7:18	0.25	0.75	1	
2016-04-09/10*	3.75	3.75	2016-04-09 19:44	2016-04-10 4:47	0.75	1.25	3.25	
Total	13.75	13.75						
Storm 8								
2017-01/17-18*	1.25	0	--	--				
E1: 2017-01-19	11.75	13	2017-01-17 3:49	2017-01-19 12:00	2.75	6	11.75	-
E2: 2017-01-20	28	28	2017-01-20 2:30	2017-01-21 23:00	4	6	14.25	-
2017-01-22*	11	11	2017-01-22 17:50	2017-01-22 23:26	1	3.5	11	
2017-01-23*	13	13	2017-01-23 3:05	2017-01-24 06:00	5.75	7	11	
Total	65.0	65.0						
Storm 9								
E1: 2017-02-17	31	33.25	2017-02-17 17:50	2017-02-18 20:00	4.25	9.5	30.5	-
2017-02-18*	8	5.75	2017-02-18 20:00	2017-02-18 23:15	1.75	3	3	
2017-02-19*	2.25	2.25	2017-02-19 2:59	2017-02-19 12:20	0.75	1	1.75	
2017-02-22*	0.5	0.5	2017-02-22 1:18	2017-02-22 7:58	0.25	0.25	0.25	
Total	41.75	41.75						

Storm 10								
2017-02-26*	2	0	--	--				
E1: 2017-02-27	74.5	83	2017-02-26 8:44	2017-02-28 13:28	1.75	6.25	33.25	-
2017-02-28*	6.5	0	--	--				
Total	83	83						

Table 13. Summary of storm events defined in Table 2.1. Source refers to which gage was used as the final observed data. Taken from Biggs et al., 2017.

Event Date*	Rainfall (mm)	Peak Discharge (cms)		Total Runoff (mm)		Runoff Ratio (Q/P)		Event	Source
		PT	IBWC	PT	IBWC	PT	IBWC		
Storm 1									
2014-02-28	12.25	1.13	0.05	0.27	0.02	0.02	0.00	E1	PT
2014-03-01	7.50	0.50	1.54	0.13	0.33	0.02	0.04	E2	IBWC
2014-03-02	7.50	0.77	6.14	0.26	1.08	0.03	0.14	E3	IBWC
Storm 2									
2015-03-01	23.25	3.36	-	1.36	-	0.06	-	E1	PT
2015-03-02	9.25	1.43	-	0.48	-	0.05	-	E2	PT
Storm 3									
2015-05-15	22.50	19.46	-	5.93	-	0.26	-	E1	PT
Storm 4									
2015-09-15	30.75	5.27	-	6.40	-	0.21	-	E1	PT
Storm 5									
2016-01-05	22.25	17.72	9.31	3.76	13.76	0.17	0.62	E1	PT
Storm 6									
2016-03-06	6.50	1.03	0.00	0.93	0.00	0.14	0.00	E1	PT
2016-03-07	23.00	1.78	5.07	1.81	4.23	0.08	0.18	E2	IBWC
Storm 8									
2017-01-19	13.00	-	5.37	-	2.57	-	0.20	E1	IBWC
2017-01-20	29.25	-	6.86	-	18.66	-	0.64	E2	IBWC
Storm 9									
2017-02-17	33.25	0.92	11.16	1.02	7.03	0.03	0.21	E1	IBWC
Storm 10									
2017-02-27	83.00	16.69	14.45	42.07	43.44	0.51	0.52	E1	CAMERA

No PT data for storm 7, IBWC rating curve discharge was zero.

Storm 2: 2015-03-01 to 2015-03-03.

This storm had three distinct storm hydrographs (Figure 2.7, Biggs et al., 2017). We separated them into two storms for the AnnAGNPS model, one for 2015-03-01 and one for 2015-03-02 (Table 2.1, Biggs et al., 2017). The third event was small and was excluded from the model calibration and validation. The rainfall was closest to a 24-hour, Type I storm (Figure 2.8, Biggs et al., 2017).

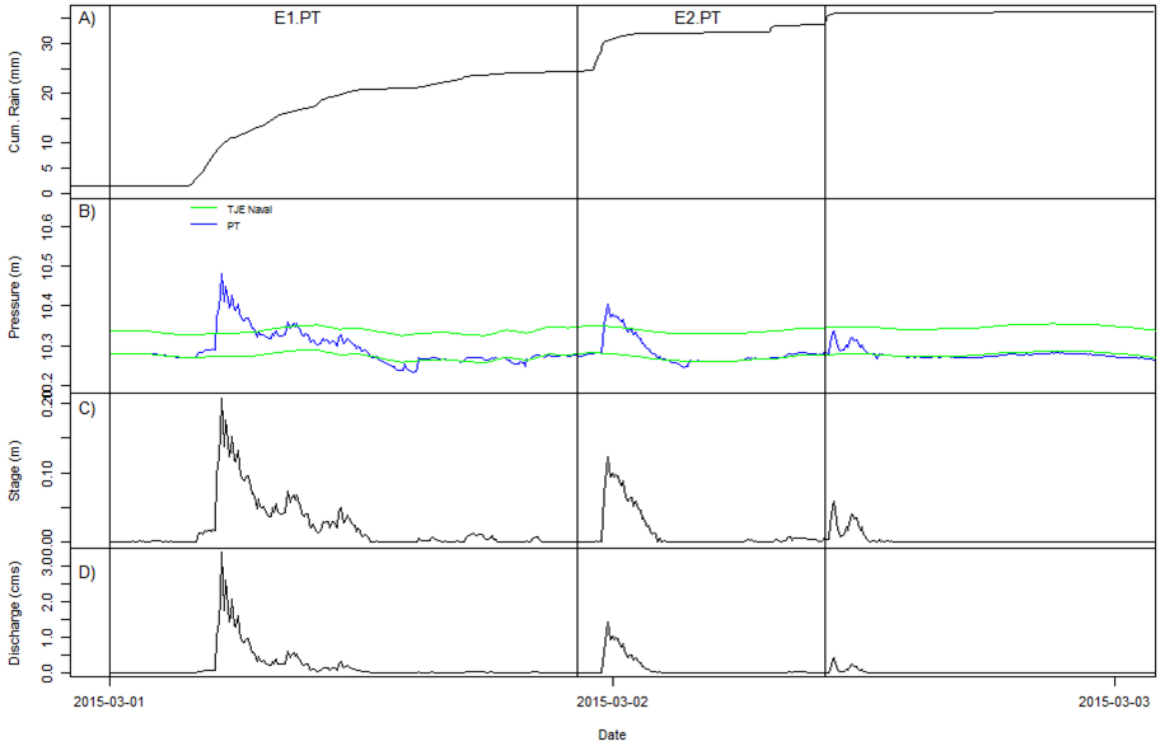

Figure 26. Storm 2, 2015-03-01 to 2015-03-03, with A) cumulative rainfall, B) pressure, including atmospheric pressure from the weather stations (upper green line), adjusted atmospheric pressure (lower green line), and pressure from the PT (blue), C) water stage, and D) discharge. The vertical dashed lines indicate where events were defined to start and end for purposes of reallocating rainfall and runoff data in Table 2 (Chapter 3). E1.PT and E2.PT indicate the two events that were retained for the model and validation from the PT. Taken from Biggs et al., 2017.

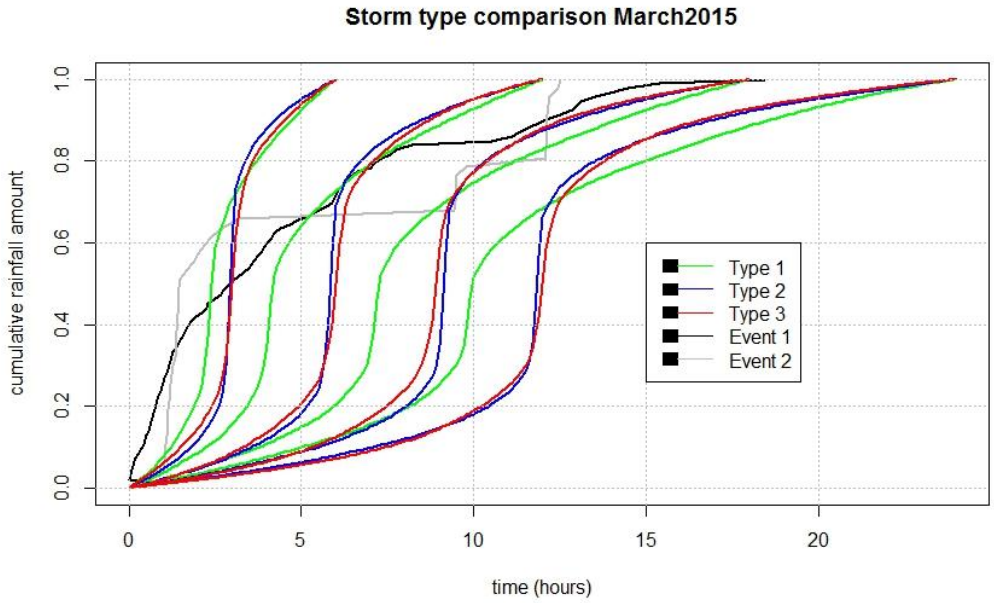

Figure 27. Cumulative rainfall amount, normalized to storm total rainfall, for the two events in March 2015. Taken from Biggs et al., 2017.

Storm 3: 2015-05-15.

This storm had one hydrograph event that occurred in the middle of the day, and the observed rainfall and runoff time series were not changed for model input (Figure 2.9, Biggs et al., 2017). This storm was an outlier for peak discharge, and had high observed peak compared with AnnAGNPS modelled peak. The storm has higher maximum intensity than the Type II storm (Figure 2.10, Biggs et al., 2017).

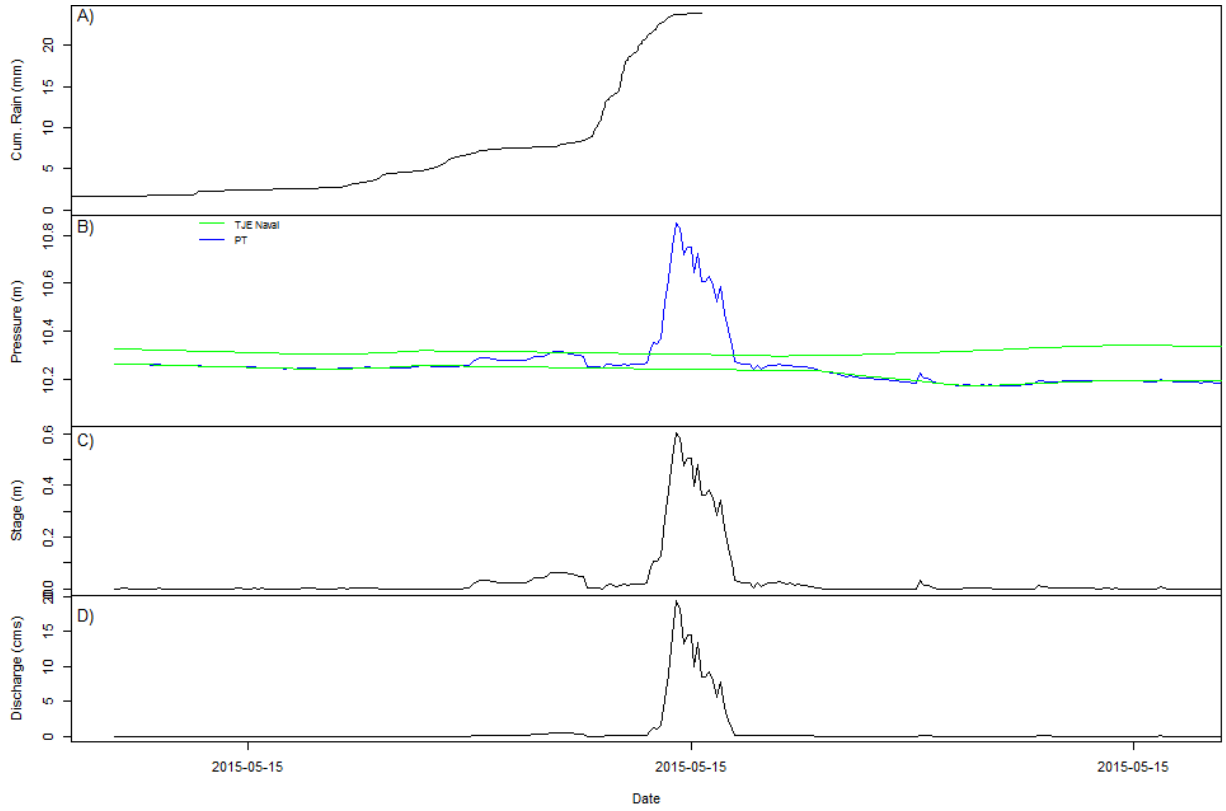

Figure 28. Storm event #3, 2015-05-15, with A) cumulative rainfall, B) pressure, including atmospheric pressure from the weather station (upper green line), adjusted atmospheric pressure (lower green line), and pressure from the PT (blue), C) water stage, and D) discharge. One event was used for model validation, on 5/15/2015. Taken from Biggs et al., 2017.

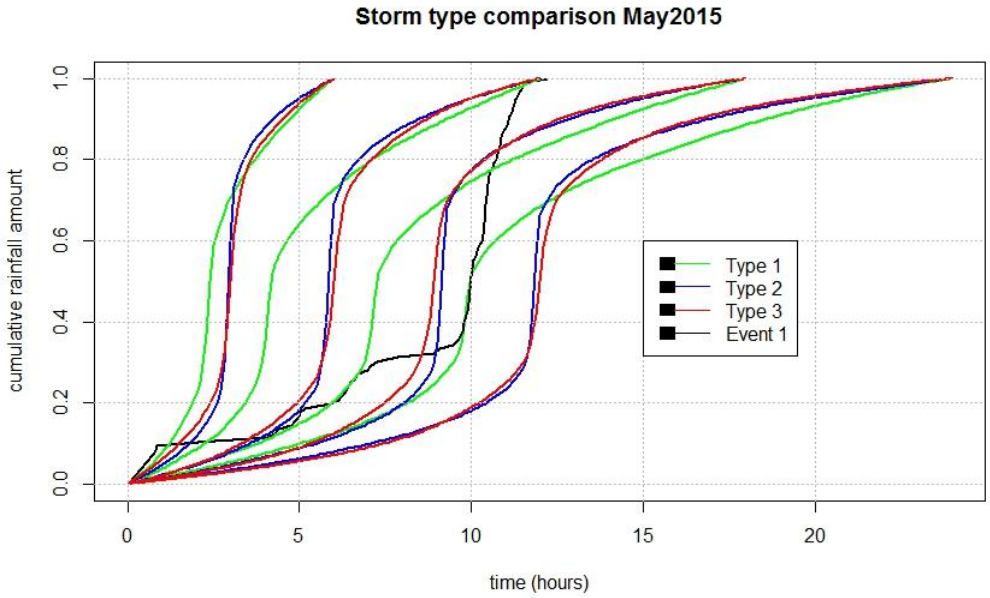

Figure 29. Cumulative rainfall amount, normalized to storm total rainfall, for the one event in May 15, 2015. This storm was an outlier for peak discharge (high observed peak compared with AnnAGNPS modelled peak). Taken from Biggs et al., 2017.

Storm 4: 2015-09-15.

This storm has one hydrograph event (Figure 2.11, Biggs et al., 2017). The event occurred on 2015-09-15 and was not changed from the observed rainfall and runoff time series. A second event, on 2015-09-16, occurred after rainfall stopped and was excluded from the AnnAGNPS model and is not shown in Figure 2.11. The reason for the second peak is not known. Subsequent tests of the PT suggest that the instrument deployed during this storm may show spontaneous fluctuation, and was replaced for subsequent events.

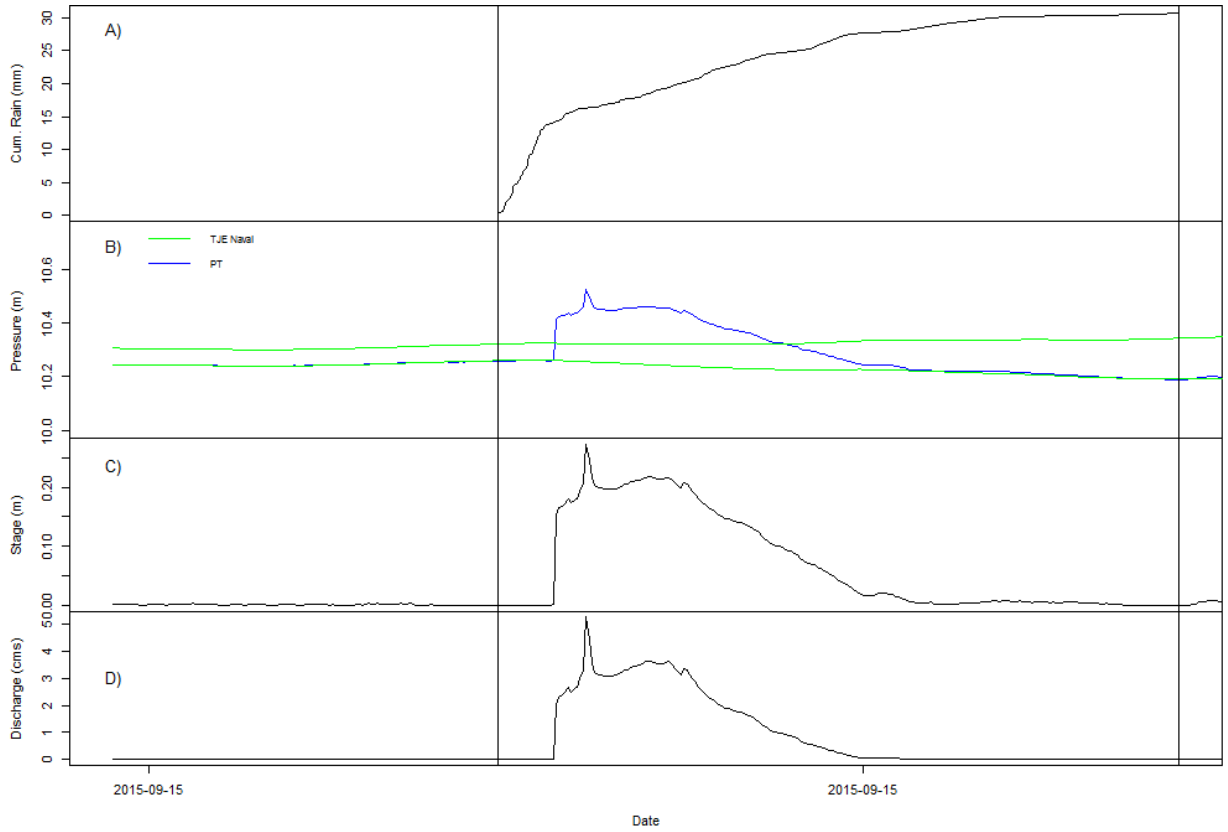

Figure 30. Storm event #4, 2015-09-15, with A) cumulative rainfall, B) pressure, including atmospheric pressure from the weather station (upper green line), adjusted atmospheric pressure (lower green line), and pressure from the PT (blue), C) water stage, and D) discharge. Vertical lines indicate the start and end of the one event retained for model validation. Taken from Biggs et al., 2017.

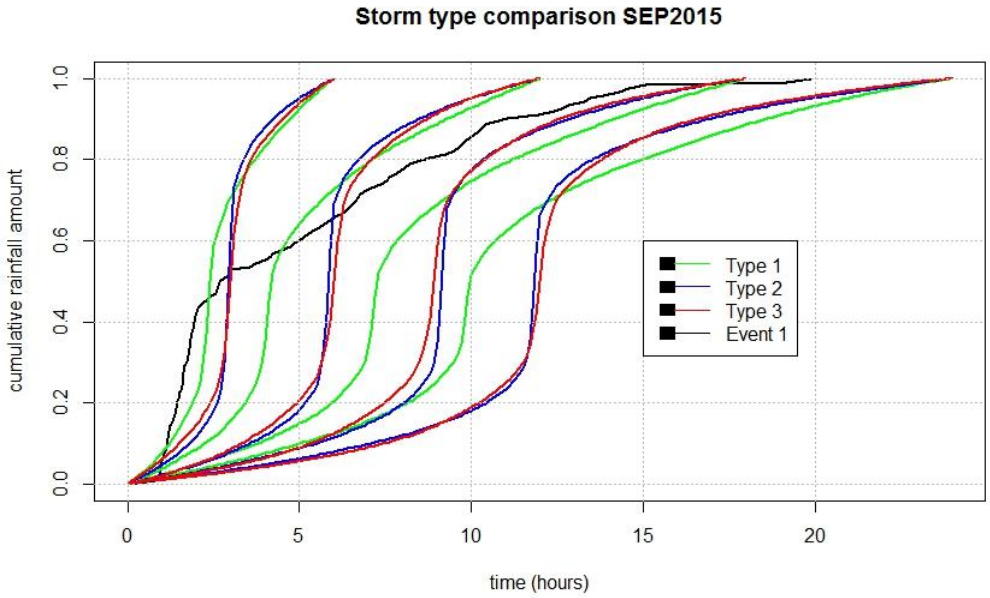

Figure 31. Cumulative rainfall amount, normalized to storm total rainfall, for the one event in September, 2015. Taken from Biggs et al., 2017.

Storm 5: 2016-01-05

This storm has one hydrograph event on 2016-01-05 (Figure 2.13, Biggs et al., 2017), so no reallocation of rainfall or runoff data was performed. The rainfall most closely matched the 12-hour Type II storm (Figure 2.14, Biggs et al., 2017).

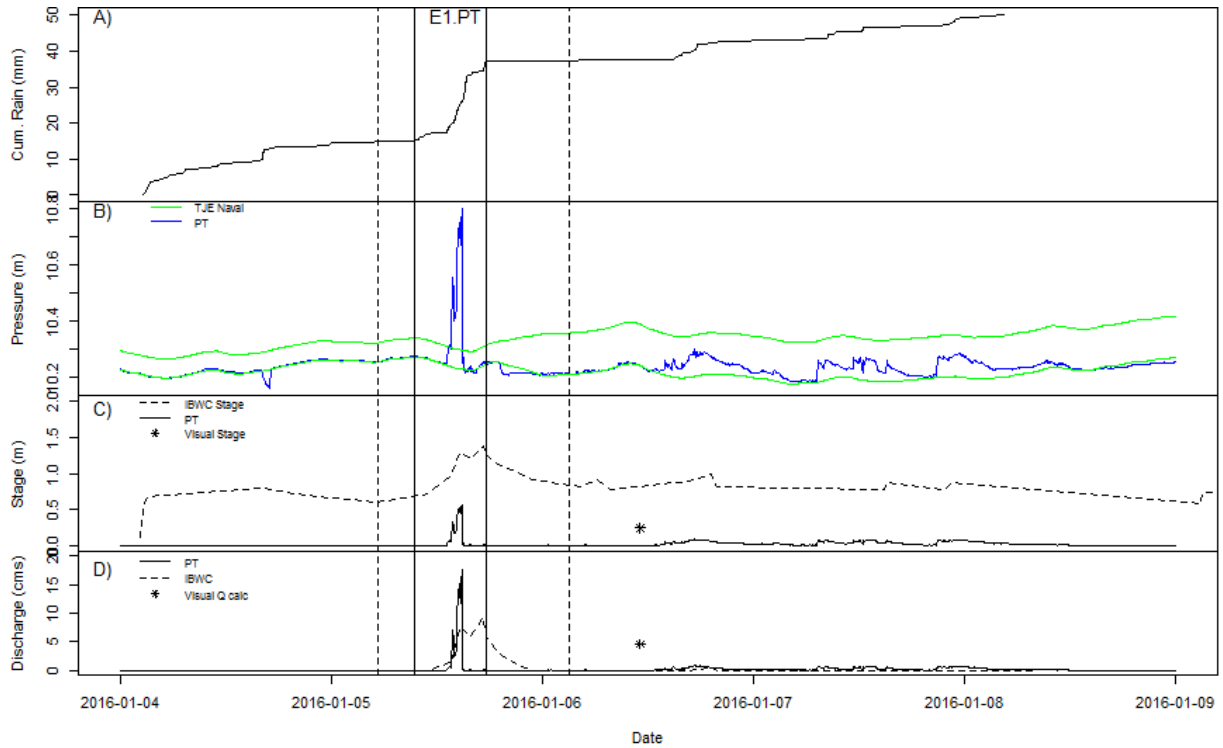

Figure 32. Storm event #5, 2016-01-05, with A) cumulative rainfall, B) pressure, including atmospheric pressure from the weather station (upper green line), adjusted atmospheric pressure (lower green line), and pressure from the PT (blue), C) water stage, and D) discharge. Vertical dashed lines indicate the start and end of the one event using IBWC. The vertical solid lines indicate the start and end of one event using the PT and was retained for model validation. Taken from Biggs et al., 2017.

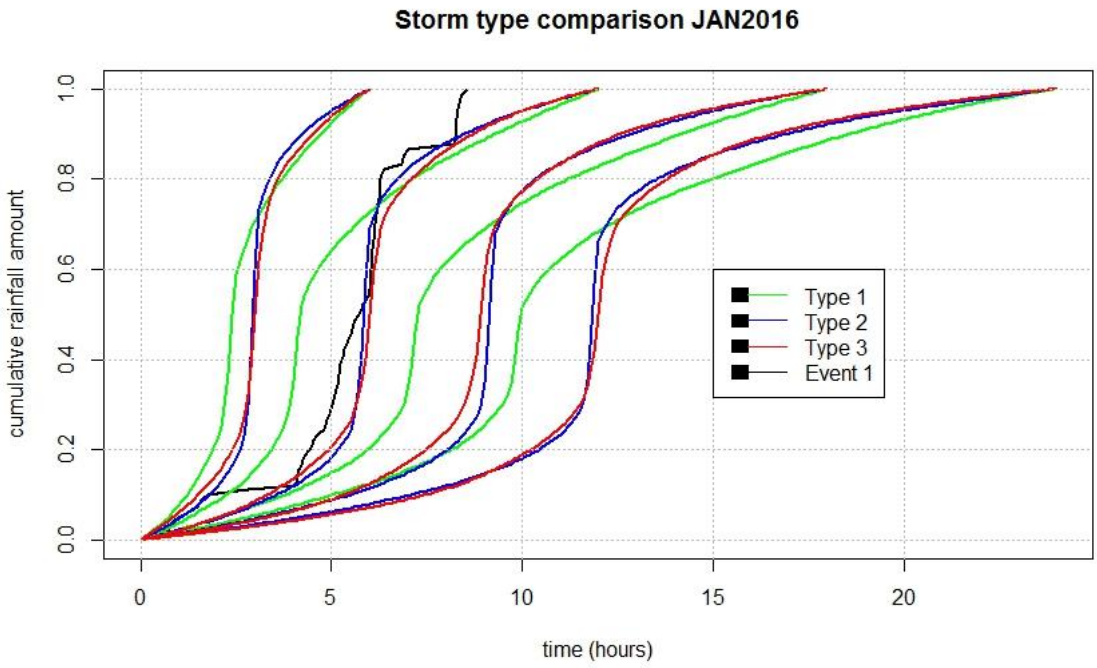

Figure 33. Cumulative rainfall for January, 2016. *** This storm was an outlier for peak discharge (high observed peak compared with AnnAGNPS modelled peak). Taken from Biggs et al., 2017.

Storm 6: 2016-03-06

This storm has one hydrograph event on 2016-03-06 and one hydrograph event on 2016-03-07 to 2016-03-08 (Figure 2.15, Biggs et al., 2017). The PT gave erratic measurements during the second event that did not correspond closely with rainfall, so the IBWC rating curve was used for that event. The rainfall did not match any storm type, but the peak intensity corresponded with a 16-hour, Type II storm (Figure 2.16, Biggs et al., 2017).

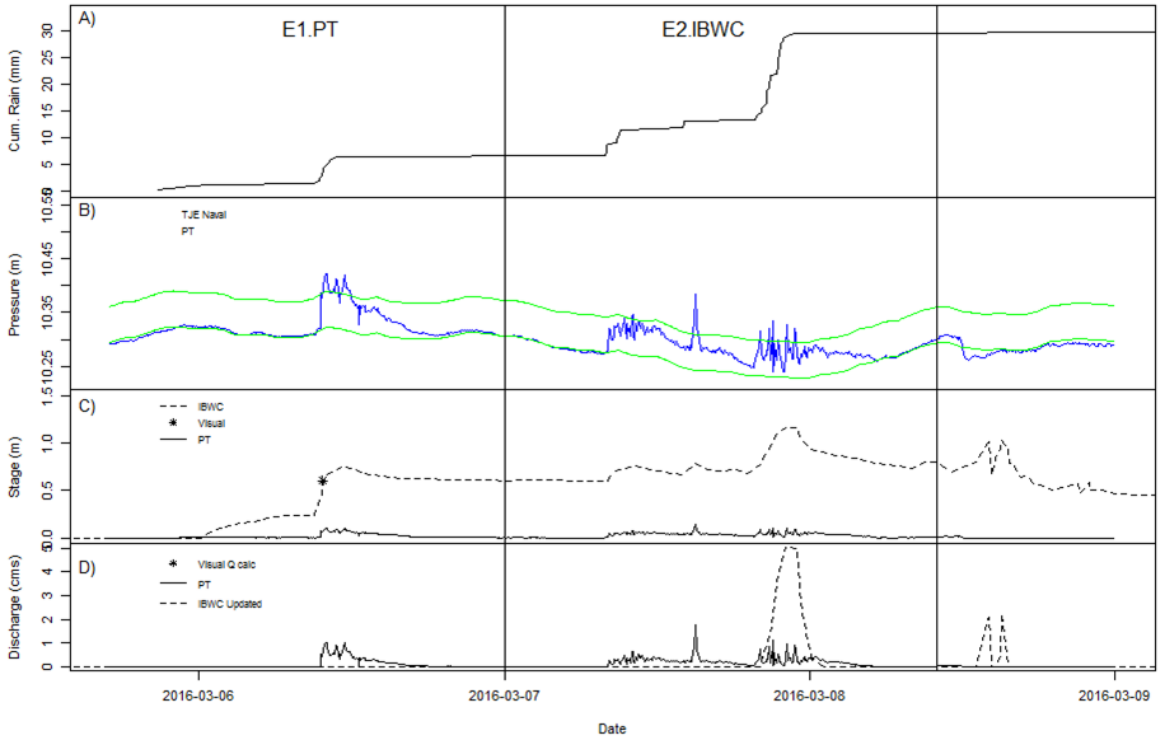

Figure 34. Storm event #6, 2016-03-06, with A) cumulative rainfall, B) pressure, including atmospheric pressure from the weather stations (upper green line), adjusted atmospheric pressure (lower green line), and pressure from the PT (blue), C) water stage, and D) discharge. Vertical lines indicate the start and end of the one event retained for model validation. . E2 PT was not used in analysis due to erratic measurements that do not correspond to the rainfall, IBWC rating from E2 was used instead. Taken from Biggs et al., 2017

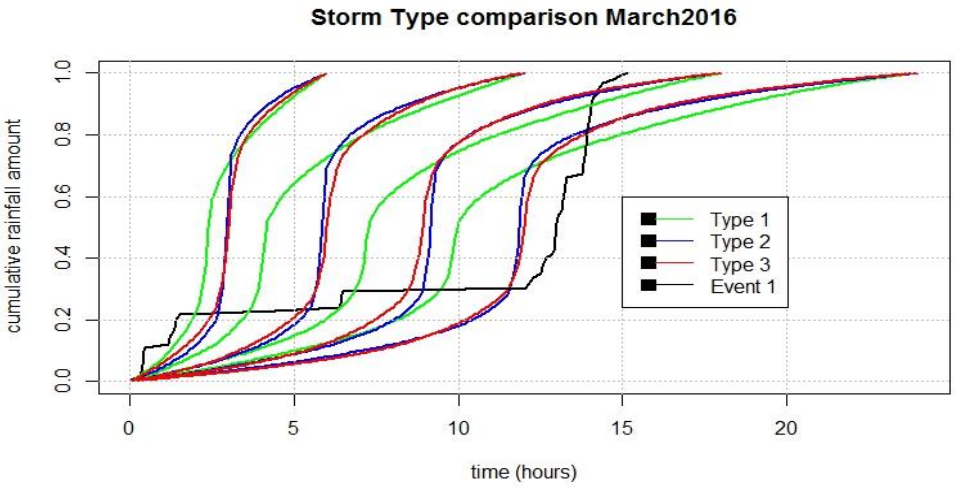

Figure 35. Cumulative rainfall for March, 2016. Taken from Biggs et al., 2017.

Storm 7: 2016-04-09

This storm did not have recorded runoff, despite having significant rainfall (Figure 2.17). A malfunction of the PT must have occurred during this storm. Additionally, IBWC rating curve gave values of zero for this storm due to low stage measurements recorded from the bubbler.

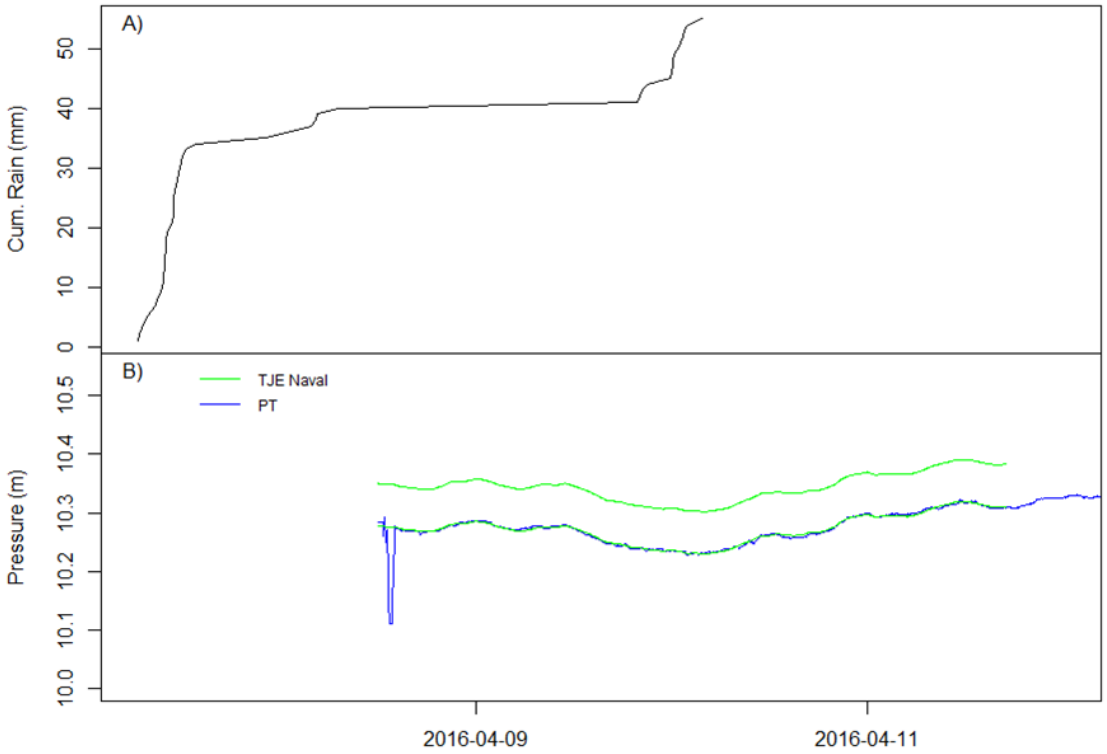

Figure 36. Storm event #7, 2016-04-09, with A) cumulative rainfall and B) pressure, including atmospheric pressure from the weather station (upper green line), adjusted atmospheric pressure (lower green line), and pressure from the PT (blue). No apparent discharge event captured with the PT, IBWC rating curve had discharge values of zero.

Storm 8: 2017-01-19

A malfunction of the PT occurred during this storm. According to the IBWC rating curve, this storm had three major storm hydrograph (Figure 2.18, Biggs et al., 2017). We separated them into two storms for the AnnAGNPS model, one for 2017-01-19 and one for 2017-01-20 (Table 2.1, Biggs et al., 2017). The third storm was erratic and didn't correspond well with rainfall and was excluded from the model calibration and validation.

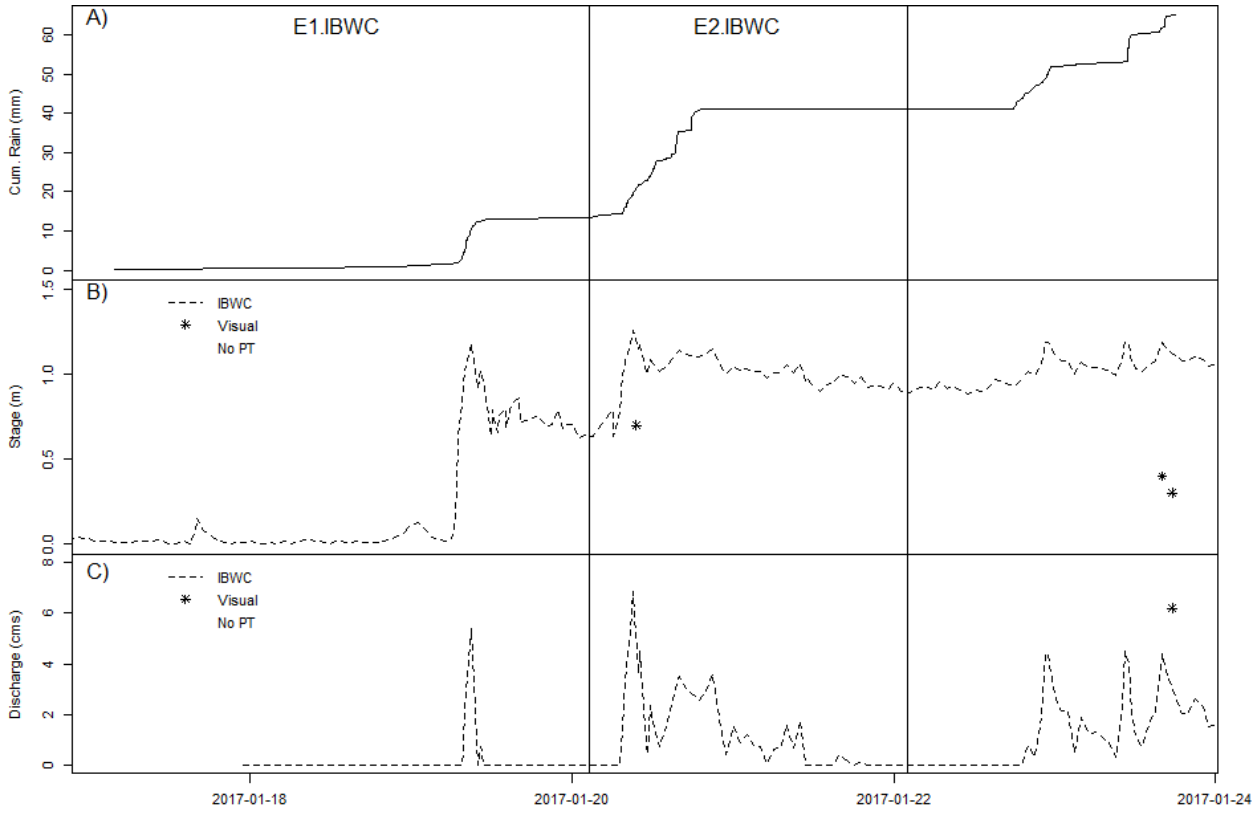

Figure 37. Storm event #8, 2017-01-18, with A) cumulative rainfall, B) stage from the IBWC bubbler, and C) discharge from the updated IBWC rating curve. No PT data, IBWC rating curve discharge used in model calibration and validation for E1 and E2. Taken from Biggs et al., 2017.

Storm 9: 2017-02-17

This storm had one distinct storm hydrograph (Figure 2.19, Biggs et al., 2017). The PT housing was damaged during this storm and gave erratic measurements. Discharge calculated from the IBWC rating curve was used for the model calibration and validation. The IBWC peak discharge (~10 cms) matched well with the observed discharge (~15 cms).

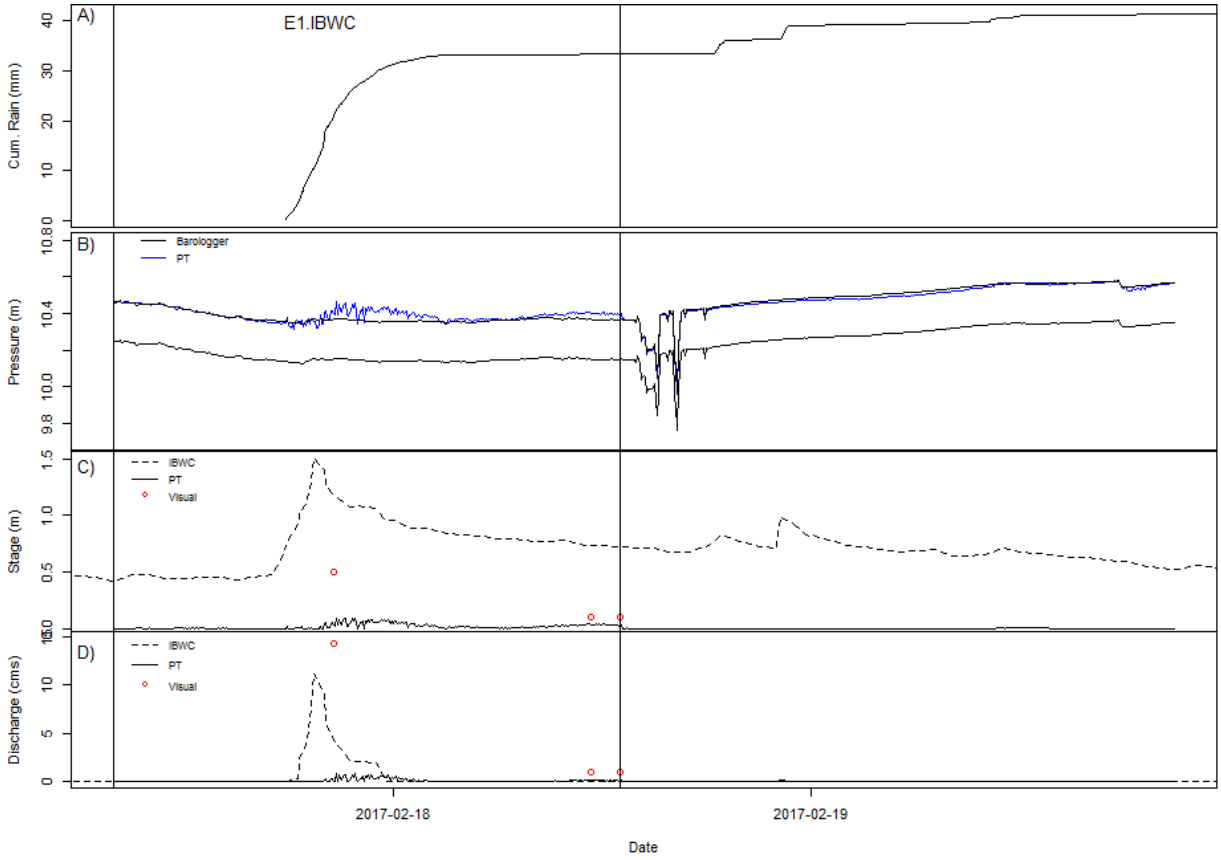

Figure 38. Storm event #9, 2017-02-17, with A) cumulative rainfall, B) pressure, including atmospheric pressure from the barologger (lower black line), adjusted atmospheric pressure (upper black line), and pressure from the PT (blue), C) water stage from the PT (solid black line) and IBWC bubbler (dashed black line), and D) discharge from the PT and IBWC rating curve. E1.IBWC indicates the one event was retained for the model and validation using the IBWC rating curve. Taken from Biggs et al., 2017.

Storm 10: 2017-02-27

This storm was the largest recorded observed storm and had one distinct storm hydrograph (Figure 2.20, Biggs et al., 2017). There was no data from the PT, but a field camera was placed at the PT location and recorded stage every 15 minutes. The IBWC rating curve was developed from this event. Discharge calculated from the field camera was used for the model calibration and validation.

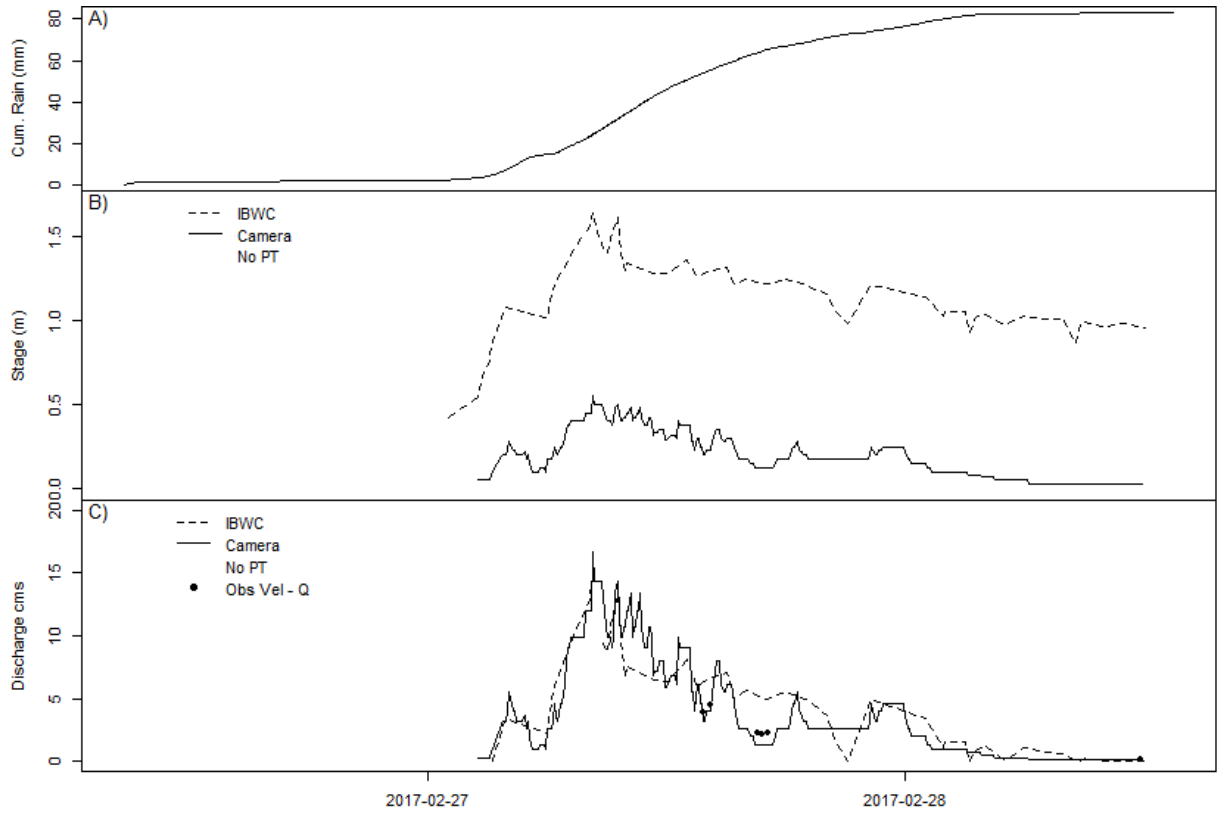

Figure 39. Storm event #10, 2017-02-27, with A) cumulative rainfall, B) stage recorded by the IBWC bubbler (dashed black line) and stage recorded by the field camera (solid black line), and C) discharge from the field camera and IBWC rating curve. IBWC rating curve was based on this event. Discharge from the field camera matched closesly with observed discharge and was used in model calibration and validation. Taken from Biggs et al., 2017.

Sediment trap texture analyses and trap efficiency

Table 14. Particle size data summary for the Goat Canyon sediment traps. All sample depths were 0-3 ft, and mean grain size description was "fine sand" for all samples. Samples SS1 through GC8 are from AMEC (2007). Samples from "Avulsion Basin #1 to Canyon Basin #2 are from de Temple et al. (1999). Taken from Biggs et al., 2017.

Sample location	Sample ID		Particle size distribution, percent							
		Median grain size mm	Gravel	Sand			Silt	Clay	Silt + Clay	Total Sand
				Coarse	Med.	Fine				
Sorted Pile	SS1	0.098	0	0	17.11	45.79	31.31	5.78	37.10	62.9
	SS2	0.101	0	0	20.07	44.32	30.91	4.71	35.61	64.39
	SS3	0.094	0	0	12.39	50.82	33.62	3.17	36.79	63.21
	Mean ± sd	0.098± 0.003	0	0	16.5±3.9	47±3.4	31.9±1.5	4.6±1.3	36.5±0.8	63.5±0.8
Native Pile	NS1	0.122	0	0	27.55	43.05	26.16	3.24	29.4	70.60
	NS2	0.146	0	0	30.01	43.93	22.81	3.25	26.05	73.95
	NS3	0.152	0	0	28.3	47.04	20.66	4	24.65	75.34
	Mean ± sd	140± 0.016	0	0	28.6±1.3	44.7± 2.1	23.2± 2.8	3.5± 0.4	26.7± 2.4	73.3± 2.4
Upper Catchbasin	GC1	0.090	0	0	7.60	53.97	33.69	4.74	38.43	61.57
	GC2	0.075	0	0	3.48	47.67	43.19	5.65	48.85	51.15
	GC3	0.085	0	0	3.95	54.83	36.4	4.82	41.22	58.78
	GC4	0.075	0	0	10.08	40.33	42.62	6.96	49.58	50.42
	GC5	0.069	0	0	5.39	41.06	47.57	5.98	53.54	46.45
	Mean ± sd	0.079± 0.008	0	0	6.1±2.7	47.6±6.9	40.7±5.6	5.6±0.9	46.3±6.3	53.7±6.3
Lower catchbasin	GC6	0.082	0	0	9.04	45.02	40.47	5.47	45.94	54.06
	GC7	0.094	0	0	3.38	61.31	30.79	4.53	35.32	64.68
	GC8	0.102	0	0	18.73	43.16	33.09	5.02	38.11	61.89
	Mean ± sd	0.092± 0.010	0	0	10.4 ± 7.8	49.8 ± 10	34.8 ± 5.1	5±0.5	39.8±5.5	60.2±5.5
Avulsion basin	#1	-	0	-	-	-	-	-	37.0	63.0
Avulsion basin	#2	-	0	-	-	-	-	-	13.1	89.6
Silt basin	-	-	0	-	-	-	-	-	39.8	60.2
Canyon basin	#1	-	5.8*	-	-	-	-	-	16.1	78.1
Canyon basin	#2	-	5.9*	-	-	-	-	-	3.4	90.7

*Coarser fractions underestimated due to sampling methods.

The settling velocity (ω) for each sediment size was estimated using the equations in the Reservoir Sedimentation Handbook referring to the Rubey (1933) equation:

$$\omega = \frac{[1636(\rho_s - \rho)d^3 + 9\mu^2]^{0.5} - 3\mu}{500d} \quad \text{(C1)}$$

where ω = terminal fall velocity (m/s); ρ_s = sediment density (kg/m^3); ρ = density of water (kg/m^3), assumed to be 1000 kg/m^3; μ = dynamic viscosity of water (N•s/m^2), assumed to be 1.31×10^{-3} N•s/m^2; and d = particle diameter (m).

The critical settling velocity (ω_c) of the sedimentation basin was calculated as:

$$\omega_c = Q/A \quad \text{(C2)}$$

where ω_c = critical settling velocity (m/s), which is the velocity of the slowest particle of the basin that will be 100% removed (Morris and Fan, 1998); Q = design discharge or inflow (m^3/s), and A = surface area of the sediment basin (m^2).

Table 15. Sediment removed from traps (Tons Removed), annual trap efficiency, and corrected sediment load from the watershed by size class. Taken from Biggs et al., 2017.

Removal Date	Tons Removed	Eann n=1	Eann n=3	Corrected Load (tons)
		2006		
Medium sand (a)	1947	1.00	1.00	1947
Fine sand (b)	15194	1.00	1.00	15194
Silt (c)	12991	0.99	1.00	12992
Clay (d)	1788	0.36	0.40	4508
Total	31920			34642
Total without Clay	30132			30133
		2007		
Medium sand (a)	1947	1.00	1.00	1947
Fine sand (b)	15194	1.00	1.00	15194
Silt (c)	12991	0.99	1.00	12992
Clay (d)	1788	0.53	0.61	2946
Total	31920			33079
Total without Clay	30132			30133
		2008		
Medium sand (a)	3115	1.00	1.00	3115
Fine sand (b)	24310	1.00	1.00	24310
Silt (c)	20786	0.96	1.00	20815
Clay (d)	2860	0.16	0.18	16339

Total	51072			64580
Total without Clay	48212			48241
		2009		
Medium sand (a)	3536	1.00	1.00	3536
Fine sand (b)	27592	1.00	1.00	27592
Silt (c)	23593	0.95	1.00	23673
Clay (d)	3246	0.22	0.23	14148
Total	57967			68949
Total without Clay	54721			54801
		2010		
Medium sand (a)	4284	1.00	1.00	4284
Fine sand (b)	33427	1.00	1.00	33427
Silt (c)	28581	0.97	1.00	28609
Clay (d)	3933	0.29	0.31	12615
Total	70224			78935
Total without Clay	66291			66320
		2011		
Medium sand (a)	3951	1.00	1.00	3951
Fine sand (b)	30833	1.00	1.00	30833
Silt (c)	26364	0.93	0.99	26764
Clay (d)	3627	0.34	0.39	9416
Total	64776			70965
Total without Clay	61149			61549
		2012		
Medium sand (a)	3505	1.00	1.00	3505
Fine sand (b)	27349	1.00	1.00	27349
Silt (c)	23385	0.99	1.00	23388
Clay (d)	3218	0.67	0.75	4271
Total	57456			58513
Total without Clay	54238			54242

1. 6.1% Medium sand: 0.25 – 0.5 mm (mean = 0.375 mm)
2. 47.6% Fine sand: 0.125 - 0.250 mm (mean = 0.1875 mm)
3. 40.7% Silt: 0.0039 - 0.0625 mm (mean = 0.0332 mm)
4. 5.6% Clay: 0.00098 - 0.0039 mm or <3.9 um (mean = 0.00244 mm)

The mean grain size diameter was used to calculate the trap efficiency for each size class.

Original data figures and reports from AMEC (2007).

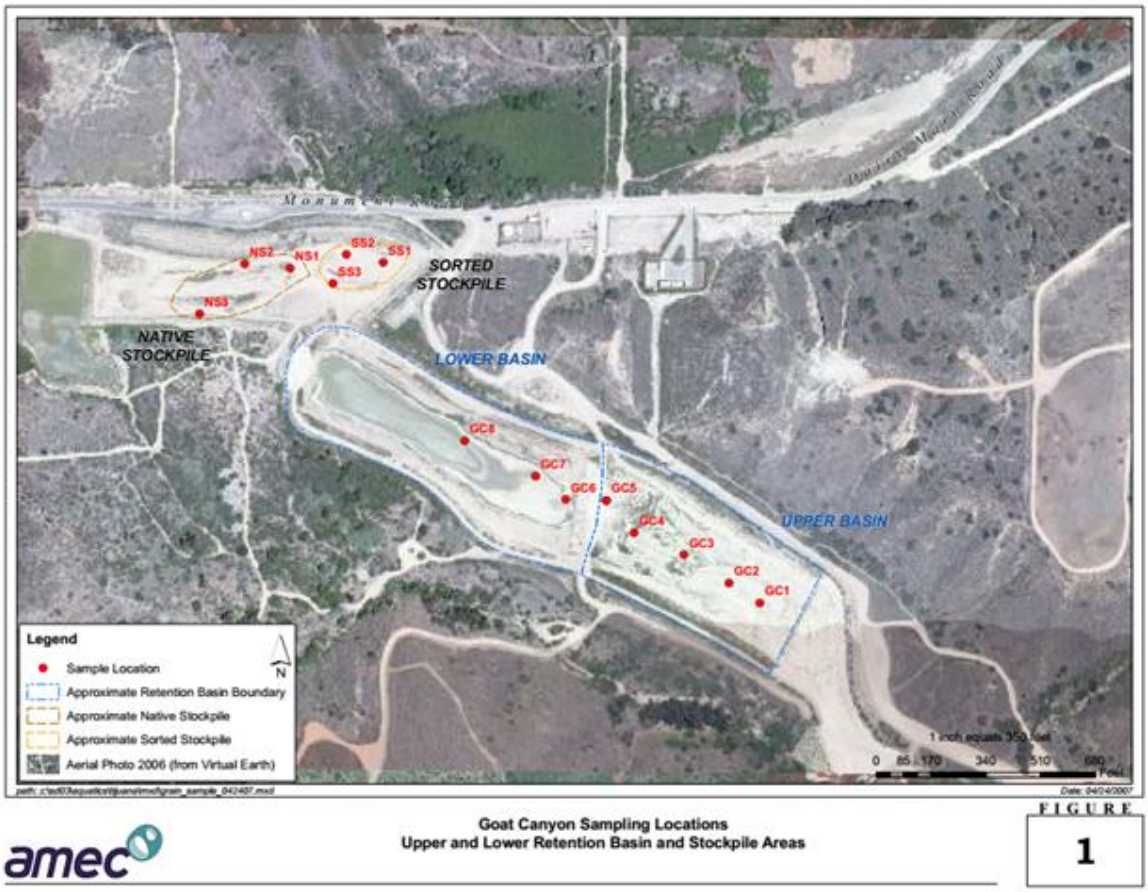

Figure 40. Sites analyzed for particle size by AMEC (2007). Taken from Biggs et al., 2017.

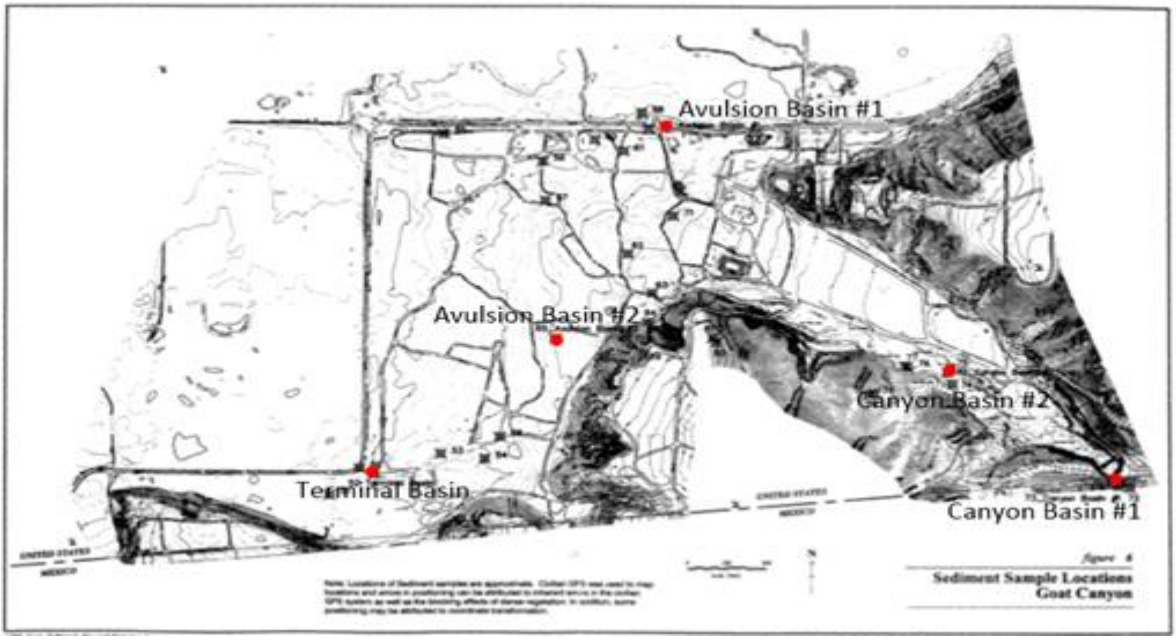

Figure 41. Sites analyzed for particle size by DeTemple et al. (1999). Sites are not located in the current sediment traps, but were taken in the Tijuana Estuary prior to constructing the sediment traps.

Table 16. Mean soil particle size data from AMEC (2007).

Table 2. Summary of Mean Soil Particle Size Data

Soil Sampling Area	Number of Samples	Percent Sand[1] (Mean ± SD)	Percent Fines[2] (Mean ± SD)	Median Grain Size (mm) (Mean ± SD)
Upper Basin	5	53.7 ± 6.3	46.3 ± 6.3	0.079 ± 0.008
Lower Basin	3	60.2 ± 5.5	39.8 ± 5.5	0.092 ± 0.010
Native Stockpile	3	73.3 ± 2.4	26.7 ± 2.4	0.140 ± 0.016
Sorted Stockpile	3	63.5 ± 0.8	36.5 ± 0.8	0.098 ± 0.003

[1] - particle size range from 0.063 to 3.363 mm.
[2] - particle size below 0.063 mm.
mm - millimeters
SD - standard deviation

Table 17. Raw data used to calculate the means in Table A.2.1 (AMEC 2007).

Table C-1. Goat Canyon Particle Size Data Summary with Statistical Comparisons.

Sample Collection Location	Sample ID	Depth, ft.	Mean Grain Size Description	Median Grain Size mm	Particle Size Distribution, wt. percent						Silt & Clay	Mean Percent Sand
					Gravel	Sand Size			Silt	Clay		
						Coarse	Medium	Fine				
Sorted Pile	SS1	0-3	Fine sand	0.098	0.00	0.00	17.11	45.79	31.31	5.78	37.10	62.90
	SS2	0-3	Fine sand	0.101	0.00	0.00	20.07	44.32	30.91	4.71	35.61	64.39
	SS3	0-3	Fine sand	0.094	0.00	0.00	12.39	50.82	33.62	3.17	36.79	63.21
	Mean			0.098	0.0	0.0	16.5	47.0	31.9	4.6	36.5	63.50
	Standard Deviation			0.003	0.0	0.0	3.9	3.4	1.5	1.3	0.8	0.78
Statistical Significance (Sorted vs Native)?				Yes			Yes	NS			Yes	
Native Pile (Unsorted)	NS1	0-3	Fine sand	0.122	0.00	0.00	27.55	43.05	26.16	3.24	29.40	70.60
	NS2	0-3	Fine sand	0.146	0.00	0.00	30.01	43.93	22.81	3.25	26.05	73.95
	NS3	0-3	Fine sand	0.152	0.00	0.00	28.30	47.04	20.66	4.00	24.66	75.34
	Mean			0.140	0.0	0.0	28.6	44.7	23.2	3.5	26.7	73.30
	Standard Deviation			0.016	0.0	0.0	1.3	2.1	2.8	0.4	2.4	2.43
Upper Catchbasin	GC1	0-3	Fine sand	0.090	0.00	0.00	7.60	53.97	33.69	4.74	38.43	61.57
	GC2	0-3	Fine sand	0.076	0.00	0.00	3.48	47.67	43.19	5.65	48.85	51.15
	GC3	0-3	Fine sand	0.085	0.00	0.00	3.95	54.83	36.40	4.82	41.22	58.78
	GC4	0-3	Fine sand	0.075	0.00	0.00	10.08	40.33	42.62	6.96	49.58	50.42
	GC5	0-3	Fine sand	0.069	0.00	0.00	5.39	41.06	47.57	5.98	53.54	46.46
	Mean			0.079	0.0	0.0	6.1	47.6	40.7	5.6	46.3	53.67
	Standard Deviation			0.008	0.0	0.0	2.7	6.9	5.6	0.9	6.3	6.27
Statistical Significance (Upper vs Lower Catchbasin)?				NS			NS	NS			NS	
Lower Catchbasin	GC6	0-3	Fine sand	0.082	0.00	0.00	9.04	45.02	40.47	5.47	45.94	54.06
	GC7	0-3	Fine sand	0.094	0.00	0.00	3.38	61.31	30.79	4.53	35.32	64.68
	GC8	0-3	Fine sand	0.102	0.00	0.00	18.73	43.16	33.09	5.02	38.11	61.89
	Mean			0.092	0.0	0.0	10.4	49.8	34.8	5.0	39.8	60.21
	Standard Deviation			0.010	0.0	0.0	7.8	10.0	5.1	0.5	5.5	5.51
Catchbasin Samples (Pooled)	Mean			0.084	0.000	0.000	7.706	48.420	38.478	5.396	43.874	49.89
	Standard Deviation			0.011	0.000	0.000	5.141	7.533	5.872	0.803	6.528	6.53